Using personalised cardiovascular models to identify new diagnostic predictors for pre-eclampsia

Claudia Mihaela Popp

Submitted to Swansea University in fulfilment of the requirements for the Degree of MSc by Research in Biomedical Engineering

Swansea University

2023

Summary

Haemodynamic adaptations play a crucial role in uteroplacental perfusion during pregnancy. In particular, modifications of the utero-ovarian arterial network cause a significant increase in blood volume distributed to the placenta and foetus. Failure to make these cardiovascular modifications results in complicated pregnancies caused by different disorders such as hypertension, pre-eclampsia, intrauterine growth restriction (IUGR), and placental insufficiency. In pre-eclampsia, the modifications of the utero-ovarian arterial network are unsuccessful and cause less blood volume to be distributed to the placenta and foetus.

Pre-eclampsia is a hypertensive disorder that is still not fully understood, and clinicians still fail at identifying pre-eclamptic women during controls, especially at differentiating between hypertensive women and pre-eclamptic women. One reason for this is that clinicians rely heavily on blood pressure when diagnosing pre-eclampsia, and this biomarker has similar readings for both pre-eclampsia and hypertension. As part of the diagnosis of pre-eclampsia, proteinuria is used. In order to improve the diagnosis of pre-eclampsia, other biomarkers are being researched.

A dataset of 21 patients was used to find novel biomarkers that can classify pre-eclampsia. The dataset is divided into two groups: uncomplicated pregnancies with hypertensive women and complicated pregnancies with pre-eclampsia. A computational model of the cardiovascular system is used to simulate blood and pressure solutions based on patient-specific observations in order to develop a new biomarker. The model employs 1D modelling which incorporates a wave intensity analysis that models forward and backward waves to provide more precise predictions of wave propagation across the artery system, particularly in the utero-ovarian system.

The proposed biomarkers will include dimensionless terms formed by global maternal parameters such as systolic blood pressure, stroke volume, pulse wave velocity, etc., or local uterine parameters such as pressure and velocity in specific vessels of the uterine system. Afterwards, their ability as a classifier of pre-eclampsia will be investigated. Besides this, a case study of the prone position in pregnancy and its effects on cardiovascular changes will be carried out. To do this, the computational model will be used to study what happens when a pregnant woman is positioned in the prone position and how vital metrics like blood pressure and cardiac output are altered.

It was found that the biomarkers based on the radial and arcuate arteries have a better classification ability for pre-eclampsia, even higher than the Doppler-measured Resistance Index (RI) and Pulsatility Index (PI). The novelty of this work is the introduction of new biomarkers through the use of a computational model, as well as the demonstration of the dependability and use of 1D modelling in pregnancy. The model demonstrated how biomarkers that could not be measured clinically may be easily calculated using 1D modelling and provide critical information about the utero-ovarian circulation.

Future work should concentrate on changing the existing solver into a much faster and simpler solver, as well as validating the biomarkers in a larger dataset.

Declarations

This work has not previously been accepted in substance for any degree and is not being concurrently submitted in candidature for any degree.

.....

Date: 23/07/2023

This thesis is the result of my own investigations, except where otherwise stated. Other sources are acknowledged by footnotes giving explicit references. A bibliography is appended.

.....

Date: 23/07/2023

I hereby give consent for my thesis, if accepted, to be available for electronic sharing

.....

Date: 23/07/2023

The University's ethical procedures have been followed and, where appropriate, that ethical approval has been granted.

.....

Date: 23/07/2023

Acknowledgements

Firstly, I would like to express my deepest gratitude to my supervisor, Dr. Raoul Van Loon, for his patience and invaluable feedback. This endeavour would not have been possible without his guidance. Additionally, I would like to thank Dr. Hari Arora for organising weekly research meetings where many discussions and questions have been raised and helped me take a critical and objective approach in my research.

Secondly, I would like to thank Dr. Edward D. Johnstone and Dr. Jenny E. Myers from Manchester University for providing the data used in this work.

Contents

Symbols and Abbreviations

Name	Symbol/Abbreviation	Units
Cross-sectional area	*A*	cm^2
Pulse wave velocity	*PWV*	$\frac{cm}{s}$
Resistance index	*RI*	-
Pulsatility index	*PI*	-
Systolic blood pressure	*SBP*, P_{syst}	*mmHg*
Diastolic blood pressure	*DBP*, P_{dia}	*mmHg*
Cardiac output	*CO*	*L/min*
Heart rate	*HR*	*Beats/min*
End-diastolic velocity	*D*	$\frac{cm}{s}$
Peak-systolic velocity	*S*	$\frac{cm}{s}$
Peripheral resistance	R_{periph}	$\frac{dynes*s}{cm^5}$
Systemic vascular resistance	*SVR*	$\frac{dynes*s}{cm^5}$
Density	ρ	$\frac{kg}{m^3}$
Wave speed	*c*	$\frac{cm}{s}$
Stroke Volume	*SV*	*L*
Compliance	*C*, C_v	$\frac{m^3}{Pa}$
Change in pulse pressure	ΔP_{pulse}	*mmHg*
Uterine artery	ut	
Ascending uterine artery	asc	
Arcuate artery	arc	
Radial/spiral artery	rad	
Left side	*L*	
Right side	*R*	
UP	Uncomplicated pregnancies	
CP	Complicated pregnancies	

1. Introduction

The main focus of this thesis is the discovery of novel pre-eclampsia biomarkers. As a result, this subject will be the main focus of the chapters from Chapter 1 through Chapter 6. The case study that follows in Chapter 7 focuses on the impact of maternal posture on the cardiovascular system. The final chapter, Chapter 8, focuses on data cleaning and provides a brief exercise for cleaning a sizable dataset of measurements collected during clinical visits to evaluate pregnancy conditions.

During pregnancy, the maternal cardiovascular system undergoes major changes to adapt to normal foetal growth, especially the uterine arterial network. The uterine arterial network consists of a symmetric network of vessels receiving blood from the internal iliac artery to the uterine and vaginal arteries, which go to the utero-ovarian communicating artery, the ovarian arteries, and spiral/radial arteries (Figure 1).

The growth of the placenta, which delivers blood to the foetus, is critical. The antenatal care starts with the first face-to-face appointment at around 10 weeks, where the woman's weight and height are taken to calculate body mass index and also a blood sample is taken to check blood count and group [1]. The next appointment can take place between 11 and 14 weeks, when an ultrasound screening is offered. Then, the pregnancy is monitored with an appointment between 18 and 20 weeks to check for foetal anomalies and placental location. The maternal circulation starts changing as early as 5 weeks into the pregnancy, with the most major changes being the increase in cardiac output [2, 3] and uterine artery blood flow rate [4], the decrease in total peripheral resistance and vessels remodelling to adapt to the increase in cardiac output and uterine blood flow rate [5, 6]. It is not recommended to use invasive procedures for diagnosis and measurement as they have a higher risk than non-invasive procedures and should be used only when appropriate [7] which makes it hard to monitor changes like heart and vessel remodelling. One method that is often used to determine uterine artery area and blood flow is Doppler ultrasound.

Doppler ultrasound is often used for the assessment of Down syndrome in antenatal care, but studies investigated the use of Doppler ultrasound in hypertensive disorders and found that an end diastolic notch at 20 – 24 weeks could be related to maternal hypertension and intrauterine growth retardation (IUGR), especially if it's present in both uterine arteries [8, 9], but it cannot be used for a clear diagnostic and only for assessing if the pregnancy is at a low or high risk of developing complications (further details on notching in Chapter 2.5. Diagnostic Techniques for Pre-eclampsia). The main measurements of Doppler ultrasound are used for calculating the diameter of the uterine artery and the blood flow volume. The downside of using Doppler ultrasound is that it is predisposed to human error, resulting in difficulty taking a reading as factors like the Doppler angle, positioning, and Doppler gain can influence the variability by as much as 20% [10]. One index that was developed using Doppler is the Resistance Index (RI) which can be calculated as the difference in the peak systolic velocity and end diastolic velocity divided by the peak systolic velocity [8]. An advantage of using RI for measurement is that it is independent of the angle of insonance [8]. Another index that is often used is the Pulsatility Index (PI) which is the difference in the peak systolic velocity and end diastolic velocity divided by the time averaged maximum velocity over the cardiac cycle, but it is slightly more complicated to calculate the mean velocity accurately compared to calculating the RI.

The hypertensive disorders of pregnancy represent one of the major causes of maternal deaths with a percentage of 16.1 in developed countries [11]. Regardless of this, it is still a challenge to diagnose and prevent complications in early pregnancy. The current practise involves assessing the risk factors to determine the risk of developing hypertension and prescribing aspirin during the first trimester [1]. Further into the pregnancy (20 + 0 weeks), women showing signs of hypertension will be offered a test to measure proteinuria, and for women with blood pressure of 140/90 mmHg or higher, they will be referred to secondary care [1, 12, 13]. Hypertensive disorders can be divided into gestational

hypertension (non-proteinuric) (GH), pre-eclampsia (PE), hypertension with proteinuria, or other organ dysfunction [14].

Pre-eclampsia is one of the most common hypertensive disorders and, because of that, one of the main causes of maternal and perinatal morbidity [15]. It is caused by failure of vascular remodelling of the uterine spiral arteries, which leads to insufficient blood flow to the foetus during gestation [16, 17] (the spiral arteries and utero-ovarian system are visualised in Figure 1).

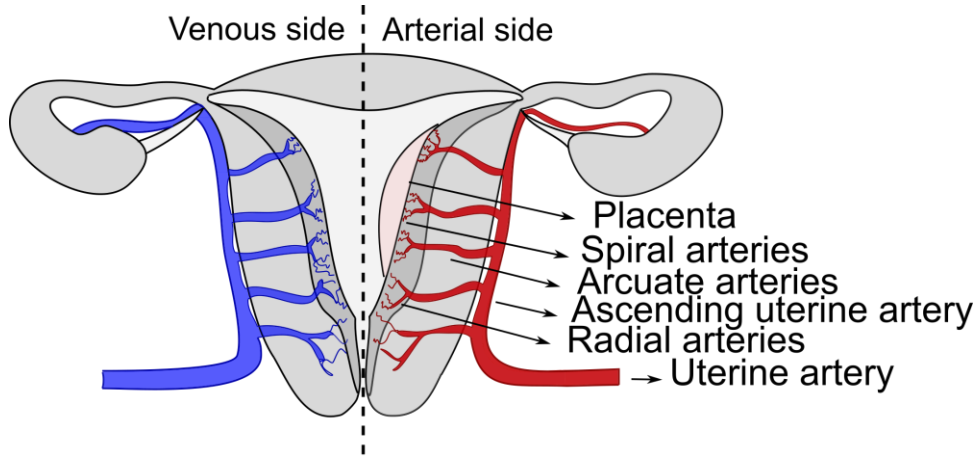

Figure 1. *Cardiovascular system of the utero-ovarian system*

A computational model of the cardiovascular circulation in the entire adult has been developed by Mynard et al. [18] and adapted by Carson et al. [19, 20] for pregnancy. The network consists of 513 1D vessels that can capture wave propagations and 61 0D vascular beds that include major organs such as the brain, liver, kidneys, placenta, and others [19–21]. The model provides information on the flow and pressure at each point in the system and also the areas of the vessels during the cardiac cycle [21] and can simulate cases of normal pregnancy or hypertension with results in the physiological ranges and the cardiovascular changes during the gestation period. Besides the vessels and vascular beds, a lumped model of the heart is present to simulate cardiac function. The use of wave intensity analysis (WIA) in this model is critical for simulating waveforms of pressure and flow that are representative of the actual waveforms found in a pregnant woman. WIA calculates the forward and backward waves, which are able to capture changes in the utero-ovarian system such as increased resistance. Without this level of complexity, it would be much harder to predict accurate pressure and flow waveforms for each patient. It is also important to mention that the radial and spiral arteries are modelled together and are referred to as only radial arteries.

In order to completely appreciate which parameters affect the utero-ovarian system, a sensitivity analysis of the computational model will be done. This allows for a better understanding of pregnancy outcomes based on cardiovascular parameters, as well as assessing the most and least sensitive parameters using a univariate and multivariate approach. Eight cardiovascular markers will be evaluated. The sensitivity analysis will be composed of 250 Monte Carlo simulations for each parameter (to display the variation throughout the cardiac cycle of each parameter). Then, the Sobol indices will be calculated to measure the variance that each parameter is causing on the pressure and flow.

Afterwards, new biomarkers that can classify pre-eclampsia will be proposed and analysed as the main objective of this work. This study proposes a set of 8 new biomarkers based on key cardiovascular parameters. To verify these new biomarkers, a classification problem that includes supervised and unsupervised machine learning was created. The classification is binary, where the data is split into uncomplicated pregnancies and complicated pregnancies. The newly proposed classifiers

will be compared to the clinical indices RI and PI. The aim is to find a biomarker that can provide better accuracy in classification compared to RI and PI.

2. Literature Review

2.1. Pregnancy and its complications

During the gestation period, the maternal body undergoes significant physiological changes. The gestation phase lasts about 40 weeks and can be divided into three semesters. The physiological changes include changes in the cardiovascular, renal, nervous, hormonal, respiratory systems and many more. During the first trimester of pregnancy, the presence of nausea and morning sickness will produce discomfort and affect the quality of life of the pregnant woman. Even so, it has been correlated with the outcome of pregnancy showing a positive relation between nausea and vomiting and a decrease in miscarriage risk, perinatal death, low infant birth weight and preterm birth [22].

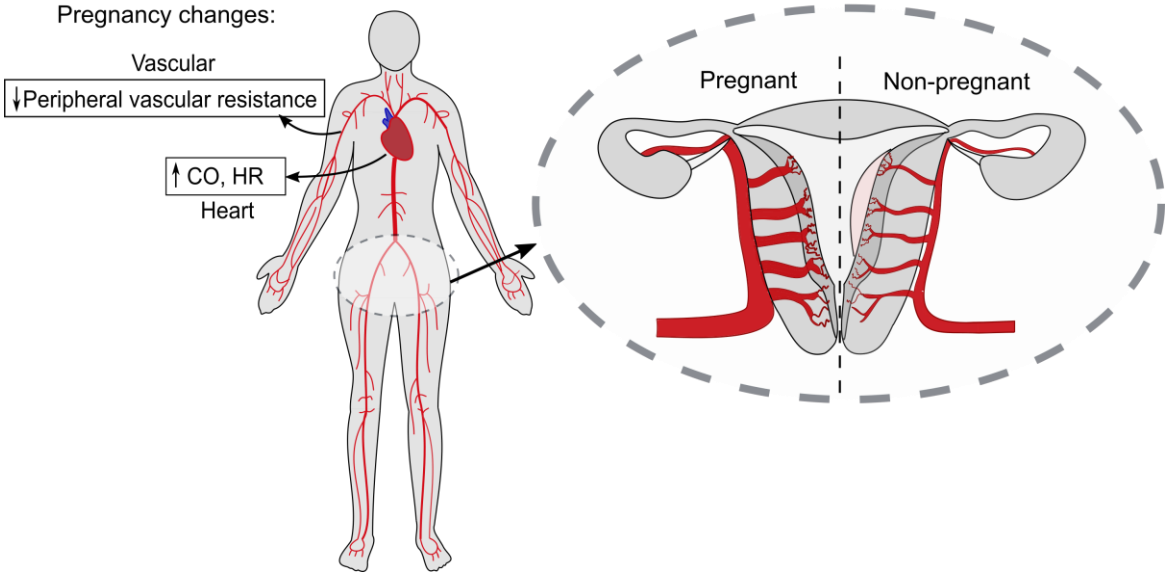

Figure 2. *Main changes in the cardiovascular system during pregnancy and uterine system comparison between pregnant and non-pregnant state.*

One of the major changes of the cardiovascular system is the invasion of the spiral arteries by trophoblasts which results in loss of musculoelastic structure of the spiral arteries and thus, a steep increase in uterine blood flow [23]. Besides the spiral arteries, the uterine arteries also increase significantly in diameter compared to the non-pregnant state and during pregnancy, there is a less significant increase in diameter [23]. It is considered that the vessels increase during pregnancy due to the increase in levels of oestrogen that has a vasodilator effect [23]. The increased levels of oestrogen, and also progesterone and prostaglandins affect the entire systemic circulation and result in vascular smooth muscle relaxation which means a decrease in peripheral vascular resistance [24]. This will affect the following parameters: heart rate, cardiac output and stroke volume (Figure 2). The cardiac output increases by 45 percent when compared to the non-pregnant state, and this increase is due to both heart rate alterations and stroke volume changes. Heart rate increases until 32 weeks of gestation and stroke volume increases until approximately 20 weeks of gestation [25]. Next, the blood pressure shows an increase during pregnancy with the systolic blood pressure having a minor linear increase (up to 5 mmHg increase) during gestational weeks and the diastolic blood pressure showing a slight decrease in the first trimester and followed by an increase in the second and third trimesters [26]. It was also noted that there might be changes masked on the heart because of the rise of the diaphragm resulting in the displacement of the heart upwards and to the left [24]. Besides that, the uterus can also compress the

abdominal aorta and inferior vena cava and result in aortocaval compression which can lead to hypotension [24].

The renal system is highly affected by the cardiovascular system with the major causes being the changes in the renal arteries which can result in increased renal blood flow due to increase in cardiac output and therefore, increase in glomerular filtration rate [24]. But, on the other hand, cardiovascular complications will also result in renal complications. Acute kidney injury (AKI) is one of the most common diseases which are hard to diagnose by clinicians and is often caused by pre-eclampsia [27]. AKI is often diagnosed based on increases in creatine and urine output levels but during gestation, these threshold levels are not reliable due to the gestational variations in serum creatine and urine [27]. Another option would be renal biopsy but is not recommended as is difficult to perform as gestation progresses and has a high risk of bleeding [27]. Other complications that could affect the renal system during pregnancy (although the chances of happening are around 1%) are thrombotic thrombocytopenic purpura (TTP; causes blood clots to form in the human body) and atypical haemolytic uraemic syndrome (aHUS; causes blood clots to form specifically in the small blood vessels in the kidneys). TTP and HUS are caused by a gestational fall in disintegrin and metallopeptidase with thrombospondin type 1 motif 13 (ADAMTS13) which overlap with the Haemolysis, elevated liver enzymes and low platelets (HELLP) syndrome (found also in the severe manifestations of pre-eclampsia) [27]. Despite this, most women with chronic kidney disease (CKD) have successful pregnancy outcomes [27].

The respiratory system is affected directly by the growing uterus during gestation that results in an uplift of the diaphragm by 4 cm above the original state [28]. This affects the respiratory rate by increasing it and will change from the coastal breathing to the diaphragm breathing in the gestational period. Another mechanical changes are that the transverse diameter expands by 2-5 cm and the subcostal angle increases by 35° which allows for the abdominal contents to move to accommodate the developing uterus [28]. The downside of these mechanical changes is that the total lung volume decreases by 5% but its accounted by the increase in respiratory rate [28, 29]. There are also biochemical changes that affect the respiratory system like an increase in progesterone which increases the minute ventilation and respiratory rate [28].

A very common symptom in pregnant women is dyspnea which is described as a breathing discomfort or “shortness of breath” [29–32] and is often present early in pregnancy, in the first and second trimesters. Clive et al. [29] have not found any correlation between the mechanical changes present in early pregnancy and dyspnea. The increase in weight during early pregnancy was mentioned to not be the reason for dyspnea as the gained weight in early pregnancy should not be as significant as in last trimester [32]. This complications are still hard to diagnose as there are no helpful investigations methods which can be used [32]. It is thought that the progesterone induced stimulation of the respiratory centre in the brain is a possible mechanism which causes dyspnea [32].

Other respiratory diseases that could also be present in pregnancy are asthma, pneumonia, acute respiratory distress syndrome (ARDS) and many more. It was found that pregnancy increases susceptibility to pneumonia [31] and two of the main ARDS causes during pregnancy are tocolytic-induced pulmonary edema and pre-eclampsia [32]. It was also found that the correlation between pre-eclampsia and pulmonary edema increases the mortality rate where 50% of maternal deaths caused by pre-eclampsia were affected by pulmonary edema [33]. It can be concluded that there is a strong relationship between the respiratory system and cardiovascular system during pregnancy and their respective complications.

The nervous system often affects the pregnancy by developing symptoms like increased migraines, stress and depression. The hormonal changes made by the maternal system to adapt during pregnancy causes these symptoms, but they often go back to the original levels postpartum. Besides this, the nervous system can also develop new-onset seizures during pregnancy. Depending on the history of the patient, epilepsy, which is the disease where one or more seizures are present, can be

diagnosed and treated. Another reason for developing epilepsy during pregnancy is pre-eclampsia or eclampsia [34]. Epilepsy can result in complications like miscarriage, hypoxia, small for gestational age, low birthweights and even maternal and foetal death in rare cases [35]. It was also noticed that anticonvulsant drugs which are used as treatment against seizures can double the risk of foetal malformations [36]. Another cause of maternal death during pregnancy or postpartum is stroke. There is not enough evidence to sustain that strokes are affected by the pregnancy, but it was correlated that eclampsia or pre-eclampsia are the most common causes of strokes during the pregnancy [36].

In the final stage of pregnancy, the delivery, it was found that the nervous system of the maternal body has an increased sensitivity to general and local anaesthetic agents [24] and in the case of local anaesthetic agents it can result in the engorgement of the epidural veins as the pressure in the respective veins reaches its peak during contractions [24].

2.2. Pre-eclampsia and hypertensive disorders

Pre-eclampsia is a hypertensive disorder that complicates 2% – 8% of pregnancies [37]. It can also be considered a multisystem disorder as it affects the maternal circulation and thus, the mother, and the placenta which affects the foetus. This can make pre-eclampsia a life-threatening disorder for both the mother and the foetus. The mortality rate associated to pre-eclampsia and eclampsia is between 10 – 15% in low and middle-income countries [37]. The majority of these deaths are caused by eclampsia and they are rare in high-income countries [37]. Regarding the morbidity, the women could suffer of renal failure, cardiac arrest, stroke, adult respiratory distress syndrome, liver failure and coagulopathy [37]. The case fatality is approximately 1% in high-income countries and triple in low-income countries [37]. Pre-eclampsia accounts for 20% of antenatal admissions and 10% of caesareans births. Regarding the neonatal deaths and stillbirths, pre-eclampsia and eclampsia are associated with one quarter of them in developing countries [37].

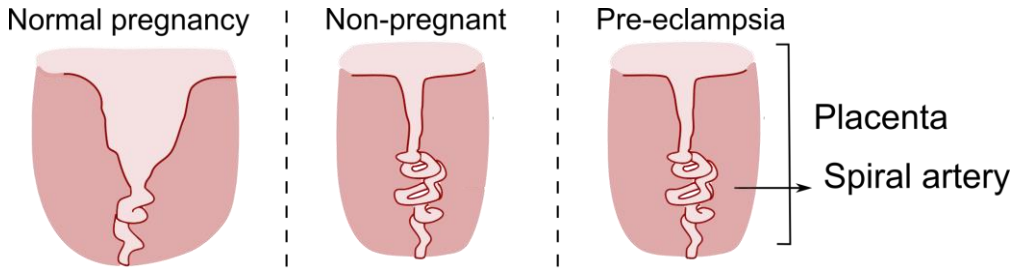

Figure 3. *Comparison of vascular remodelling of spiral artery for normal pregnancy, non-pregnant and pre-eclampsia*

As mentioned in the Introduction, pre-eclampsia is caused by failure of remodelling of the spiral arteries, as seen in Figure 3. Specifically, the villous cytotrophoblasts invade the inner third of the myometrium and the spiral arteries lose their endothelium and most of their muscle fibres which in turn, results in low-resistance vessels that are less sensitive to vasoconstrictive substances during the normal pregnancy [17]. However, in pre-eclampsia, the invasion of cytotrophoblasts is defective, and the vessels remain highly resistive which makes them more sensitive to vasoconstrictive substances, resulting in placental ischemia and oxidative stress [17]. Placental ischemia causes fetal complications such as intrauterine growth retardation (IUGR) and intrauterine death [17]. On the other side, oxidative stress is causing vascular hyperpermeability, thrombophilia, and hypertension to account for the decrease in flow in the uterine arteries [17].

The hypertensive disorders are listed in the table below. Eclampsia is the most dangerous of all the hypertensive disorders followed by Haemolysis, elevated liver enzymes and low platelets syndrome (HELLP), chronic hypertension with superimposed pre-eclampsia, pre-eclampsia, gestational hypertension and finally, chronic hypertension. The most common disorders are chronic hypertension,

Table 1. *Hypertensive disorders and its definitions*

Name	Definition
Chronic hypertension	Pre-existing hypertension; elevated blood pressure; diagnosed before 20 weeks of gestation [17]
Gestational hypertension	Hypertension that develops during pregnancy (after 20 weeks) and disappears after 12 weeks postpartum [17]
Pre-eclampsia	Mostly hypertension and elevated proteinuria concentration
Chronic hypertension with superimposed pre-eclampsia	Chronic hypertension and followed by new onset proteinuria, thrombocytopaenia or other feature of the pre-eclampsia syndrome
Eclampsia	Seizures in a pre-eclamptic woman that cannot be attributed to other cause
Haemolysis, elevated liver enzymes and low platelets syndrome (HELLP)	Severe form of pre-eclampsia; involves hepatocellular injury

gestational hypertension and pre-eclampsia. Categories of pre-eclampsia based on gestational age at diagnosis: early-onset and late-onset. Early on set is defined as developing before 34 weeks and it can also be called preterm preeclampsia and late-onset preeclampsia develops beyond 34 weeks [38]. Women with early-onset pre-eclampsia have a higher risk of stillbirths and recurrence compared to late-onset pre-eclampsia [38].

Prior pre-eclampsia, chronic hypertension, pregestational diabetes mellitus, and an elevated maternal BMI are all clinical risk factors for pre-eclampsia [39]. In terms of their relative risk, the ones that present a higher risk are antiphospholipid antibody syndrome (disorder of the immune syndrome that causes an increased risk in blood clots), renal disease, prior pre-eclampsia, systemic lupus erythematosus, nulliparity, chronic hypertension, Diabetes mellitus, high altitude, multiple gestations and a strong family history of cardiovascular disease [17]. Other risk factors include smoking and nulliparity such as nulliparous women have a higher risk compared to multiparous women [38].

Once the risk factors have been established, clinicians usually consider the prediction and prevention of pre-eclampsia. One method used for a woman that has a high risk of developing pre-eclampsia is using low dosage of aspirin before 20 weeks as a means to prevent preterm pre-eclampsia [39, 40].

The management of pre-eclampsia is critical after diagnosis as there is no set treatment currently. Thus, there are some factors that need to be considered for the management of pre-eclampsia. The main factors are the severity of the disorder and gestational age at diagnosis [17]. In the case of severe pre-eclampsia discovered before 24 weeks, the possibility of terminating the pregnancy needs to be considered due to the high risk for the mother, as well as the foetus [17]. For the cases that are not life-threatening, the first step is managing the blood pressure. The blood pressure needs to be monitored consistently and lowered using antihypertensive drugs [39]. Other maternal monitoring should include repeated testing of proteinuria, blood tests and liver and renal assessments [39]. Fetal monitoring is crucial and after the diagnosis of pre-eclampsia, the well-being of the foetus needs to be assessed [39]. It is usually recommended for regular ultrasound scans for observing any growth restrictions [39].

2.3. Vascular stiffness changes during pregnancy

It is important to understand the changes of vascular stiffness during pregnancy as these changes affect the pulsatile blood waveform which is delivered to the placenta. The arterial stiffening is caused by the loss of elastin fibres that reduces the elasticity of the artery [41] and is linked to diseases such as renal disease, stroke, and hypertension. It was also shown that age can affect the degradation of elastic fibres resulting in stiffer arteries for older people [42, 43] and that arterial stiffness can be a risk predictor for hypertensive patients [44].

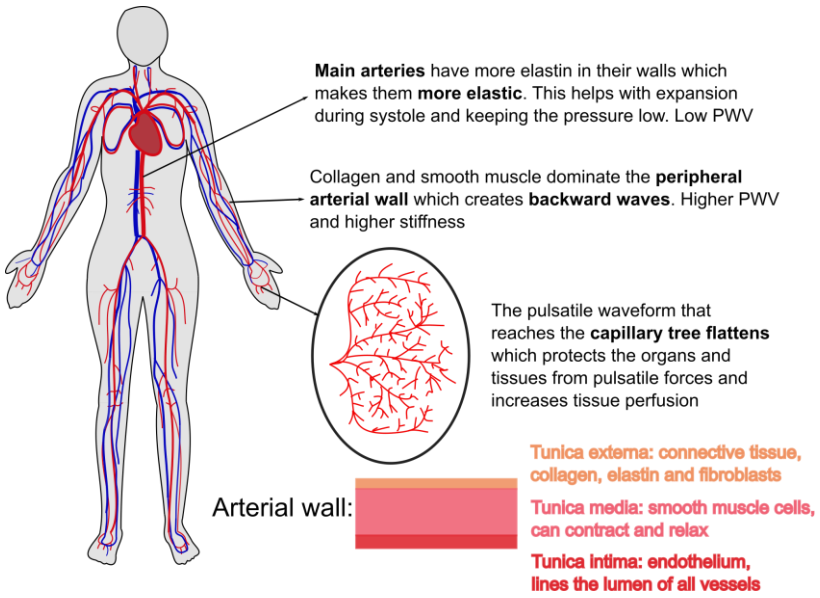

***Figure 4**. Schematic of arterial wall and central to peripheral arterial stiffness gradient*

The arterial wall determines the elasticity of the artery, and it can be viewed in Figure 4. The wall is formed of three main layers: the outer layer or adventitia, the middle layer or media and the inner layer or intima. The wall is formed of two main fibres, collagen and elastin, which provide stability and elasticity to the wall. The collagen will strengthen the wall as it is formed of an unorganised crosslinked matrix while the elastin fibres will provide elasticity to the wall as the elastic modulus of elastin is approximately 1 MPa [45] and the breaking strain (extensibility) of 150% compared to collagen which can have an elastic modulus of 300-500 MPa and breaking strain of 10-50% [45]. The elastin fibres have the role to allow the stroke volume to pass during systole while the collagen fibres should prevent overdistention and rupture [46]. The arterial wall changes throughout the vascular tree with central vessels having more elastin fibres that makes them more elastic while peripheral arteries such as muscular arteries have more collagen fibres which makes them stiffer [47]. These ratios of collagen/elastin are made to regulate the pulsatile flow as explained in Figure 1 and is called a stiffness gradient. For the case where the central arteries show an increased arterial stiffness, the pulsatility in the microcirculation increases which affects the tissue perfusion and can cause organ damage meaning an increased risk of cardiovascular disease [47]. The PWV (pulse wave velocity), compliance and Augmentation Index (AI, to not be confused with Artificial Intelligence) are often used to evaluate the arterial stiffness.

The PWV is the rate at which forward pressure waves propagate. The most common are carotid-femoral PWV (cf-PWV) which measures the PWV non-invasively as the time it takes the wave to propagate from the carotid to the femoral artery (distance / time measurement) [48] and brachial-ankle (baPWV) which measures the time it takes the wave to propagate from brachial artery to the ankle. The time point where the forward and backward waves meet, and the amplitude affect the level of central BP. The AI has been derived to measure the wave reflection and is calculated as follows [49]:

$$AI = \frac{\Delta P}{PP} \times 100 \quad (1)$$

where ΔP is the difference in peak pressure and augmentation pressure. The augmentation pressure is the pressure at the first shoulder in the cardiac cycle. PP is the pulse pressure.

Finally, the compliance is less used in studies but there are still multiple methods to measure it. One of them is calculating the compliance as the ratio of stroke index (volume of blood pumped by heart divided by body surface area) and pulse pressure [50]. Another method is measuring the diameter of the vessel using Doppler and together with pressure, finding the compliance as the change in area over change in pressure [51]. There are also devices such as CR-2000, Research Cardiovascular Profiling System, Eagan, MN [52] that can measures the distal and proximal compliance [53].

Many studies investigated the arterial stiffness of the aorta in relation to hypertension or PE. On one hand, studies focused on the effect of PE on the arterial stiffness post-partum and on the other hand, studies looked at arterial stiffness as a possible indicator for detection of PE.

It is a well-known fact that PWV and AI, which are used to evaluate arterial stiffness, have increased values for pre-eclamptic pregnancies [48, 50, 54–56]. Phan et al. [57] found that the cf-PWV was increased in weeks 14-17 and the group who had increased values later developed PE. Turi et al. [58] showed that for hypertensive pregnancies, aortic PWV (PWVao) remained high throughout the pregnancy while for healthy pregnancies, PWVao decreased from the second trimester and only started increasing post-partum. Similarly, Myers et al. [59] found that PWV together with placental growth factor (PIGF) in early pregnancy show significant differences between the women who developed placental disease and healthy women.

For the studies that looked at arterial stiffness post-partum, it is worth noting that the period when PE developed is important. Orabona et al. [60] investigated the area of the aorta and PWV in pregnancies with previous EO-PE (early onset PE, < 34 weeks) and LO-PE (late onset, > 34 weeks) and found that pregnancies affected by EO-PE showed increased PWV values and larger aortas with impaired elastic function compared to pregnancies with no history of PE. Also, history of LO-PE showed larger ascending aortas but no impairment of the elastic function. This suggests that women affected by EO-PE in a previous pregnancy will have a more complicated future pregnancy compared to LO-PE. It can also be stated that women affected by EO-PE will have arterial dysfunction post-partum, showing as, for example, hypertension 1-2 years after birth and Melchiorre et al. [61] found that 40% of women result in hypertension due to EO-PE. One explanation of why PE affects the arterial function post-partum could be due to the oxidative stress from the placenta which can persist years after birth [62]. Another study [63] shows similar results as it found increased arterial stiffness in the cases affected of a hypertensive disorder such as gestational hypertension or PE in a previous pregnancy. Another study [64] states that the effects of LO-PE are small and transient 6 months post-partum which is in line with the findings of Orabona et al. Based on this, it is important to consider any complications in a previous pregnancy as they can affect current pregnancies.

2.4. Placenta formation development

The placenta is the interface between the maternal circulation and foetal circulation, it anchors the foetus to the uterine wall, it is used for nutrients, gas, and waste exchanges between the two and it also adapts to the developing foetus and directs any changes made by the maternal system to the foetus [65]. The placenta is formed of mainly two plates, the basal plate which is towards the maternal side, and the chorionic plate which faces the foetus and is also penetrated by the umbilical cord [65]. The space between the two plates is called intervillous space and is filled with the maternal blood that is supplied by the spiral arteries that penetrate the basal plate [65].

The placement of the placenta is important, and it can affect the pregnancy outcome. The typical locations of placement are anterior, posterior, lateral, fundal and low-lying. The anterior placenta is located in the front of the stomach while the placenta which is attached to the back of the uterus is called posterior. The low-lying location is when the placenta is placed on the internal os of the cervix (i.e. the opening of the cervix with the uterus) whilst the fundal placenta is at the opposite end (top of the uterus). One of the reasons why the location of the placenta affects the pregnancy outcome is that the blood circulation in the uterus is not uniformly distributed. A study has shown that posterior placenta is related to preterm labour [66] which is in accordance with Janewarland et al. [67]. Other findings are related to pregnancy induced hypotension (PIH) and placental abruption (i.e. the separation of the placenta from the uterus) for anterior and fundal placenta [66]. This subject still needs additional research as other studies found slightly different results [68, 69] and most studies focus on investigating placental previa as a pregnancy complication rather than the overall relationship between placental location and adverse pregnancy outcomes. The overall conclusion is that the location is definitively a factor affecting the pregnancy with the fundal placenta showing the adverse outcomes during pregnancy and delivery.

As mentioned above, many studies focus on placental previa when investigating placental placement. Placental previa (PP) is defined as abnormal implantation of placental tissue overlying the internal cervical os [70] which was defined before as low-lying placenta and it affects a low number of pregnancy (0.5% of pregnancies [71]), but the pregnancies affected by it, can result in haemorrhage, prematurity, stillbirth, and neonatal death [72, 73]. However, it was found that the majority of PP cases could be resolved prior to delivery due to placental migration [70]. Placental previa is usually diagnosed in the second trimester and is usually related to risk factors like advanced maternal age, history of caesarean delivery or other complicated deliveries and abuse of substances or smoking [70, 74–76].

The placenta is also renowned for its endocrine function. During pregnancy, the placenta produces enough progesterone for maintaining the pregnancy and by the end of it, it can reach even ten times the normal amount of progesterone production [65]. It also produces oestrogen, human chorionic gonadotropin (hCG), and human chorionic somatomammotropin (hCS, or human placental lactogen, hPL) [65].

Pre-eclampsia is affecting placental formation by reducing the perfusion as the maternal vessels supplying the placenta fail to meet adequate perfusion due to their improper remodelling [77]. A similar complication that could affect the development of placenta is fetal growth restriction (FGR). FGR is defined as the failure of the foetus to grow properly [78] and is often diagnose by estimating fetal size during ultrasound measurement. The difference between FGR and preeclampsia in placental development is that FGR shows to have smaller placental diameter compared to normal, while in preeclampsia, the placenta is not supplied properly [78].

2.5. Diagnostic techniques for pre-eclampsia

The two standards of diagnosing pre-eclampsia are SBP > 140 mmHg or DBP > 90 mmHg on two occasions at least 4 hours apart and proteinuria level of > 0.3g of protein in a 24-hour urine collection [79, 80]. In the absence of proteinuria, the number of platelet needs to be < 100,000 / mL or serum creatine concentration > 1.1 mg/dL or elevated blood concentration of liver transaminases to twice of normal [79]. For patients with existing medical conditions or previous pregnancies with maternal diseases, the risk score for developing preeclampsia is high [81]. Examples of these diseases are diabetes, autoimmune disease, chronic renal disease and previous pregnancies affected by pre-eclampsia [81].

From 1985, Doppler ultrasound has become a useful tool in the diagnosis of complicated pregnancies such as pre-eclampsia as it is a non-invasive and harmless diagnostic technique used in many clinical settings [82]. Currently, the practice offers a scanning after 28 weeks to monitor the baby and additional scans for pregnancies at risk [1]. The uterine artery velocity waveform is composed of

the sum of forward and backward (i.e. reflected) waves which could occur due to branching and in the case of complicated pregnancies, the waveform is changed [83]. When the reflected waves have a high amplitude, they will be delayed and cause the appearance of the dicrotic notch [83]. The amplitude of the waveform is also changed in complicated pregnancies as it is caused by the changes in the uterine vasculature and is assumed to be related to the resistance of the vessels as high resistance will result in a high amplitude of the waveform [83]. There are three main measurements taken, the peak systolic velocity (S), the end diastolic velocity (D), and the time average maximum velocity (A) which can then be used to calculate the pulsatility index (PI) and resistance index (RI) [8].

$$PI = \frac{S - D}{A} \tag{2}$$

$$RI = \frac{S - D}{S} \tag{3}$$

The pulsatility index is said it is describing the velocity waveform better than the resistance index as it includes the area below the curve into the formula [84, 85] and is often mentioned in clinical studies. It was found that for pre-eclamptic women, PI is increased (1.36 vs 1.02) and the usage of bilateral notches did not improve the assessment of pre-eclampsia by Papageorgiou et al. [86]. In another study, it was found that the presence of notching predicted 3 out of 4 cases of severe pre-eclampsia [84] which makes the notching a promising indicator of pre-eclampsia.

The presence of notching in Doppler ultrasound was highly researched as a possible indicator of pre-eclampsia in high-risk pregnancies [87–90] [91]. In the majority of the studies, the group of high risk women showed an increase in the presence of notching compared to healthy women. The studies were performed in the second trimester and based on Schiffer et al. [92] the vascular resistance in the spiral arteries starts to drop due to the vascular remodelling of the spiral arteries which could influence the presence of notching [90]. Also, bilateral notching was researched by Zimmermann et al. [91] where the bilateral notching was present in 58% of women with proteinuric pregnancy-induced hypertension or intrauterine growth retardation and stated that a combination of several Doppler parameters such as notching and RI are better than a single parameter at predicting disease as they are correlated to each other and bilateral notching is superior to unilateral notching as it can reduce diagnosis error.

In a more recent study, it was found that the relationship between the metrics and the waveform analysis is much more complex and they should be assessed together to get a proper understanding of the cardiovascular changes of the utero-placental circulation [83]. More and more computational models of the foetal and maternal circulations emerge and aim to improve the current assessment of complicated pregnancies as the advantage of using computational models is that they provide an overview of the changes present in the cardiovascular system which cannot be measured (e.g. smaller uterine arteries such as spiral arteries that cannot be properly measured using Doppler) [21, 83, 93, 94].

Currently, the research on other biomarkers that can facilitate early diagnosis of pre-eclampsia is of interest. Other biomarkers besides hypertension and proteinuria are BMI, nulliparity, age etc. The advantage of these biomarkers is that they are non-invasive and cost affective but their effectiveness in identifying pre-eclampsia is reduced. There was also PWV investigated as a biomarker, but it was shown that there is not a statistically high enough difference between pre-eclampsia and healthy pregnancies.

This resulted in the development of a new first-trimester screening test that showed an accuracy of 82% in the detection of pre-eclampsia. The test involves the uterine artery resistance from Doppler measurement, mean arterial blood pressure, and the level of placental growth factor (PlGF). The benefit of this test is that it can be performed early in the pregnancy but this would mean performing a Doppler measurement earlier than usual, which is not typical [81]. This will also result in additional costs which could affect the implementation of it. It is worth noting that the rate of early onset preeclampsia is significantly lower than late onset preeclampsia (0.75% vs 1.5% in Iacobelli et al. [95] and 0.38% vs

2.72% in Lisonkova et al. [96]) which means the development of biomarkers for early pregnancy is not the only answer to the diagnosis and management of pre-eclampsia.

A new biomarker developed for the diagnosis of late onset pre-eclampsia is using soluble fms-like tyrosine kinase I (sFlt-I) and PlGF as a test. The negative predictive value (women with negative results is very likely to not be affected by the disease) is 99.3% and it can assess whether a woman will develop pre-eclampsia in the following week (the increased negative predictive value helps with the exclusion of the disease) [81]. Again, this test includes additional costs and time which resulted in not being opted for in some practices.

Thus, the need for a biomarker that can identify those who will develop pre-eclampsia with a high accuracy is still present and is still being researched. One limitation that hinders the progress for many of these studies is the cohort number as collecting large cohorts involves more resources being used, many studies use small cohorts. The disadvantage of using small cohorts is the increase variability of how the biomarker will perform. Hence, the introduction of computational models to run simulations of pregnancy could become a turning point in the development of new biomarkers that consider typical measurements taken.

2.6. Computational cardiovascular model

Cardiovascular models of pregnancy can be split in two categories: models of the foetal-placental circulation (excluding the maternal circulation) and models of the maternal circulation with most models focusing on the foetal-placental circulation. The models focusing on the maternal circulation need to be complex and be able to simulate the wave propagation throughout the system as the wave propagation plays a key role in the development of pregnancy and its disorders. Wave propagation and wave reflection (wave propagation: as the heart beats, the wave generated propagates or advances throughout the system from the heart to the peripheral arteries and reaches the capillary beds; wave reflection: with each boundary in the path of the wave, be it an artery bifurcation, a part of the wave will continue to travel forward while the rest of the wave is reflected and will travel back, being called a backward wave) provide essential information regarding the stiffness of the vessels (refers back to Figure 4) and are required as waveform measurements through Doppler scanning aid clinical diagnosis and monitoring.

The cardiovascular model consists of the maternal circulation during pregnancy and has been developed by Carson et al. [19, 21]. It consists of a heart model, 1D arteries and veins, smaller arteries and lumped capillary beds. To capture the main changes during pregnancy, the utero-ovarian circulation was modelled in detail.

Carson et al. [20, 21] explains how it uses a cardiovascular network with the majority of anatomical and functional data from Mynard et al. [18] and adapting this cardiovascular network to a pregnant woman by adding a vessel network of the utero-ovarian circulation to capture the pregnancy related changes. The network used for modelling the utero-ovarian circulation includes the relationship between the ovarian artery and the uterine artery how they are connected through the utero-ovarian communicating artery [20]. The majority of the vessels diameters are taken from literature. One difference between the computational model of the utero-ovarian network and the actual utero-ovarian network is that the model uses a symmetric network, so the right side is the same as the left side of the network which is not reflective of the actual utero-ovarian circulation. This assumption will cause small discrepancies between the measurements and the results of the simulations.

Firstly, the 1D modelling was done assuming that the fluid (i.e. blood) is incompressible, constant density, Newtonian. The Navier-Stokes equations were solved after they were reduced to an one-dimensional system by assuming axial symmetry (all quantities including velocity will be independent of the angle), radial displacement (no circumferential or axial displacement), constant

pressure in each cross-section, neglecting radial and circumferential velocity by considering axial velocity considerably larger than the other two [19]. To solve the governing equations, a constitutive law is needed. The constitutive law provides a relation between the cross-sectional area and the transmural pressure (i.e. difference between pressure inside and external pressure). The model chosen for this is the viscoelastic model and it includes terms as stiffness, wave speed, area at the reference pressure and pressure at which the vessel collapses. From the constitutive law, the initial area and compliance can be calculated.

The wave propagation can be modelled using Fourier analysis or wave intensity analysis (WIA). The reason why using Fourier analysis is not the most appropriate method is that it is performed in the frequency domain, which assumes that the cardiovascular system is a linear system and is in steady-state oscillation. The cardiovascular system adapts to changes in heart rate, flow, resistances (especially in the pregnancy state) and the fluid flow behaviour and vessel wall behaviour are not linear, especially in the case of veins which are highly compliant and have valve which impacts the flow behaviour to promote upstream flow to return to the heart. The benefit of using WIA is that is performed in the temporal domain and can separate the forward and backward waves from each other. The disadvantage of WIA is that it is more mathematically intensive compared to Fourier.

To find the wave intensity, the forward and backward components pressure and velocity need to be defined:

$$dP_{\pm} = \frac{1}{2}\left(dP \pm \rho c dU\right) \tag{4}$$

$$dU_{\pm} = \frac{1}{2}\left(dU \pm \frac{dP}{\rho c}\right) \tag{5}$$

where P is pressure, U is velocity, ρ is density and c is wave speed. The wave intensity can be calculated as the product of the dP and dU with respect to the time step dt [97]:

$$wi_{\pm} = \frac{dP}{dt}\frac{dU}{dt} = \frac{\pm 1}{4\rho c}\left(\frac{dP}{dt} \pm \rho c \frac{dU}{dt}\right)^2 \tag{6}$$

The 1D modelling is used to model the bigger vessels where monitoring the flow is important while the vascular beds were modelled using 0D lumped parameter model as the global aspects of the cardiovascular system are of interest here. The 0D model can be summarised as three basic elements: the resistance element, the compliance element and the inductance element. The combinations of these elements are called Windkessel models, and the inductance element is not used often as it is difficult to estimate the inertance. Usually, a three element Windkessel model is used and is formed of a resistance in series with a resistance and compliance in parallel. The first resistance is also called characteristic impedance and can help with capturing the wave propagating aspects from a vessel.

The heart model is formed of the valve model and the chambers and is also modelled as a lumped parameter model. The atria and ventricle are modelled similarly as a native elastance (modified compliant element) in series to a source resistance. The valve model uses three elements: a Bernoulli resistance, a viscous resistance and an inertial element which depend on the current orifice area and an effective length. The valve model uses two equations to model the opening and closing of the valve.

The final part of the model which is important during pregnancy is the utero-ovarian system. The model assumes symmetry between left and right sides of the system and is using the same configuration for the arterial and venous loops of the utero-ovarian system.

The cardiovascular modelling is similar to [98] with the majority of 1D arteries and veins dimensions being scaled based on the patient height as following:

$$L_{vessels} = \gamma L_{vessels,base} \tag{7}$$

where $\gamma = \frac{Patient\ Height}{Base\ Height}$ and a base height of 185.4 cm. For the scaling of diameters, the model uses the Murray's Law with an exponent of 2.76.

The model consists of 513 1D vessels and 62 vascular beds. The vessels are arteries and veins, and they cover all circulations inside the body such as the pulmonary circulation, the cerebral circulation, the coronary circulation, the hepatic-portal circulation and especially the utero-ovarian circulation. The vascular beds include organs such as brain, stomach, spleen, liver, intestines, right and left kidneys, and also body parts such as left and right shoulder, arms, legs, chest, face and others. The vascular beds significant in pregnancy are the uterus, placenta, ovaries, and cervix.

The initial conditions assume no flow at the start of the iterations and pressure of 5 mmHg in the venous systemic circulation, measured DBP of patient in the arterial systemic circulation, 10 mmHg in the venous pulmonary circulation, 11 mmHg in the arterial pulmonary and 8.5 mmHg in the hepatic portal veins. The initial pressure in the heart is different for each chamber and is calculated based on the initial blood volume in the chamber and elastance. The venous valves are open, and the vascular beds initial pressure is calculated by ignoring the compliance, resulting in a steady state problem. Next, the model is adapting to patient data. This is done by using an iterative parameter estimation loop that runs the model using the heart rate and mean arterial pressure when setting up the initial conditions, compares the model systolic pressure, diastolic pressure and cardiac output with measured data and adapts the peripheral resistances, arterial compliances and blood volume until convergence is met. After this, the model will be reduced to only the arterial system and transformed in an open-loop forward model (Figure 5). This second loop uses the solutions found in the first loop such as the flow in the aorta and uses it as the initial condition. The main aim of the second loop is the uterine system and adapting its vessels to fit the Doppler scan data. The open-loop forward model adapts the peripheral resistances and arterial compliances until the SBP and DBP converge to patient measured values. Next, it adapts the main areas of the arteries to converge to the measured PWV. In the last step, only the areas of the uterine, arcuate and radial arteries are adapted to converge to the systolic and end-diastolic velocities from the Doppler scans data.

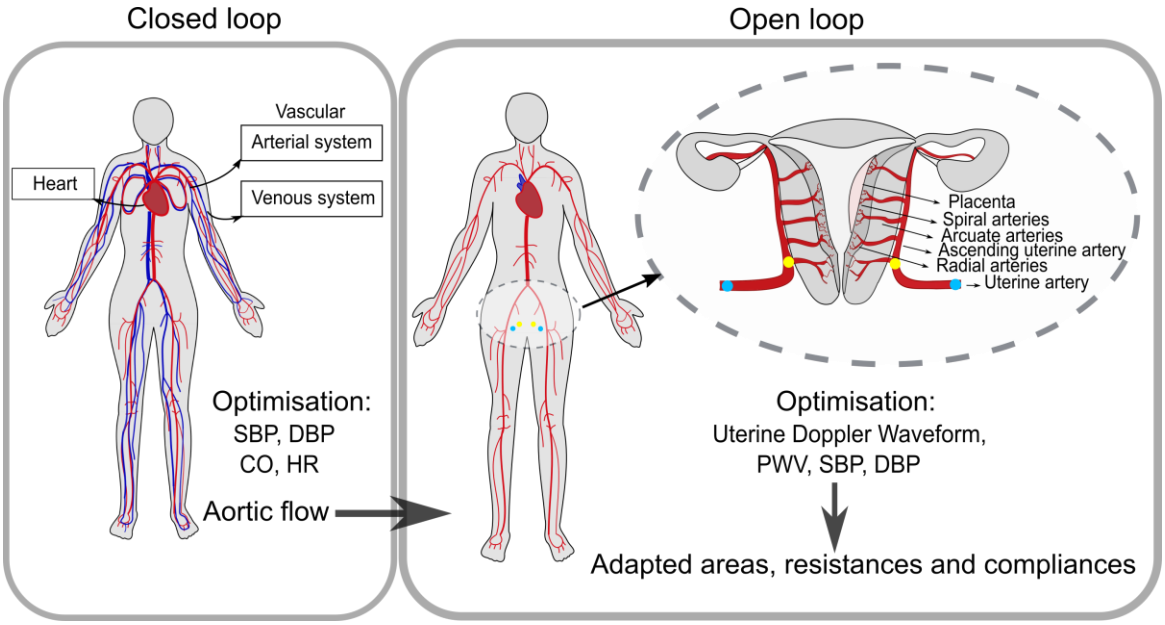

***Figure 5**. Diagram of the maternal arterial network model (left) with close-up on the utero-ovarian system (middle). The diagram also shows the measurements that are taken during check-up. In essence, the pressure upstream of the uterine artery (blue dots) are calculated using some global maternal measurements of heart and vasculature, which, together with the uterine doppler waveform (S – peak systolic velocity, D – end-diastolic velocity), allows the prediction of downstream pressures (yellow dots)*

3. Materials and Methods

3.1. Patient characteristics

The data has been collected from St. Mary's Hospital, Manchester, UK with the approval of NHS Research Ethics Committees (RECs). The data consists of routine measurements such as SBP, DBP, CO, HR, PWV, height, weight and birth weight. During the check-up, the patients underwent a Doppler ultrasound scan of the uterine artery that provides information on peak systolic velocity, minimum diastolic velocity, S/D ratio, PI, RI and presence of notching. Full data is attached in the Appendix. The dataset is comprised of 12 uncomplicated patients (UP – uncomplicated pregnancies) and 9 pre-eclamptic or complicated by other conditions patients (7 pre-eclamptic + 2 chronic hypertension with fetal growth reduction and placental dysfunction, CP – complicated pregnancies). The table below shows the Mean $\pm$ SD of the parameters measured. The mean of the SBP for the UP group is raised, suggesting that the group has patients with high blood pressure. Because of that, it will be hard to differentiate the groups as it is known that blood pressure is one of the key parameters monitored by clinicians in pre-eclamptic patients. So, finding other biomarkers that can be used by clinicians besides blood pressure is beneficial.

***Table 2.** Mean $\pm$ SD of parameters measured for UP and CP where L – left, R – right, V_{sys} – systolic velocity, V_{dia} – diastolic velocity*

Parameters measured	**Mean $\pm$ SD**	
	UP	**CP**
Gestational age (weeks)	23.0 $\pm$ 0.7	24.8 $\pm$ 2.1
Height (cm)	162 $\pm$ 5.5	163.9 $\pm$ 7.1
Weight (kg)	79.0 $\pm$ 22.6	75.8 $\pm$ 8.5
SBP (mmHg)	133.9 $\pm$ 13.0	140.9 $\pm$ 17.6
DBP (mmHg)	89.6 $\pm$ 8.2	90.7 $\pm$ 12.2

HR (beats/min)	91.6 ± 11.9	81.9 ± 11.3
CO (L/min)	4.6 ± 1.4	6.0 ± 1.1
PWV (cm/s)	7.2 ± 1.7	8.9 ± 1.5
V_{sys} (L/R)	64.7 ± 31.8 / 67.9 ± 30.1	56.9 ± 18.3 / 47.1 ± 11.7
V_{dia} (L/R)	29.6 ± 15.1 / 33.6 ± 18.0	14.4 ± 6.0 / 14.1 ± 9.8
S/D (L/R)	2.2 ± 0.5 / 2.1 ± 0.3	4.3 ± 1.6 / 4.4 ± 2.8
PI (L/R)	0.9 ± 0.3 / 0.8 ± 0.2	1.7 ± 0.6 / 1.7 ± 0.7
RI (L/R)	0.5 ± 0.1 / 0.5 ± 0.1	0.7 ± 0.1 / 0.7 ± 0.1
Gestational age – outcome (weeks)	37.6 ± 1.7	27.1 ± 2.4
Birth Weight (g)	2774.3 ± 1035.3	540.5 ± 220.5
Outcome (% live birth)	100	55.6

The information regarding the notching can be found in the Appendix. The data does not include any information regarding patient history of any other conditions. The data regarding the *SBP*, *DBP*, *HR*, *CO*, *Height*, *PWV*, V_{sys}, and V_{dia} was used to personalise the computational model as described in the section above.

3.2. Sensitivity analysis

Before proceeding with developing new biomarkers, a sensitivity analysis of the computational model is beneficial as it will provide more information on which parameters affect the pressure and flow in the main arteries (e.g. aorta) and in specific arteries such as the uterine artery. The uterine artery is of interest here as it is the main blood supply from the system to the placenta and understanding how different parameters such as resistances or compliances affect the blood flow in the uterine artery is essential for finding new parameters that can be used in developing new biomarkers. There are two type of sensitivity analysis, a local sensitivity analysis and a global sensitivity analysis (Table 3). A local sensitivity analysis uses the method of varying one parameter at a time and seeing how the output changes. A global sensitivity analysis is a more complex analysis as it can analyse the effect of varying multiple parameters at a time and calculate the effect of two or more parameters (for example, 1 parameter will not affect the model output that much on its own but when paired with another parameter, their effect together is greater than when they are on their own). The global sensitivity analysis is favourable in complex models (such the cardiovascular model where there are many equations and many parameters).

A local sensitivity analysis will be performed by varying 8 different parameters resulting in 250 Monte Carlo simulations. The parameters will be varied by taking random values from a given range. Besides that, the first and second order Sobol indices will also be calculated. Sobol method is used to calculate the global indices for non-linear models [99]. Another method to calculate global sensitivity indices would be Fourier Amplitude Sensitivity Test (FAST), however it can provide less accurate indices and more bias indices at the cost of lower computational time [100]. Compared to FAST, Sobol method has a much higher computational time, but it compensates by being able to evaluate the full range of the input parameter variation and it does not make any assumptions between the input and output (no bias). Thus, Sobol method will be able to provide objective assessments of the interactions between parameters and of the variation of the parameters. It is desired to understand if the interactions between parameters in the cardiovascular system will affect the output in a different way than expected.

Table 3. *Comparison between Local and Global Sensitivity Analysis*

Local Sensitivity Analysis	Global Sensitivity Analysis
Variation of model input on model output	Variation of the model inputs and their interactions on the model output
Better for linear models or models where input parameters have little interaction between themselves	It is more computationally expensive and time consuming Better for non-linear models such as chemical/biological models

A more in-depth explanation of Sobol' method is presented below.

Sobol et al. [99] defined $u = f(x)$ as the model that is under investigation. $f(x)$ is defined in I^n. I^n is a n-dimensional unit hypercube and x belongs to it. x is the input of function f and $x = (x_1, \dots, x_n)$ (i.e. x is a point in the n-dimensional box). u is a scalar output of function f with input x.

$$f(x) = f_0 + \sum_{s=1}^{n} \sum_{i_1 < \cdots < i_s}^{n} f_{i_1 < \cdots < i_s}(x_{i_1}, \dots, x_{i_s}) \tag{8}$$

where $1 \leq i_1 < \cdots < i_s \leq n$ (and s: $1 \leq s \leq n$) . This is called an ANOVA (Analysis of Variances) Representation. It is assumed that $f(x)$ is square integrable and results in:

$$\int f^2(x)dx - f_0^2 = \sum_{s=1}^{n} \sum_{i_1 < \cdots < i_s}^{n} \int f_{i_1,\dots,i_s}^2 \, dx_{i_1}, \dots, dx_{i_s} \tag{9}$$

$$D = \int f^2(x)dx - f_0^2 \text{ and } D_{i_1 \dots i_s} = \int f_{i_1,\dots,i_s}^2 \, dx_{i_1}, \dots, dx_{i_s} \tag{10}$$

New terms, D and $D_{i_1 \dots i_s}$, are constants and are called variances and:

$$D = \sum_{s=1}^{n} \sum_{i_1 < \cdots < i_s}^{n} D_{i_1 \dots i_s} \tag{11}$$

So, if x is a random number from I^n, then $f(x)$ and $f_{i_1 < \cdots < i_s}(x_{i_1}, \dots, x_{i_s})$ would be random variables with variances D and $D_{i_1 \dots i_s}$, respectively [99].

The ratio of the two variances results in the global sensitivity indices, $S_{i_1 \dots i_s}$:

$$S_{i_1 \dots i_s} = \frac{D_{i_1 \dots i_s}}{D} \tag{12}$$

All terms $S > 0$ and their sum is equal to 1:

$$\sum_{s=1}^{n} \sum_{i_1 < \cdots < i_s}^{n} S_{i_1 \dots i_s} = 1$$

The first order indices only considers the variance of one input to the output. There are higher order indices such as second order, third order and so on until the total order indices. The second order measures the sensitivity between two inputs while the total sensitivity measures the sensitivity of one input with all other inputs. This means that the sum of total indices can be greater than 1 and increases with increasing correlation between inputs [101]. The downside of dealing with dependent inputs is that it gets harder to interpret and the indices can take negative values [102]. The sensitivity index can be described as the following example:

Model: $f(a,b,c) = a + 2bc + ac - c$

For three inputs (or parameters), a, b and c, S_a^{tot} (total-order index of input a) will be:

$$S_a^{tot} = S_a + S_{ab} + S_{ac} + S_{abc}$$

where S_a is the first-order index of a (so S_a will calculate how much a affects the output of $f(a,b,c)$), S_{abc} is the second-order index of a in correlation to b, S_{ac} is the second-order index of a in correlation to c and S_{abc} is the third-order index of a in correlation to b and c.

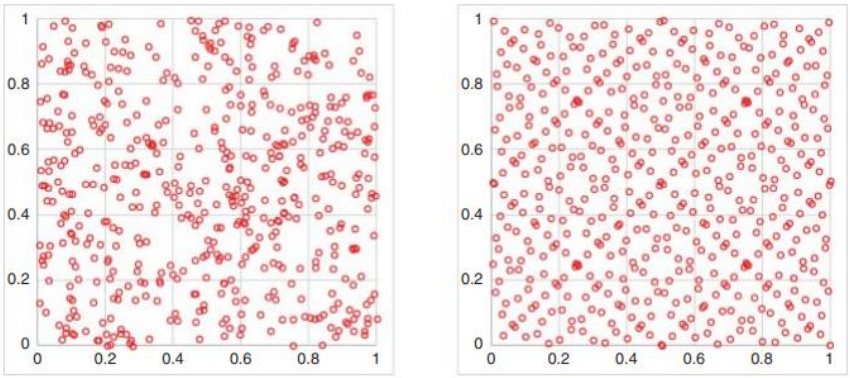

Figure 6*. left - Pseudorandom, right – Quasi-random. Figure taken from [103]*

There are many sampling techniques used in the Monte Carlo method like pseudorandom sampling, importance sampling or Latin hypercube sampling [104]. The Latin hypercube sampling is often used in computationally demanding models while the importance sampling is effective when large sample sizes are required [104]. The computational model is not very computational demanding, and the analysis does not require a large sample size so pseudorandom sampling is an appropriate choice compared to the other two. This will be used in the 250 Monte Carlo simulations.

The Sobol Analysis uses a Quasi-random sampling technique as it is converging faster than ordinary Monte Carlo and it uses a low-discrepancy sequence (a sequence that has its values better distributed compared to random distribution) for sampling compared to the ordinary Monte Carlo which uses pseudorandom sampling (it's called 'pseudorandom' as a software generated random number is not a real random number due to its predictable and highly deterministic nature, see Figure 6).

Sampling techniques used:

1. 250 Monte Carlo simulations – pseudorandom sampling.
2. Sobol Analysis – quasi-random sampling.

The sensitivity analysis was performed only on the forward arterial model and without the parameter estimation. The parameter estimation was replaced with a convergence criteria of running 15 iterations as it was observed that the solution becomes periodic after 15 iterations. The sensitivity analysis will be performed on different patients as some parameters will use patient specific measurements as baseline values. Multiple patients are selected to compare the variations between them. The software used for the analysis is MATLAB version 2021b. The toolbox for performing the analysis is Global Sensitivity Analysis Toolbox [105].

The parameters chosen for the sensitivity analysis are:

- Pressure used at the start of the model (P_o) takes part in calculating other variables such as initial area and compliance of the vessels which gives information on the state of stiffness of the vessels at the beginning
- Systemic vascular resistance (SVR) or the peripheral resistance affects the resistance distribution in the arterial system
- Total compliance at the start (C) includes the 1D and 0D compliances
- Initial compliance estimation (Ca0) or the 1D compliance; it calculates the compliance of the arterial vessels
- Initial flow in the aorta ($Q_{aorta,initial}$) affects the flow waveform and cardiac output in the system

- Initial area in the uterine vessels (A_{ut}) varies the area at the beginning of the model in the left and right side of the uterine vessels
- Initial area in the arcuate vessels (A_{arc}) varies the area at the beginning of the model in the left and right side of the arcuate vessels
- Initial area in the spiral/radial vessels (A_{spi}) varies the area at the beginning of the model in the left and right side of the spiral vessels

P_o will take the DBP of the patient measurement as the baseline value around which the parameter will vary. Similarly, $Q_{aorta,initial}$ will take the flow solution from running the closed loop model (that includes the heart and venous side) and use it as the initial flow in the aorta for the forward arterial model on which the sensitivity analysis is performed. The initial flow in the aorta will also depend on the patient. The baseline value for SVR is calculated based on the following equation:

$$SVR = \frac{(MSAP - MSVP)}{CO} \tag{13}$$

where MSAP is the mean systolic arterial pressure, MSVP is the mean systemic venous pressure, and CO is the cardiac output. MSAP is 1/3 SBP + 2/3 DBP while MSVP is 1/3 SVBP + 2/3 DVBP. SBP and DBP are based on patient measurements and SVBP and DVBP are commonly 5 mmHg and thus, they have been set to 5 mmHg. Following this, the initial compliance estimation (Ca0) can be calculated using the constitutive law (Eq. 14, [19]) and C is the addition of Ca0 (1D vessels) and vascular beds (0D) compliance. The initial areas of the vessels are the same, regardless of the patient and were estimated based on literature.

$$P_{tm} = \frac{2\rho c_0^2}{b}\left(\left(\frac{A}{A_0}\right)^{\frac{b}{2}} - 1\right) + P_0, \qquad b = \frac{2\rho c_0^2}{P_0 - P_{collapse}} \tag{14}$$

where A = area, P_{tm} = transmural pressure, A_0 = initial area , ρ = density, P_0 = initial pressure, $P_{collapse}$ = collapse pressure, c_0 = reference wave speed.

The Sobol analysis focuses only on one point in time and calculates the index based on the variation at that time point. The Sobol indices were calculated for the maximum flow and pressure during the cardiac cycle in the aorta and uterine artery. So, it results in 4 indices for each parameter.

These parameters and the same ranges were used for calculating the sensitivity indices and running the Monte Carlo simulations. The range for all parameters was $\pm$ 30 % variation around the baseline values. These ranges will differ based on the patient selected when performing the analysis and it was chosen to be varied by 30% to include the measurement values of the patients whilst keeping a physiological range. A smaller variation would not include some of the extremes of the patient measurements.

As mentioned before, the Monte Carlo method was also applied separately as the Sobol Analysis computational algorithm could not save the simulation results, and only save the sensitivity indices. So, a further analysis was performed on 250 simulations results for each varying parameter, similar to Carson et al. [21]. The Monte Carlo simulations can identify new insights on the variation of the parameters along the cardiac cycle.

3.3. Defining Potential Biomarkers

New dimensionless terms will be proposed in this section as biomarkers that will classify the two groups. There will be two sets of biomarkers, one that focuses on the general maternal circulation and the other that focuses on the localised uterine circulation. The first set will use the Buckingham Pi method to define the dimensionless terms. This method will investigate the ability of general maternal cardiovascular parameters to classify pre-eclamptic patients from non-pre-eclamptic patients as it was

shown in the previous sections that there are differences SBP or PWV between them. The Buckingham Pi method will be able to formulate terms in unique ways.

The second set will use the formulation of RI ((maximum – minimum) / maximum) on pressure and velocity for different vessels found in the uterine system. This approach will provide more dimensionless terms that will assess vessels that cannot be reach clinically.

Buckingham Pi is a method used in dimensional analysis. It is popular in the Fluid Mechanics area and one of its famous application is the Reynolds number. The benefit of performing dimensional analysis is that the number of variables is reduced, it helps in understanding the physics of the model and is useful in data analysis.
The variables chosen for this method are:

Table 4. *Summary of variables used in Buckingham Pi analysis; MLT = Mass, Length and Time*

Symbol	Name	SI Unit	MLT
R_{ut}	resistance in the uterine vessel	$\frac{Pa\ s}{m^3}$	$M\ L^{-4}\ T^{-1}$
SV	stroke volume	m^3	L^3
CO	cardiac output	$\frac{m^3}{s}$	$L^3\ T^{-1}$
R_{periph}	peripheral vascular resistance	$\frac{Pa\ s}{m^3}$	$M\ L^{-4}\ T^{-1}$
C_v	compliance (systemic compliance	$\frac{m^3}{Pa}$	$M^{-1}\ L^4\ T^2$
PWV	pulse wave velocity	$\frac{m}{s}$	$L\ T^{-1}$
P_{syst}	systolic blood pressure	Pa	$M\ L^{-1}\ T^{-2}$
ΔP_{pulse}	change in pulse pressure	Pa	$M\ L^{-1}\ T^{-2}$
A	area (of maternal circulation; ascending aorta	m^2	L^2

As previously discussed, the *PWV*, C_v, *A* and ΔP_{pulse} are parameters related to arterial stiffness which can be linked to hypertension and thus could be shown to be useful in the assessment of pre-eclampsia. R_{periph} and R_{ut} will be affected by the lack of adaptation of spiral and radial vessels to pregnancy due to pre-eclampsia which can be of use. P_{syst} was shown to be higher in patients with hypertension and thus it could be used as an addition to pulse pressure. *CO* and *SV* are similar as *CO* is just *SV* multiplied by *HR*. These variables will then be assessed to check the level of importance of each variable on the outcome of the patient, healthy/pre-eclamptic. The classification was performed using MATLAB version 2021b.

There are 9 variables and 3 primary dimensions (M, L, T) that result in 9 - 3 = 6 dimensionless groups or pi terms. The repeating variables are: A, R_{periph}, P_{syst}.
The following equations represent the dimensionless groups:

$$\pi_1 = \frac{R_{ut}}{R_{periph}} \tag{15}$$

$$\pi_2 = \frac{SV^2}{A^3} \tag{16}$$

$$\pi_3 = \frac{CO\ R_{periph}}{P_{syst}} \tag{17}$$

$$\pi_4 = \frac{C_v\ P_{syst}}{A^{\frac{3}{2}}} \tag{18}$$

$$\pi_5 = \frac{R_{periph}\, A\, PWV}{P_{syst}} \tag{19}$$

$$\pi_6 = \frac{\Delta P_{pulse}}{P_{syst}} \tag{20}$$

Besides these 6 dimensionless groups or pi terms, two more dimensionless indices were calculated inspired by the definitions of PI and RI. The benefit of using the computational model is that arteries downstream of the uterine artery can be used to calculate indices beyond areas that are clinically accessible. As such, the ascending uterine, arcuate and radial arteries were selected as the vessels in which to calculate 2 indices: pressure pulsatility index (*PPI*) and resistance index in specific arteries (, RI_{artery}). The usage of pressure as a measure for pulsatility has been proposed in Adamson et al. [106] where $P_{max} - P_{min}$ represents the pulsatile component and P_{mean} is the mean component. This formulation is similar to the PI where the difference between maximum and minimum velocity divided by the mean over a cardiac cycle is used. Another derivation of a parameter using the pressure for assessing the pulsatility is Pulmonary artery pulsatility index (PAPi) [107]. PAPi has been defined as the pulmonary artery pulse pressure divided by the right atrial pressure [107]. This predictor will provide new insight into the pressure changes in the utero-ovarian circulation.

$$PPI = \frac{P_{max} - P_{min}}{P_{mean}} \tag{21}$$

where P_{min} is the minimum pressure in the selected artery while P_{max} is the maximum pressure in the selected artery during the cardiac cycle. For the case of velocity, RI_{artery} has been defined as the resistance index and has the same formulation to RI, just that RI_{artery} is measured in the selected artery (e.g. arcuate, radial etc.).

$$RI_{artery} = \frac{V_{max} - V_{min}}{V_{max}} \tag{22}$$

These two new predictors will investigate both the right and left side of the circulation, and thus, a total of 16 terms ($RI_{ut}, RI_{asc}, RI_{arc}$ and RI_{rad} for left and right; $PPI_{ut}, PPI_{asc}, PPI_{arc}$ and PPI_{rad} for left and right).

The new predictors will provide a better image of the effects of pre-eclampsia in the maternal circulation, both locally and globally. Finally, the *PI* and *RI* will be included in the classification analysis where the results will be compared to the newly defined predictors.

***Note**: RI* or *RI-L/RI-R* = clinically measured *RI*

$RI_{artery}, RI_{ut}, RI_{asc}, RI_{arc}, RI_{rad}$ = RI calculated using the computational model

3.4. Classification Analysis

The data presented in Chapter 3.1. Patient characteristics is formed of two groups, one group that does not include pre-eclamptic patients but includes patients with raised *SBP* and another group that includes patients with pre-eclampsia (an emphasis is put on the group with the healthy patients but with increased *SBP* as it will be harder to classify the patients as pre-eclamptic or not due to the raised *SBP*). Because of this, the problem becomes a classification problem where the biomarker are used to classify the patients as pre-eclamptic or not.

The classification will include the following methods:

- Ranking features
- Using supervised Machine Learning classifiers from the MATLAB built-in Classification App
- Using unsupervised Machine Learning classifiers such as k-means (MATLAB built-in function)
- Assessing the accuracy, sensitivity, specificity and confidence intervals for all classifiers

The classification will use the leave-one-out cross-validation method as it is optimal for small datasets, then the number of folds is 19. The data is split in training data and testing data as 90% will be used for training and 10% for testing. As the dataset contains only 21 patients, a higher percentage of the dataset was allocated to training. The testing set includes 2 patients from each group and their values for each classifier was close to the mean of the group. However, only 2 patients will affect the testing and the assessment of the predictive ability of the model. To account for this, 28 models will be used during the supervised classification and the mean of these models will be shown. These models will be discussed later in this Section.

Ranking the features uses feature importance. Feature importance assigns scores to each feature and indicates the importance of the feature when predicting the model output. The feature importance will be performed using 4 methods: FSCMRMR, FSCCHI2, FSRFTEST, and RELIEFF. All methods are built-in functions in MATLAB. The values of the features were normalised. All methods rank the predictors using the response variable (uncomplicated/complicated). The higher the score, the more important the predictor is. FSCMRMR and FSCCHI2 are typically used in classification problems while FSRFTEST and RELIEFF are also used in regression problems. The main difference between the methods are the algorithms used (Table 5). Implementing the methods was straightforward so it was decided that using all methods and comparing the results would be ideal as it would also serve as validation of the result (if one parameter shows to rank first regardless of the method used it suggests that the parameter is important).

Table 5. *Comparison between the feature importance methods*

FSCMRMR	FSCCHI2	FSRFTEST	RELIEFF
Minimum Redundancy Maximum Relevance algorithm	Uses p-values of Chi-square tests	Uses p-values of F-tests	ReliefF algorithm
Classification problem	Classification problem	Regression/Classification problem	Regression/Classification problem
Categorical and continuous features	Categorical and continuous features	Categorical and continuous features	Categorical or continuous features
Ranks features sequentially	Examines whether each predictor is independent of the response	Examines the importance of each predictor individually Only captures linear relationships between features	Works best for distance-based supervised models

Supervised machine learning algorithms are widely used in data analysis, and they use training data to learn a mapping function that can then be used to test the model. The algorithms chosen are Linear Discriminant (LD), Decision Trees, Support Vector Machine (SVM), Naive Bayes, k-nearest Neighbour (KNN) and Neural Networks (a table of all 28 variants is presented in the Appendix). LD and SVM use a similar algorithm that splits the data into groups. Decision trees operates by splitting the dataset into smaller subsets and based on this the decision tree is formed.

The decision tree has decision nodes, branches and leaf nodes. KNN assigns a data point to a class based on the k-nearest neighbours. As the method uses the distance for classification, normalising the data will increase the accuracy of the classification. Neural Networks are often used for pattern recognition. They can have multiple layers and use a forward model where the input is fed through a function and passed to the next layer. The variants of these methods have different levels of complexity such as Fine, Medium, Coarse and so on. Figure 7 shows the simplified working principles of these methods.

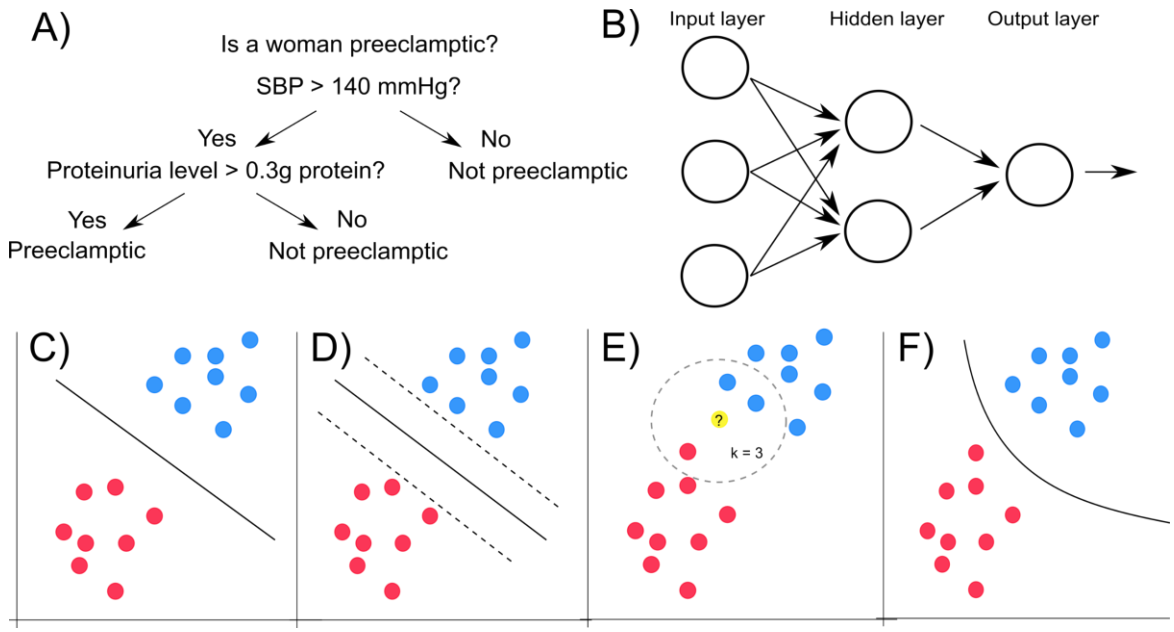

Figure 7. *Working principles of A) Decision Trees, B) Neural Networks, C) Linear Discriminant, D) Linear SVM, E) KNN, F) Naïve Bayes*

To assess the model's classification results, the next metrics were used: Accuracy *(A)*, Sensitivity *(SE)*, Specificity *(SP)*, and 95% Confidence *Interval (CI)*. As 28 methods were assessed, the mean of all methods is calculated and displayed in the final results. The choice of using 28 methods was made as selecting only a few would not give a clear image of how well a predictor performs.

$$A = \frac{Correct\ predictions}{All\ predictions} \tag{23}$$

$$Se = \frac{True\ positives}{True\ positives + False\ negatives} \tag{24}$$

$$Sp = \frac{True\ negatives}{True\ negatives + False\ positives} \tag{25}$$

where *True positive* = the predicted value is positive, and the actual value is positive while *False positive* = the predicted value is positive, but the actual value is false; *True negative* = the predicted value is negative and the actual value is negative and lastly, *False negative* = the predicted value is negative, and the actual value is positive.

$$CI = z \cdot \sqrt{\frac{A\,(1-A)}{n}} \tag{26}$$

where z is the number of standard deviations from the Gaussian distribution and for *95% CI*, z = 1.96; n is the size of the sample, and in this case, it is 19 for the supervised ML and 21 for the unsupervised ML classification.

Unsupervised ML is using k-means as the sole technique for classification. K-means clustering is one the most popular and simple techniques used in unsupervised ML. It groups the data points in k clusters and tries to identify any underlying patterns. The cluster is formed based on the distance from the centroid. The centroid is found by using iterative calculations: first, the centroids are allocated randomly and from iterative calculations, the centroids locations get optimised until a stable location is found. In this work, k was set to 2, the distance metric used is 'cityblock' (each element is the component wise median of the points in that cluster), the maximum number of iterations was set to 1000, and the

number of times to repeat clustering using new initial centroid position was set to 20. Other variations of these settings were tried but the difference between clustering was insignificant. The *A*, *CI*, *SE*, and *SP* were calculated for k-means.

4. Results and Discussion

4.1. Personalised solutions of the cardiovascular model

The personalised model was used for finding the flow and pressure solutions for all 21 patients. Four of these patients included Doppler scans that did not specify the maximum and minimum velocity like for all other patients. This resulted in manually extracting peak systolic and end diastolic velocities that are used in the open loop and the difference in the Doppler scans can be observed in Figure 8. This process could involve errors that could affect the final results. The Doppler scans were taken for the left side and right side of the uterine artery and because of that, the cardiovascular model has two sets of solutions, one which converged to the left uterine artery ultrasound and the other one which converged to the right uterine artery ultrasound.

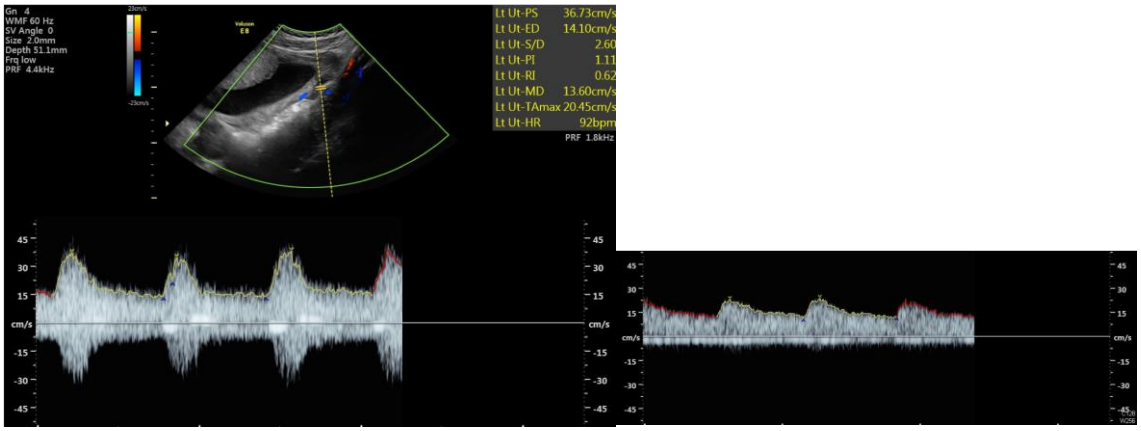

***Figure 8**. Comparison of a Doppler scan (Left) where the data of peak systolic and end diastolic velocity, PI and RI is displayed in the top right corner and another Doppler scan (Right) where the information on velocity, PI and RI is missing*

When running the computational model in MATLAB, there were two patient datasets for which the code did not converge and therefore it was manually stopped. This suggests that for some specific input parameters groups, model convergence might be compromised. These observations need to be kept in mind and can be used to improve the robustness of the approach in the future.

Figure 9. *Comparison between measured values of key parameters and simulated values using the computational model. R – simulated results. The patient number is displayed on the horizontal axis.* V_{min}, V_{max} *are from the Right uterine artery and RI was calculated using these two.*

The results of the 21 patients were compared to the key measured parameters such as *SBP*, *DBP*, *CO*, *PWV*, end-diastolic velocity or minimum velocity (V_{min}) in the uterine artery, peak systolic velocity or maximum velocity (V_{max}) in the uterine artery, and *RI*. The error was calculated as (*(Measured value – Simulated value)/Measured value*)*100* and the mean value is displayed in Table 6.

Table 6. *Mean error for key parameters*

	SBP	*DBP*	*CO*	*PWV*	*RI*	V_{min}	V_{max}
Error (%)	0.510	0.691	1.287	1.598	9.86	22.86	8.96

As observed in Figure 9 and Table 6, the simulated results diverge from the measured values for V_{min} and V_{max} which then affects the *RI* calculation. Thus, a discrepancy between the measured

and simulated results in the uterine system has formed which will impact the following analysis. However, a smaller difference resulted in the convergence of some patients to local minima.

The results include 'left-side convergence to Doppler velocity' results and 'right-side convergence to Doppler velocity' results (Figure 9 shows the velocity difference when the simulated results uses the right side velocities to convergence while Figure 10 uses the left side velocities to converge). The global parameters such as *SBP*, *DBP*, *PWV* etc. were similar while the localised uterine parameters showed differences. Due to this, the *PPI* and RI_{artery} were calculated using both the left and right side of the results (*PPI-L* uses 'left-side convergence to Doppler velocity' results while *PPI-R* uses 'right-side convergence to Doppler velocity' results).

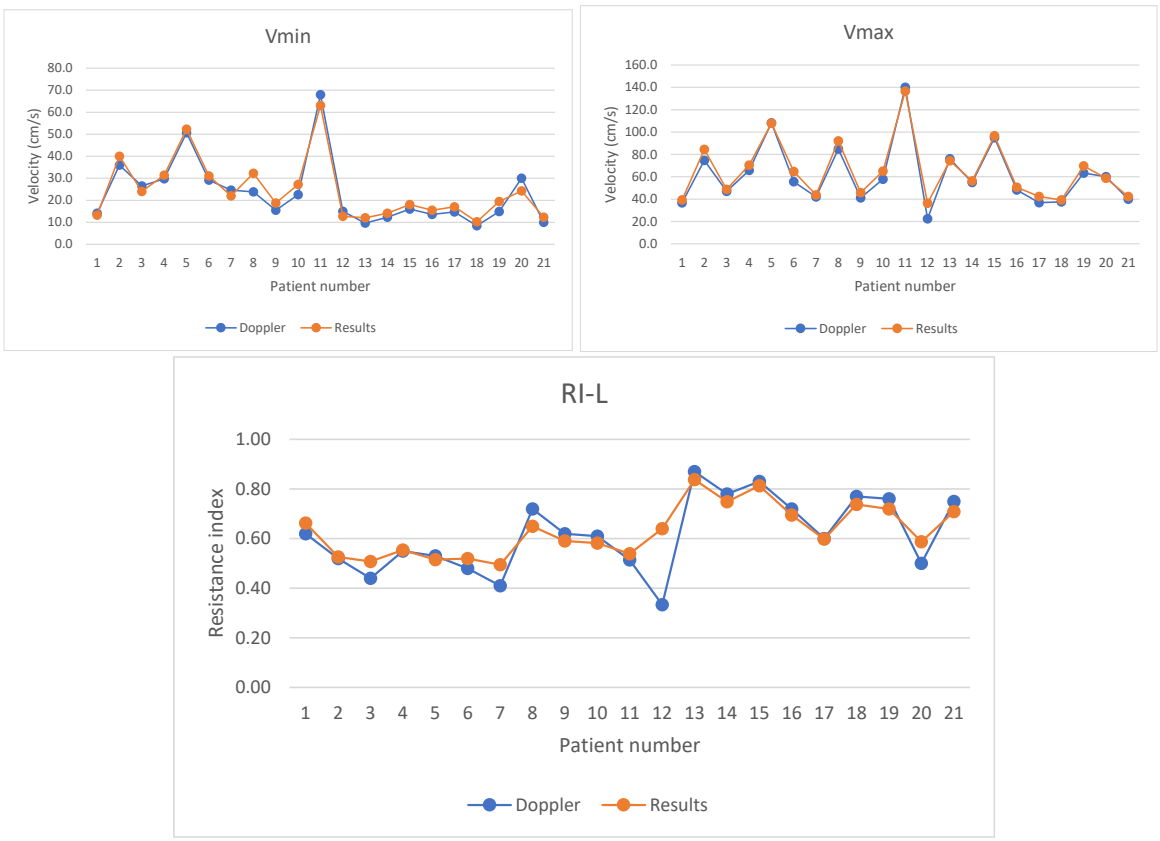

Figure 10 . *Comparison between measured values of key parameters and simulated values using the computational model.* V_{min}, V_{max} *are from Left uterine artery and RI was calculated using these two.*

4.2. Sensitivity analysis

The Monte Carlo simulations results and Sobol' indices results will be presented together in this section. In the first part of the results section, the Monte Carlo simulations results will be presented.

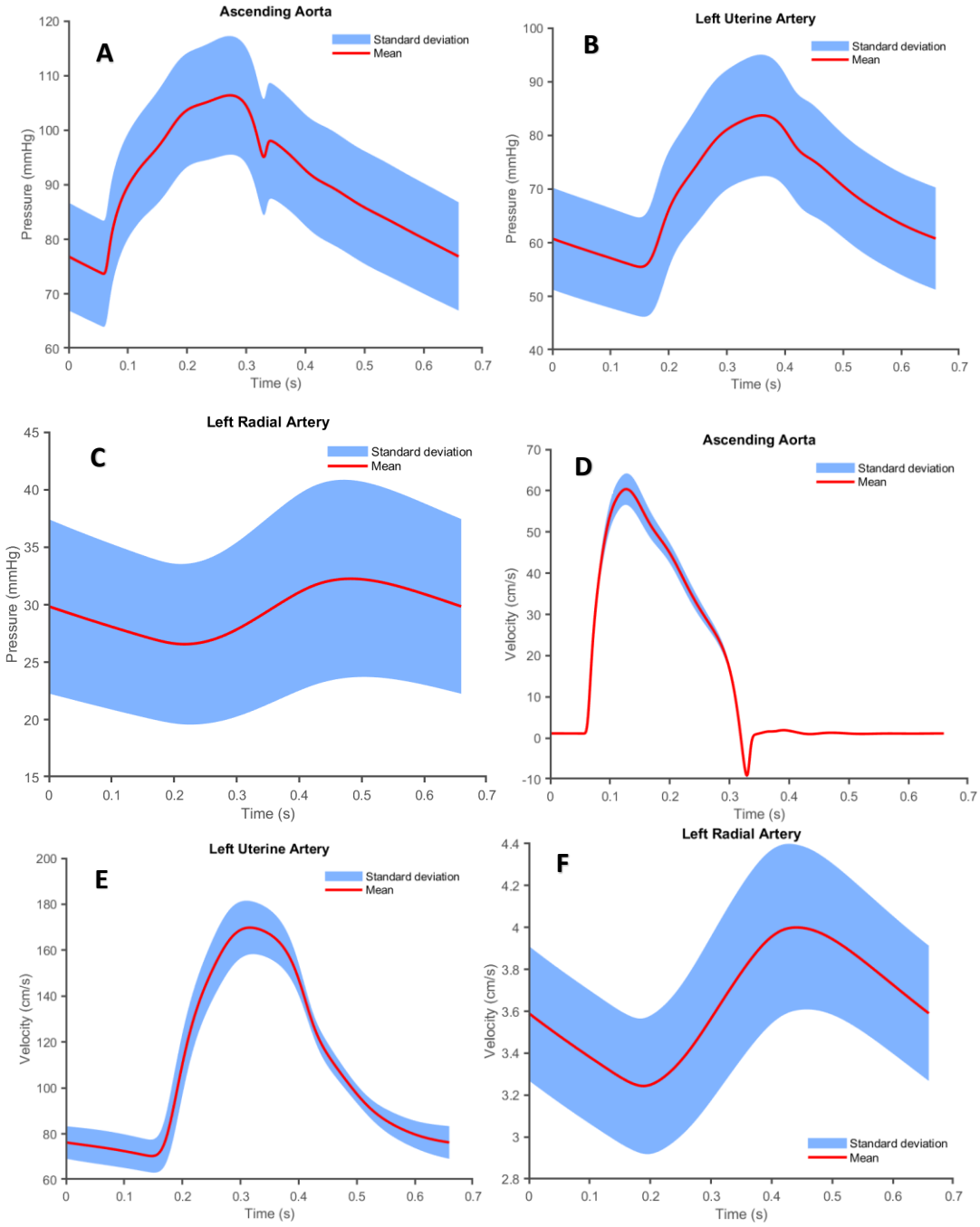

Figure 11. *Monte Carlo simulation results for parameter SVR (patient 1)**;** first three show the mean and standard deviation for pressure, last three show the mean and standard deviation for velocity*

Figure 11 shows the effect of one of the parameters, *SVR*, on the pressure and velocity in the aorta, left ascending left uterine artery, left uterine artery, left arcuate artery and left radial artery. Following this, Figure 11 shows the variance in each of these vessels of pressure and velocity. It can be seen that the variance changes during the cardiac cycle and the pressure variance in the uterine artery is highest during peak systole while the variance in the aorta during diastole is higher. For the velocity on

the other hand, the variance in the uterine artery is much greater compared to all other vessels. Comparatively, Figure 11C shows a wider range for the standard deviation in the radial artery which could be misleading as the velocity in the radial artery is considerably lower than the velocity in the uterine artery. Overall, it can be said that varying the parameter *SVR* will affect the pressure and velocity in the uterine artery the most. Looking at the third graph in Figure 12, it can be seen that the highest variance is in the aorta over the whole cardiac cycle. This is expected as the parameter is the initial flow in the aorta, but surprisingly, the second highest variance is in the uterine artery meaning that the flow in the aorta will drastically affect the pressure in the uterine artery, even if the pressure in the vessels ahead of the uterine artery will not be affected as much. Similarly to *SVR*, the velocity variance is greatest in the uterine artery for the parameter $Q_{ao,in}$ as the velocity amplitude is higher in this vessel compared to the aorta. Even so, the standard deviation range and variance in the aorta are higher when varying the $Q_{ao,in}$ compared to *SVR*.

In comparison to Figure 11, Figure 31-37 (Appendix) does not show high variance in pressure for left uterine artery when varying the A_{ut} and A_{rad} as when varying *SVR*.

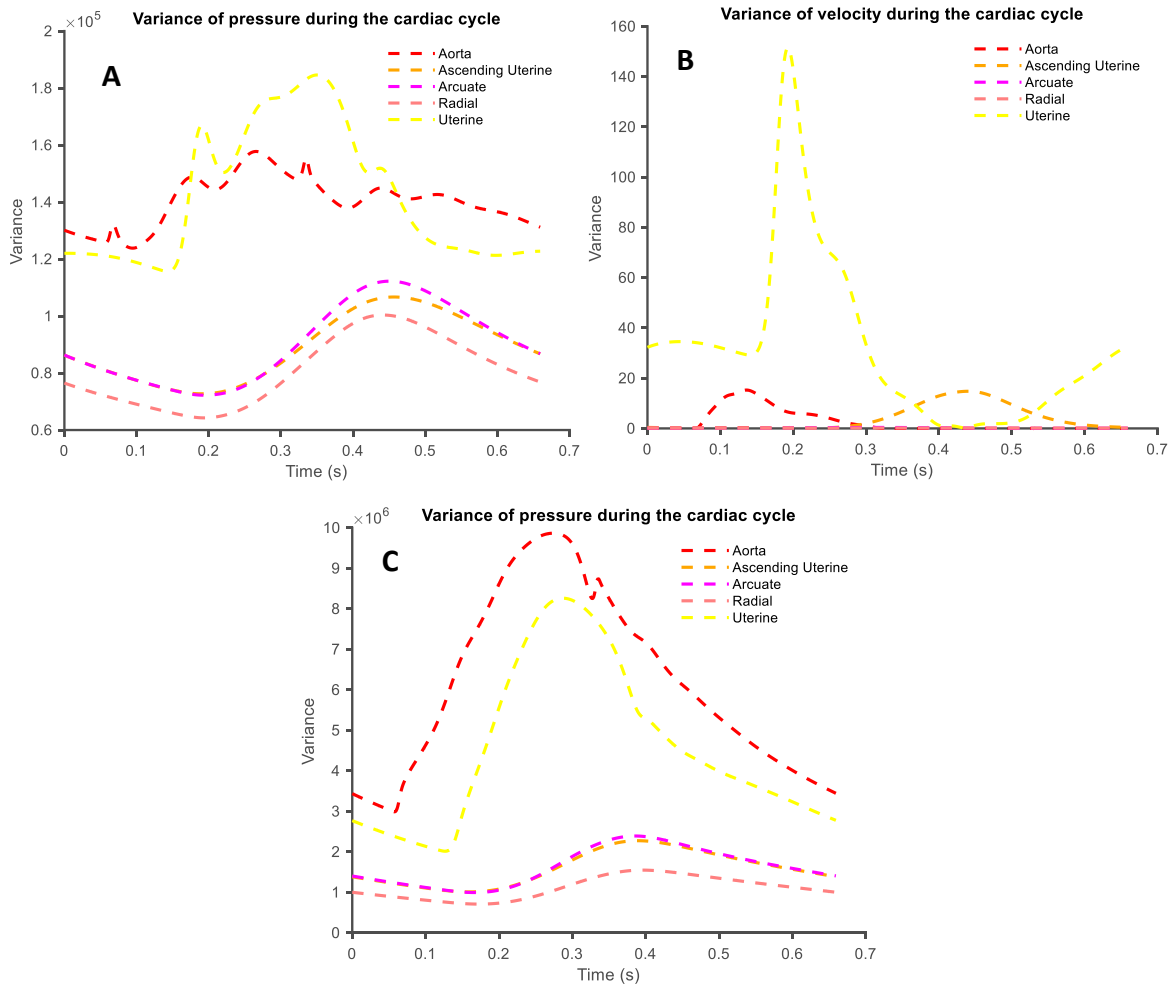

Figure 12. *Variance of parameter SVR on pressure and velocity (A and B) and parameter $Q_{ao,in}$ on pressure (C)*

The ascending uterine artery and arcuate artery show higher variability in pressure for varying the three initial areas. Moving to the variance of velocity in Figure 12B, the highest velocity is in the uterine artery as mentioned before and because of that, the highest variance of velocity between the vessels is in the uterine artery.

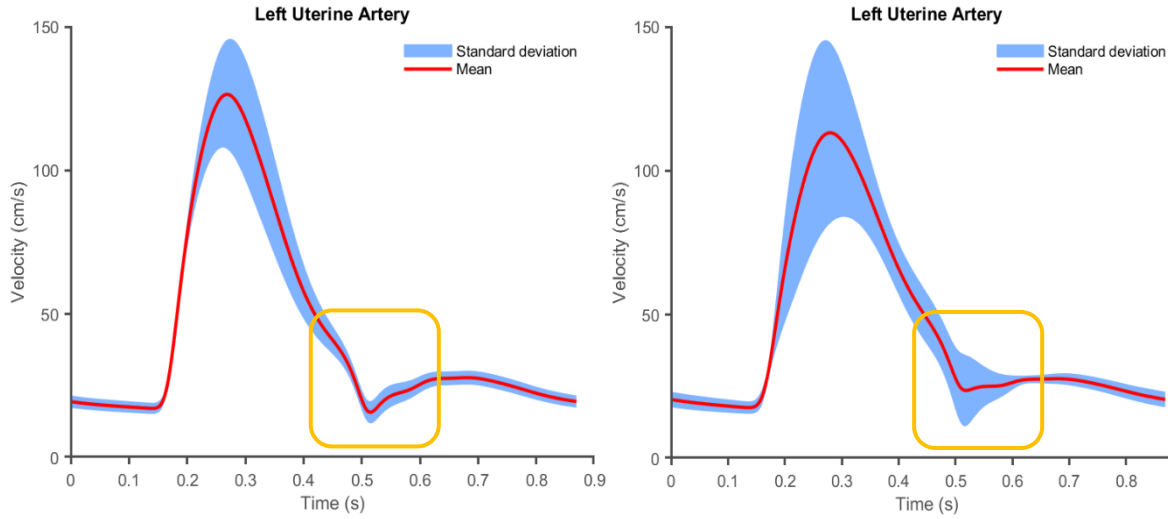

Figure 13. *Monte Carlo simulations results for patient 14 (pre-eclamptic) when varying* A_{rad} *(Left) and* $Q_{ao,in}$ *(Right); highlighted area (orange): notch (around 0.5 s)*

As the notch in Doppler ultrasound plays a role in the diagnosis of pre-eclampsia, it is of interest to assess how it is affected by different parameters and this can be seen in Figure 13. The variance in the dicrotic notch area for varying the initial area of the spiral arteries is lower than for varying the initial flow in the aorta and it results in a more accentuated notch determined by the mean line compared to the notch in the mean line of the $Q_{ao,in}$. This suggests that the initial flow in the aorta is more important compared to the initial area in the spiral arteries on the formation of notching.

Based on Cannavó' definition, the Sobol indices values can be classified as insignificant if the value is less than 0.5 [105]. But Zhan et al. [108] classified parameters with sensitivity indices over 0.1 as highly sensitive and less than 0.01 as insensitive. Thus, the best approach is to analyse the sensitivity indices values based on this model and not compare it to other models.

Table 7 shows the results for first-order coefficients with their respective errors. Coefficients with negative values or values less than 0.05 will be considered as zero which causes an insignificant effect to the model output. As the values increase, they have increasing significance and thus, the model output is more sensitive to that parameter. It will be considered that values between 0.05 and 0.3 have a low effect, 0.3 – 0.6 medium effect and 0.6 – 1 high effect (classification of how important the variables are).

Having two vessels considered as the model output can provide a better view on how the parameters affect the main vessels such as the aorta or the peripheric vessels such as the uterine artery. From Table 7, it can be seen that the initial flow in the aorta highly affects the final solution of flow in aorta compared to the flow in the uterine artery. Another parameter that has high values for the first order coefficients is *SVR*. When looking back at the Monte Carlo results, it was discussed that variations in *SVR* cause a high variability in pressure in the uterine system compared to the velocity. This is confirmed by the first-order coefficient as the value for $Q_{uterine,max}$ is 0.061 which is much smaller comparatively to 0.308 of $P_{uterine,max}$.

Table 7*. First-order sensitivity coefficient values and error of sensitivity values for the 8 parameters. The model output is formed of the maximum flow and pressure in aorta and uterine artery during the cardiac cycle. The baseline values used are based on patient 1. The highlighted values show larger values compared to others*

	Output variable							
	$Q_{aorta,max}$		$Q_{uterine,max}$		$P_{aorta,max}$		$P_{uterine,max}$	
	Value	Error	Value	Error	Value	Error	Value	Error
S1 (P_0)	0.010	0.0005	0.014	0.0005	0.009	0.0004	-0.012	-0.0005
S2 (SVR)	0.189	0.009	0.061	0.003	0.472	0.021	0.308	0.015
S3 (C)	0.012	0.0006	0.010	0.0004	0.012	0.0005	-0.009	-0.0004

S4 (Ca0)	0.0007	0.00003	0.0008	0.003	0.005	0.0002	-0.015	-0.0006
S5 $(Q_{ao,in})$	0.610	0.033	0.082	0.004	0.378	0.018	0.199	0.011
S6 (A_{ut})	-0.001	-0.00006	0.076	0.004	-0.00002	-0.00001	0.019	0.0008
S7 (A_{arc})	-0.004	-0.0002	0.02	0.0009	-0.0008	-0.00001	-0.002	-0.00007
S8 (A_{rad})	0.005	0.0002	0.014	0.0007	0.006	0.0002	0.114	0.005

Table 8*. First-order sensitivity coefficient values and error of sensitivity values for the 8 parameters. The model output is formed of the maximum flow and pressure in aorta and uterine artery during the cardiac cycle. The baseline values used are based on patient 2. The highlighted values show larger values compared to others*

	Output variable							
	$Q_{aorta,max}$		$Q_{uterine,max}$		$P_{aorta,max}$		$P_{uterine,max}$	
	Value	Error	Value	Error	Value	Error	Value	Error
S1 (P_0)	0.032	0.003	0.014	0.003	0.003	0.0001	0.004	0.0001
S2 (SVR)	0.014	0.001	0.012	0.002	0.133	0.006	0.126	0.006
S3 (C)	-0.002	-0.0002	0.0002	0.00004	0.002	0.0001	0.002	0.0001
S4 (Ca0)	-0.0008	-0.00007	0.0009	0.0002	0.003	0.0001	0.003	0.0001
S5 $(Q_{ao,in})$	0.868	0.045	0.056	0.011	0.814	0.034	0.4	0.02
S6 (A_{ut})	-0.001	-0.00001	0.62	0.047	0.004	0.0002	0.074	0.003
S7 (A_{arc})	-0.0001	-0.00001	0.017	0.003	0.002	0.0001	0.006	0.0002
S8 (A_{rad})	0.005	0.0004	0.014	0.003	0.035	0.001	0.315	0.014

Table 9*. First-order sensitivity coefficient values and error of sensitivity values for the 8 parameters. The model output is formed of the maximum flow and pressure in aorta and uterine artery during the cardiac cycle. The baseline values used are based on patient 4. The highlighted values show larger values compared to others*

	Output variable							
	$Q_{aorta,max}$		$Q_{uterine,max}$		$P_{aorta,max}$		$P_{uterine,max}$	
	Value	Error	Value	Error	Value	Error	Value	Error
S1 (P_0)	-0.002	-0.0001	0.017	0.002	-0.005	-0.0002	-0.008	-0.0003
S2 (SVR)	-0.002	-0.0001	0.014	0.002	0.1	0.004	0.098	0.004
S3 (C)	-0.002	-0.0001	0.01	0.001	-0.005	-0.0002	-0.009	-0.0004
S4 (Ca0)	-0.002	-0.0001	0.01	0.001	-0.004	-0.0002	-0.009	-0.0004
S5 $(Q_{ao,in})$	0.9	0.03	0.071	0.011	0.862	0.035	0.377	0.019
S6 (A_{ut})	-0.002	-0.0001	0.54	0.04	-0.003	-0.0001	0.07	0.003
S7 (A_{arc})	-0.002	-0.0001	0.018	0.002	-0.005	-0.0002	-0.00007	-0.0003
S8 (A_{rad})	-0.002	-0.0001	0.014	0.002	0.008	0.0003	0.307	0.013

Tables 7 and 8 show the differences between the first-order coefficients of patient 1 and 2. It can be seen that the majority of the parameters show similar values for the indices, but one noticeable difference is *SVR*. For patient 1, it was found that *SVR* has a medium effect on the pressure and a lower impact on the maximum flow in the aorta while for patient 2, *SVR* has smaller values for the indices that relate to the flow output. When comparing with the last patient tested, patient 4 (Table 9), the SVR had an even smaller effect on the aortic flow output, and it mostly affected the uterine pressure output which is similar to patient 2. As such, it can be concluded that the parameter with the most effect on the pressure and flow outputs is the initial flow in the aorta which indicates that the main maternal circulation does indeed affect the peripheral circulation of the uterine system. Another parameter that heavily affects the uterine system is the initial area of the radial arteries. In all three patients (Table 7, 8 and 9), A_{rad} had a high effect on the pressure in the uterine artery. This confirms through computational modelling that the changes in the radial/spiral arteries will affect the uterine artery.

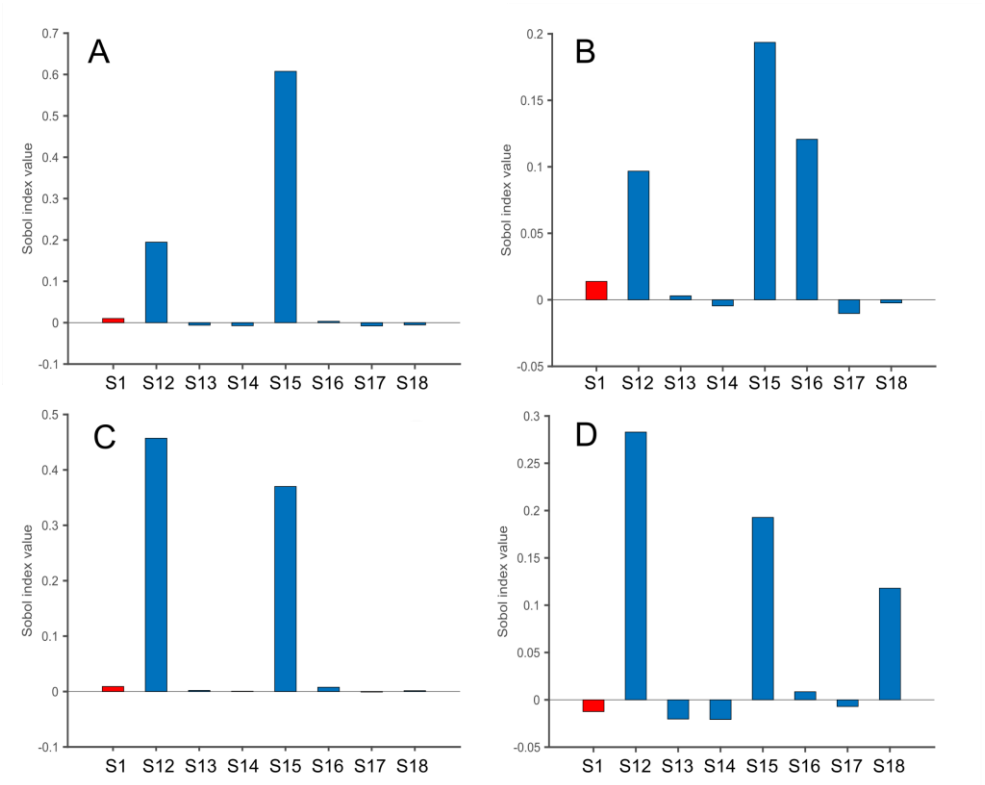

Figure 14. *First-order coefficient (red; S1) and second-order coefficients (blue) of parameter P_0 with all other parameters; A) output: flow in aorta, B) output: flow in uterine artery, C) output: pressure in aorta, D) output: pressure in uterine artery; S12 – sensitivity coefficient of 1st parameter, P_0, and 2nd parameter, SVR. S13 – sensitivity coefficient of 1st parameter, P_0, and 3rd parameter, C, S14 - sensitivity coefficient of 1st parameter, P_0, and 4th parameter, Ca0, S15 – sensitivity coefficient of 1st parameter, P_0, and 5th parameter, $Q_{ao,in}$, S16 – sensitivity coefficient of 1st parameter, P_0, and 6th parameter, A_{ut}, S17 – sensitivity coefficient of 1st parameter, P_0, and 7th parameter, A_{arc}, S18 – sensitivity coefficient of 1st parameter, P_0, and 8th parameter, A_{rad}*

Next, first-order coefficients are compared to the second-order coefficients in Figure 14 where the red bar is the effect of the first-order index, and the blue bars are the effects of the given parameter to each of the other parameters. From Figure 13, it can be seen that the second order effect of P_0 together with *SVR* or $Q_{ao,in}$ has the highest impact compared to all other parameters. This is caused by the main effect of *SVR* and $Q_{ao,in}$ which already had a higher effect than P_0.The addition of P_0 does not greatly increase the second order effect and is similar to the main effect of *SVR* or $Q_{ao,in}$. On the other hand, the second-order effect of $Q_{ao,in}$ and *SVR* (Fig. 13, S52) increases from their individual first-order coefficient values of 0.378 and 0.472 to a second order coefficient of 0.948. Similarly for Figure 15A where the second-order coefficient is over 0.9 too which can be concluded that the relationship between *SVR* and $Q_{ao,in}$ is highly important as it greatly affects the flow and pressure in the aorta.

This research leads to the relatively intuitive conclusion that the initial flow in the aorta has a significant impact on the flow and pressure in the aorta. However, its significance reduces downstream, as shown in Figure 15, where the coefficients for when the output is the uterine artery (B and C) are lower. This is not to say that the initial flow in the aorta has no effect on the flow and pressure in the uterine artery because their first order coefficients are greater than 0.05 and the value of the second order coefficient S52 (initial flow in aorta and *SVR*) increases dramatically.

The sensitivity analysis helped to identify the level of impact that various parameters have on the vascular system. The results are consistent with the literature, as *SVR* and $Q_{ao,in}$ have the greatest

effect on velocity and pressure in the uterine system, while A_{rad} has a considerable effect on uterine artery pressure, which is related to spiral artery resistance and hence crucial during pregnancy. The initial pressure and compliances had little effect on the output and can be considered unimportant in terms of their impact on the model's output. The initial flow in the aorta is affected by characteristics such as SV, Area, and aortic stiffness.

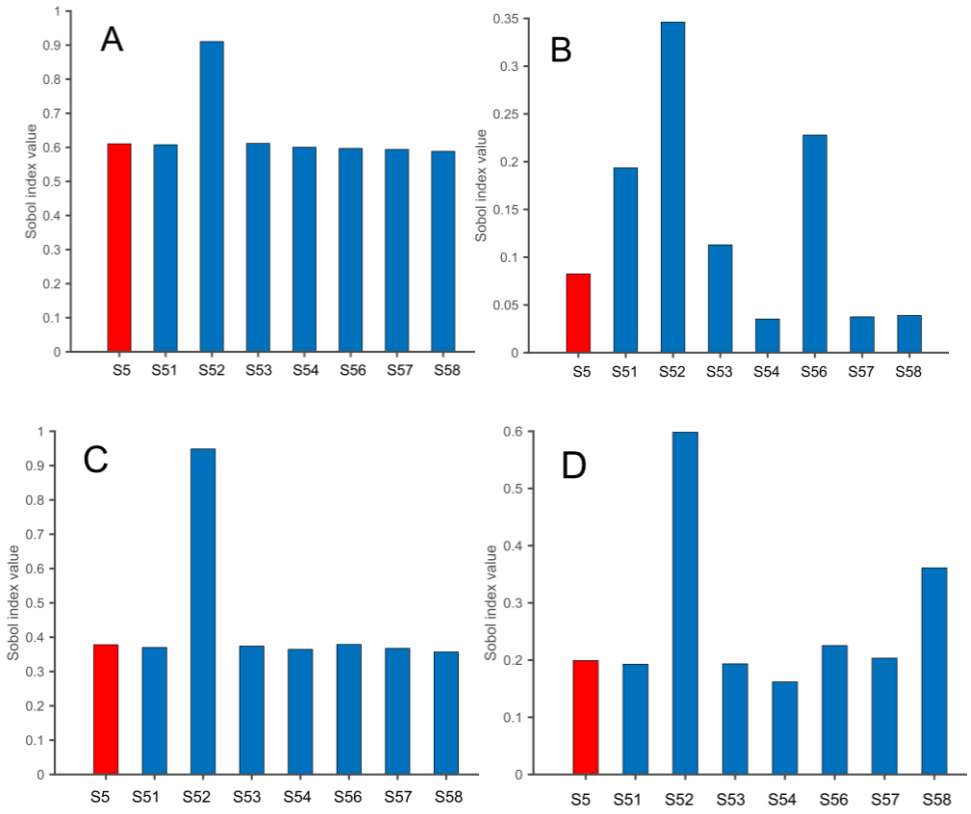

Figure 15. *First-order coefficient (red) and second-order coefficients (blue) of parameter $Q_{ao,in}$ with all other parameters; A) output: flow in aorta, B) output: flow in uterine artery, C) output: pressure in aorta, D) output: pressure in uterine artery; S5 – first order index of $Q_{ao,in}$; S51 – sensitivity coefficient of 5th parameter, $Q_{ao,in}$, and 1st parameter, P_0, S52 – sensitivity coefficient of 5th parameter, $Q_{ao,in}$, and 2nd parameter, SVR, S53 – sensitivity coefficient of 5th parameter, $Q_{ao,in}$, and 3rd parameter, C, S54 - sensitivity coefficient of 5th parameter, $Q_{ao,in}$, and 4th parameter, Ca0, S56 – sensitivity coefficient of 5th parameter, $Q_{ao,in}$, and 6th parameter, A_{ut}, S57 – sensitivity coefficient of 5th parameter, $Q_{ao,in}$, and 7th parameter, A_{arc}, S58 – sensitivity coefficient of 5th parameter, $Q_{ao,in}$, and 8th parameter, A_{rad}*

4.3. Classification Analysis

Assessment of importance of variables used in the Buckingham Pi method

Figure 16 shows the level of importance of the variables and of the dimensionless groups for the classification of the two groups (i.e. how good the variable is at classifying which patient is in CP or UP group; CP – complicated pregnancy group and UP – uncomplicated pregnancy group). For all the methods used in Figure 16 the most influential three variables were *Area*, *PWV* and *SV*. For FSCCHI2 and FSRFTEST the top three variables show the same score of importance while FSCMRMR shows the *Area* to be at the highest level and *PWV* and *SV* much lower compared to *Area*. Comparatively, RELIEFF shows that *SV* has the highest score, followed by Area and then *PWV*. From this, it can be considered that *Area*, *PWV* and *SV* will affect the outcome (UP/CP) the most which can be interpreted as in arterial stiffness of aorta due to *PWV* and *Area*.

As discussed before in the Literature Review section, it was found that arterial stiffness of aorta is increased in pre-eclamptic patients and that it could be used as a predictor when accompanied by placental growth factor to classify placental diseases [50, 54, 55, 59]. These studies are in line with our findings below. Based on this, the pi terms that include these variables should show a higher importance score.

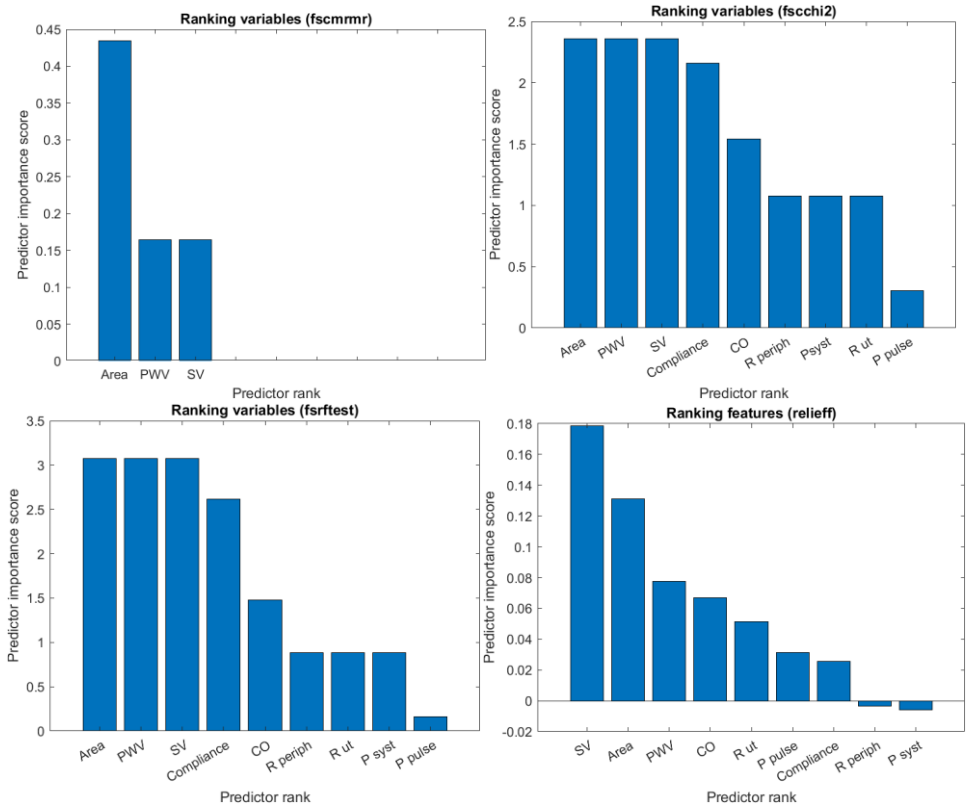

Figure 16. *Ranking the variables used for the Buckingham Pi method to understand their level of importance on the outcome (UP/CP) for all 4 methods of feature importance*

The normalised values of these parameters have been attached in the Appendix. The mean, standard deviation and p-value of the t-test have been displayed in Table 10.

Table 10. *Normalised parameters, mean ± Std where Std = standard deviation, p-value = t-test p-value using two-tailed distribution and two-sample equal variance type*

	UP	**CP**	
	Mean ± Std	**Mean ± Std**	**p-value**
Area	0.32 ± 0.11	0.58 ± 0.18	0.0009
PWV	0.58 ± 0.12	0.70 ± 0.12	0.0322
R_{ut}	0.42 ± 0.24	0.50 ± 021	0.4409
R_{periph}	0.61 ± 0.20	0.49 ± 0.13	0.1660
P_{syst}	0.72 ± 0.07	0.76 ± 0.10	0.3662
ΔP_{pulse}	0.61 ± 0.09	0.68 ± 0.18	0.2535
Compliance	0.66 ± 0.19	0.44 ± 0.13	0.0115
CO	0.63 ± 0.19	0.83 ± 0.15	0.0229
SV	0.56 ± 0.15	0.83 ± 0.13	0.0008

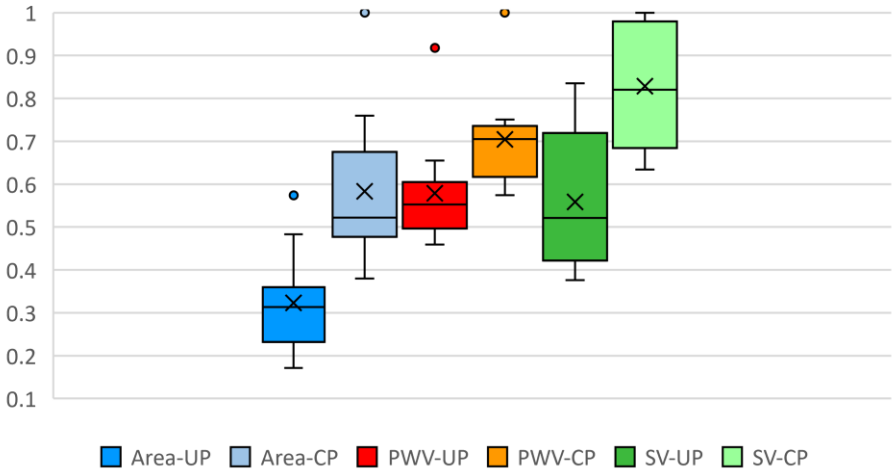

Figure 17*. Comparison of highest ranked parameters, Area, PWV, SV for UP and CP (values are normalised); the horizontal line represents the median while the x marker represents the mean*

In Figure 17, the *Area*, *PWV* and *SV* have been plotted for the two groups using boxplots. From this figure, it can be seen that *PWV* shows the lowest difference between the medians of the two groups. Comparatively, *Area* and *SV* have a bigger difference between the medians of the groups, but *SV* has a larger range which results in a bigger spread of the population. When assessing Table 10 p-values, *Area* and *SV* have the lowest p-values of 0.0009 and 0.0008 which confirms the parameters ranking score in Figure 16 Strangely, *PWV* p-value is much higher than *Area* and *SV* with *CO* and *Compliance* having smaller values than *PWV*. It is understandable that *CO* has a low p-value as *SV* and *CO* are directly related while *Compliance* further confirms the association of arterial stiffness and pre-eclampsia.

Assessment of PPI and RI_{artery} for the utero-ovarian selected vessels

Before assessing the importance score of all predictors, the *PPI* and , RI_{artery} need to be calculated. *PPI* and , RI_{artery} have been assessed for key vessels in the uterine system: uterine artery, ascending uterine artery, arcuate artery, and radial artery (radial arteries and spiral arteries have been modelled together as a lumped model), for both left and right sides of the circulation. The results can be seen in Figure 18.

The values calculated in the uterine artery are significantly worse predictors than the vessels downstream of the uterine artery, particularly the arcuate and radial arteries. These two groups have a lower interquartile range for the radial *PPI* and RI_{artery}, resulting in a better differentiation of the two groups. It was also noticed that the CP group shows higher values for RI_{artery} which is in line with the findings on *RI*. In our dataset, the mean for *RI* is higher for the CP group and it is an accepted fact that pre-eclampsia can cause an increase in the *RI* [109, 110]. Similarly, a difference between *PPI* and RI_{artery} can be seen as the values of *PPI* are smaller compared to RI_{artery}.

Figure 18 shows some outliers, the most persistent of which is patient 9. Patient 9 is a healthy patient in the UP group and in Figure 18, it is represented by the red dot, together with patient 10.

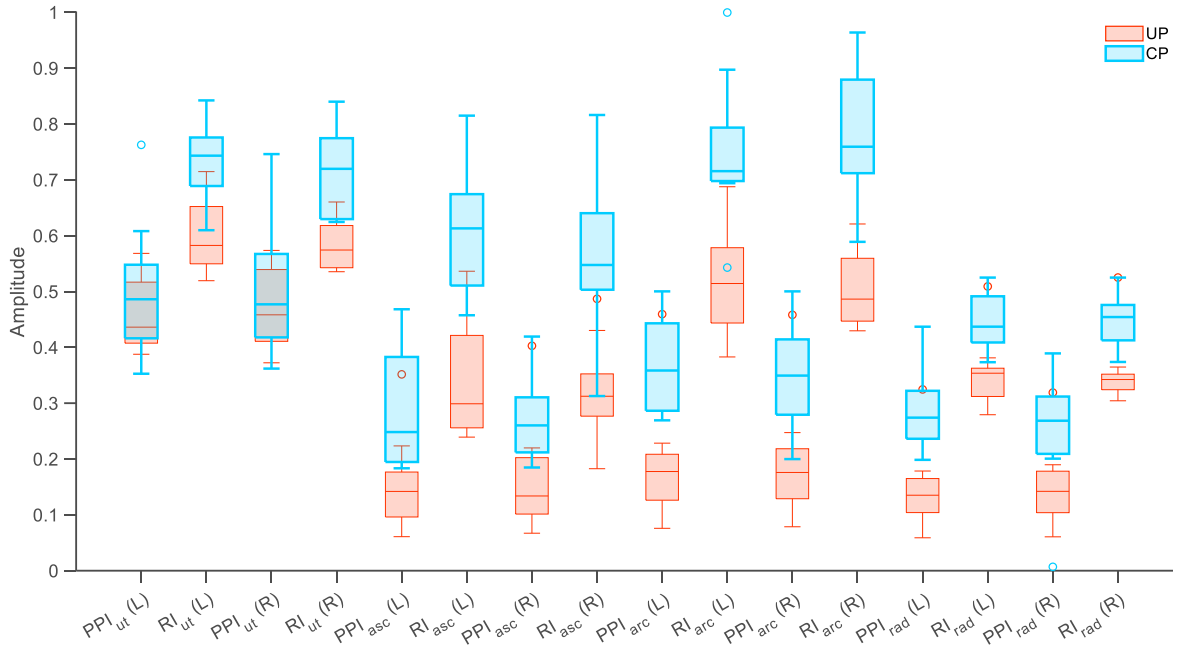

Figure 18. *All values for PPI and RI_{artery} where artery: ut – uterine artery, asc – ascending uterine artery, arc – arcuate artery, rad – radial artery and L – Left, R – Right; the UP outliers are patient 9 and 10 while the CP outliers are patients 13, 18 and 20*

It can be observed from this that, in most situations, patient 9 falls well inside the range for the CP group, increasing the likelihood of misclassifying this specific patient. One explanation for these findings is because the customised model's input parameters for optimisation, such as SBP, DBP, PWV, and CO, are not within normal limits for a disease-free pregnancy. In Appendix, the measurements for patient 9 can be seen and as an example of abnormal value is blood pressure as patient 9 had a blood pressure of 145/96 mmHg. This emphasizes the need of a biomarker that is not heavily based on blood pressure to classify pre-eclampsia. Besides the blood pressure, patient's 9 *PWV* was clearly above the mean of the UP group with a value of 12.3 m/s. The *HR* was also higher than normal and when calculating the BMI of the patient, the result showed a raised BMI of 44.1. These values might suggest an underlying disease, but the patient's history is not included in the dataset, so there is no information if this could have been caused by the raised BMI or an unknown disease.

Table 11 contains additional analysis of the predictors in Figure 19, including the mean and standard deviation for the two groups. The mean of RI_{artery} for the uterine and arcuate are in similar ranges while the mean of RI_{artery} for the ascending and radial are lower. The UP group shows lower mean values for both *PPI* and RI_{artery} for all vessels than the CP group. The greatest difference between the two groups has been noticed to be for VI_{asc} and RI_{arc}, however, RI_{arc} has a lower standard deviation than RI_{asc}, making it a better predictor.

Table 11. *Mean and standard deviation of the predictors from Figure 18 for the two groups*

	UP	**CP**
	Mean ± Std	**Mean ± Std**
$PPI_{ut}\ (L)$	0.46 ± 0.06	0.50 ± 0.12
$RI_{ut}\ (L)$	0.59 ± 0.05	0.73 ± 0.07
$PPI_{ut}\ (R)$	0.46 ± 0.06	0.51 ± 0.11
$RI_{ut}\ (R)$	0.59 ± 0.04	0.69 ± 0.08
$PPI_{asc}\ (L)$	0.15 ± 0.07	0.28 ± 0.10
$RI_{asc}\ (L)$	0.34 ± 0.09	0.61 ± 0.11
$PPI_{asc}\ (R)$	0.16 ± 0.08	0.28 ± 0.07

$RI_{asc}\ (R)$	0.32 ± 0.06	0.55 ± 0.13
$PPI_{arc}\ (L)$	0.19 ± 0.09	0.37 ± 0.08
$RI_{arc}\ (L)$	0.51 ± 0.08	0.74 ± 0.13
$PPI_{arc}\ (R)$	0.19 ± 0.09	0.36 ± 0.09
$RI_{arc}\ (R)$	0.51 ± 0.05	0.74 ± 0.09
$PPI_{rad}\ (L)$	0.14 ± 0.06	0.29 ± 0.07
$RI_{rad}\ (L)$	0.36 ± 0.05	0.44 ± 0.05
$PPI_{rad}\ (R)$	0.15 ± 0.06	0.26 ± 0.10
$RI_{rad}\ (R)$	0.36 ± 0.05	0.45 ± 0.04

When looking at literature, Schiffer et al. [92] presented a systematic review of the blood flow in the spiral artery. It was shown here that the RI in the spiral arteries which has the same formulation as RI_{rad} for uncomplicated pregnancies in the second trimester has a mean value of 0.39 which is slightly higher than 0.36 found in this study. Unfortunately, this study has not found any data on second trimester measurements comparing normal pregnancies and pre-eclamptic pregnancies. It can be observed that there is an increase in the RI_{rad} mean for the CP group, but it cannot be validated or compared using literature. Similarly, the arcuate and ascending uterine arteries are overlooked in literature so the results cannot be compared against literature. On the other hand, there is vast information regarding the uterine artery *RI* which can be used to assess the simulated RI_{ut} results. Madina et al. [109] found a mean of 0.50 ± 0.08 for normotensive women in second-trimester which is lower than 0.59 ± 0.05 found for $RI_{ut}\ (L)$. As mentioned at the beginning of this section, the tolerance set for the optimisation could have affected the simulation's results and result in this discrepancy between the actual measurements and simulated measurements. However, the measured value of *RI* for our dataset shows a mean of 0.53 which is closer to 0.50 and suggests that the simulated results have higher values for the uterine artery *RI* (PPI_{ut}) than the actual measurements. Hence, the simulated results are still in a similar range (0.59 vs. 0.53) and can be considered reliable. For the CP group, Melchiorre et al. [111] found that RI had a mean of 0.72 ± 0.11 for term pre-eclampsia and 0.79 ± 12 for pre-term pre-eclampsia. $RI_{ut}\ (L)$ has a mean of 0.73 ± 0.07 and $RI_{ut}\ (R)$ has a mean of 0.69 ± 0.08 which are closer to the mean of term pre-eclampsia found by Melchiorre et al. although the CP group fits in the category of preterm pre-eclampsia. Even so, the two standard deviation for Melchiorre et al. results is moderately high and the range overlaps with the RI_{ut} ranges.

PPI reveals a substantial difference between groups for the arcuate artery, which is followed by the radial artery. The examination of the arcuate artery, in conjunction with RI_{asc} demonstrates a statistical difference between problematic and uncomplicated pregnancies. $RI_{asc}\ (L)$ on the other hand, exhibited a similar difference between the two groups, but when tested as a prospective classifier, it performed poorly.

Feature selection and ranking

The selected features include the π terms, the clinical *PI* and *RI*, and the *PPI* and RI_{artery} for the arcuate and radial arteries. The uterine and ascending *PPI* and RI_{artery} were not included as the ranges of the two groups overlapped to a greater extent compared to the radial and arcuate arteries.

The importance scores for the selected features can be seen in Figure 19. The majority of the methods used (results presented in Figure 19) show *PPI* and RI_{artery} as the most important features for the classification. FSCMRMR shows PPI_{ut} as the most important feature which is similar to most of the other methods. π_4 was also found as one of the more important features by FSCCHI2 and FSRFTEST but the gap between *PPI*, RI_{artery} and π_4 is big. π_4 is one of the dimensionless terms that include *Area* in its formulation. Another π term also showed high score in FSCMRMR and RELIEFF result, and that term is π_1. Lastly, it can be seen that in all methods except FSCMRMR, *PPI* and RI_{artery} have significantly higher scores that the clinical parameters currently used, *RI* and *PI*.

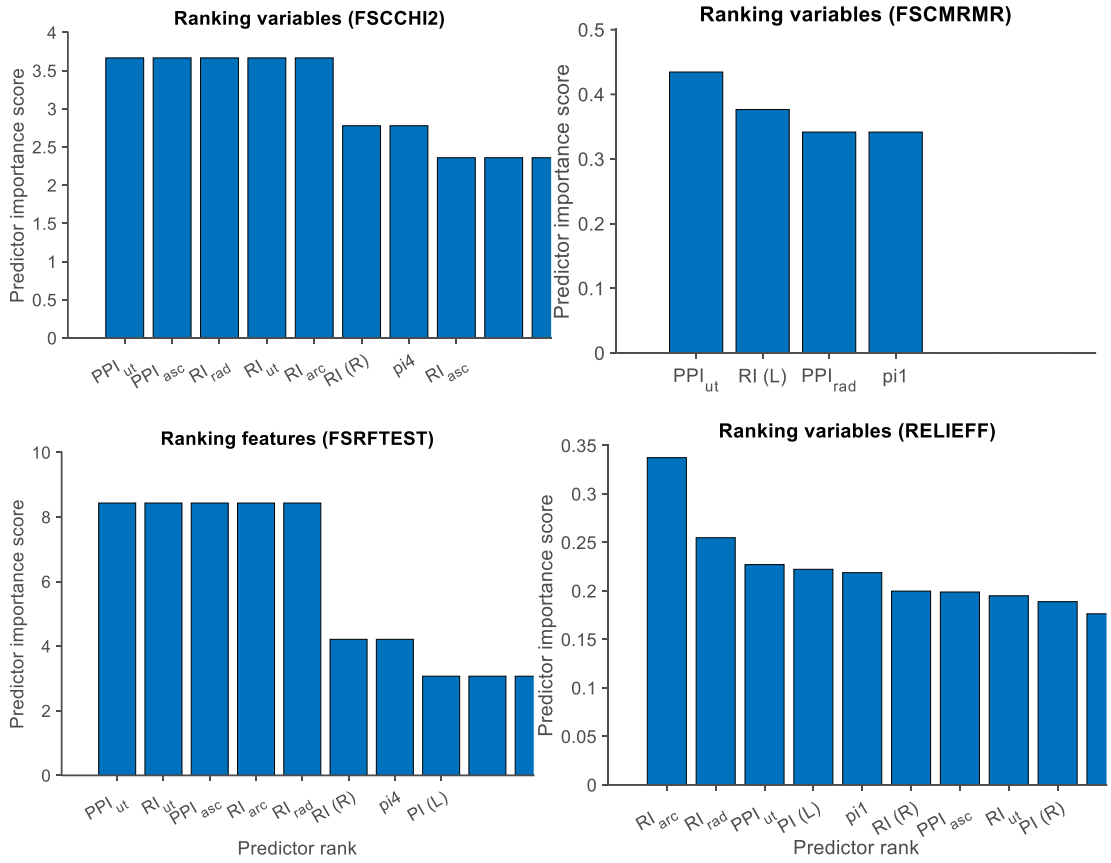

***Figure 19**. Assessing the predictors rank based on the outcome (normotensive/pre-eclamptic) of the selected features.*

Performance of the selected features for classifying pre-eclampsia

To provide a full understanding of the classification abilities of the selected features, Supervised ML and unsupervised ML was performed using 28 different models that have been detailed in the Appendix. The results of the analysis are displayed in Table 12 where the mean of all 28 ML models has been shown to minimise bias.

***Table 12.** Classification analysis of selected predictors; the results of the Supervised ML display the mean value of the 28 models trained; A – accuracy (%), CI – 95% confidence interval (%), SE – sensitivity (%), SP – specificity (%). The highlighted values in green show values that are above 85% and in yellow are values between 80% and 85%*

	Supervised ML					**Unsupervised ML**			
	Training				**Testing**				
Features	**A**	**CI**	**SE**	**SP**	**A**	**A**	**CI**	**SE**	**SP**
π_1	62.4	21.8	65.5	55.3	82.1	76.2	18.2	88.9	66.7
π_2	70.3	20.5	77.2	64.6	16.1	76.2	18.2	100	64.3
π_3	56.9	22.3	61.5	50.0	42.8	57.1	21.2	71.4	50
π_4	82.9	16.9	92.1	75.2	51.8	76.2	18.2	100	64.3
π_5	70.9	20.4	78.1	65.3	25	66.7	21.2	85.7	57.1
π_6	59.2	22.1	63.6	39.5	64.3	47.6	21.4	60	45.4
PPI_{arc} (L/R)	87.2/ 80.1	15.0/ 18.0	85.8/ 80.1	83.5/ 80.7	83.9/ 96.4	80.9/ 85.7	16.8/ 15	78.6/ 84.6	85.7/ 87.5

RI_{arc} (L/R)	78.9/ 87.8	18.3/ 14.7	80.7/ 88.3	77.5/ 85.7	96.4/ 98.2	85.7/ 95.2	15/ 9.1	90.9/ 92.3	80/ 100
PPI_{rad} (L/R)	83.1/ 78.2	16.8/ 18.6	85.0/ 77.4	82.0/ 81.5	98.2/ 98.2	85.7/ 80.9	15/ 16.8	84.6/ 78.6	87.5/ 85.7
RI_{rad} (L/R)	77.8/ 81.7	18.7/ 17.4	79.6/ 82.5	76.4/ 81.3	87.5/ 98.2	76.2/ 90.5	18.2/ 12.5	73.3/ 91.7	83.3/ 88.9
PI (L/R)	74.6/ 76.7	19.6/ 18.9	75.7/ 76.1	68.9/ 82.3	89.3/ 62.5	85.7/ 85.7	15/ 15	84.6/ 80	87.5/ 100
RI (L/R)	78.0/ 80.4	18.6/ 17.8	77.7/ 81.0	78.9/ 81.2	91.1/ 91.1	80.9/ 80.9	16.8/ 16.8	83.3/ 90	77.8/ 72.7

When looking at the results in Table 12, it can be seen that only one pi term showed good results and that is π_4. Next, the local biomarker PPI_{arc}, RI_{arc}, PPI_{rad}, and RI_{rad} showed even better results than the more global biomarker π_4. When comparing the *PPI* and RI_{arc}/RI_{rad} terms to the clinical *PI* and *RI*, it's also shown that the accuracy of the classification modelling is higher for *PPI* terms and RI_{arc}/RI_{rad}. When looking at the sensitivity of the models, the *PPI* and RI_{arc}/RI_{rad} terms show a higher sensitivity in general compared to clinical *PI* and *RI*. This suggests that in general, the *PPI* and RI_{arc}/RI_{rad} terms will be better at showing a positive result among the women which actually have pre-eclampsia. This result is important when considering the nature of the dataset (CP – complicated pregnancies; UP – uncomplicated pregnancies or pregnancies that are not complicated by pre-eclampsia, but the majority still suffer of hypertension). Similar to sensitivity, the specificity of the *PPI* and RI_{arc}/RI_{rad} terms is higher on average compared to clinical *PI* and *RI*. The values of specificity and sensitivity are similar to each other for the *PPI* and RI_{arc}/RI_{rad} terms which means that these biomarkers are performing highly when identifying both actually complicated pregnancies as complicated and uncomplicated pregnancies as uncomplicated.

It is also worth discussing the difference between the left side and right side for the *PPI*, *PI* and *RI* terms. There is not enough convincing evidence to say which side performs better when classifying the 2 groups. For the clinical terms, the *RI* (R) showed slightly better results compared to *RI* (L), but for *PI*, the results were very similar. As *PPI* and RI_{arc}/RI_{rad} terms are converged from the Doppler measurements (the uterine velocity which is the main parameter used to calculate *PI* and *RI*), it is less likely they would show a significant difference. It was noticed that for RI_{arc}/RI_{rad} terms, the results from the right side performed better compared to left side (which is similar to clinical *RI*). However, PPI showed that the results of the left side performed better than the left side. As the research related to the differences between left and right side is limited, it would be hard to come to a conclusion related to the relevance of the side from which the biomarkers are calculated.

Coming back to π_4, the biomarker showed an accuracy of 82.9% during training and only 51.8% during testing. This was caused by the low specificity of the classifier which resulted in many cases of false positive predictions (uncomplicated pregnancy being classified as complicated) which can also be seen in Figure 19 where the spread of the UP group for π_4 is considerably higher than CP and the minimum limit of UP almost overlaps with the minimum of CP. It means that π_4 has a predictive ability close to *PI* and *RI*. The formulation of π_4 which includes *aortic Area*, *SBP* and *systemic compliance* could indicate that there is a difference in aortic area for pre-eclamptic women as found by Spaanderman et al. [112]. Spaanderman et al. [122] found that hypertensive women with a history of pre-eclampsia had a lower compliance and increased area of large arteries. On the other hand, the terms containing *PWV* or *SV* did not show a higher accuracy of classification compared to π_4. This means that *PWV* is not an adequate biomarker for classifying complicated pregnancies with pre-eclampsia from uncomplicated hypertensive pregnancies this early in pregnancy (< 28 weeks). In a study performed on healthy, pre-eclamptic and hypertensive pregnancies for gestational age of > 33

weeks, it was found a high increase in *PWV* from healthy to hypertensive and when compared to pre-eclamptic there was a 1 m/s higher *PWV* in pre-eclamptic patients [50].

With the purpose of investigating the blood circulation in uterus and placenta, studies focused on the analysis of the uterine arteries and its association with the risk of pre-eclampsia, IUGR, gestational hypertension and other placental diseases. There is a general consensus that the *RI* and *PI* are related to the vascular resistance in the uterine circulation and pre-eclamptic patients will show an increase in *RI* and no decrease in *PI* which usually occurs in normal pregnancy due to the vascular remodelling from high resistance vessels to lower resistance vessels [83, 88, 113–116]. Moreover, studies also looked at notching and it was revealed that bilateral notching had higher maternal and foetal morbidity compared to unilateral [83, 90, 113, 117].

The investigation of smaller arteries such as the radial and spiral arteries is still limited as the current technology is not at an adequate level for clinical use. Makikallio et al. [118] analysed the spiral arteries using Doppler parameters and found that uterine and spiral artery *RI* and umbilical *PI* cannot identify changes in maternal remodelling early in pregnancy. Similarly, Hung et al. [119] found a detection sensitivity of PIH and IUGR of around 50% in low-risk population for a gestational age of 20 – 25 weeks and concluded that the measurement of utero-placental blood velocity waveforms is not sensitive enough. A more detailed study focused on the spiral artery flow measurements using Colour Doppler was performed by Deurloo et al. [120] and found that there was no significant difference between pregnancies complicated by pre-eclampsia and IUGR compared to uncomplicated pregnancies for gestational age of 18 – 24 weeks.

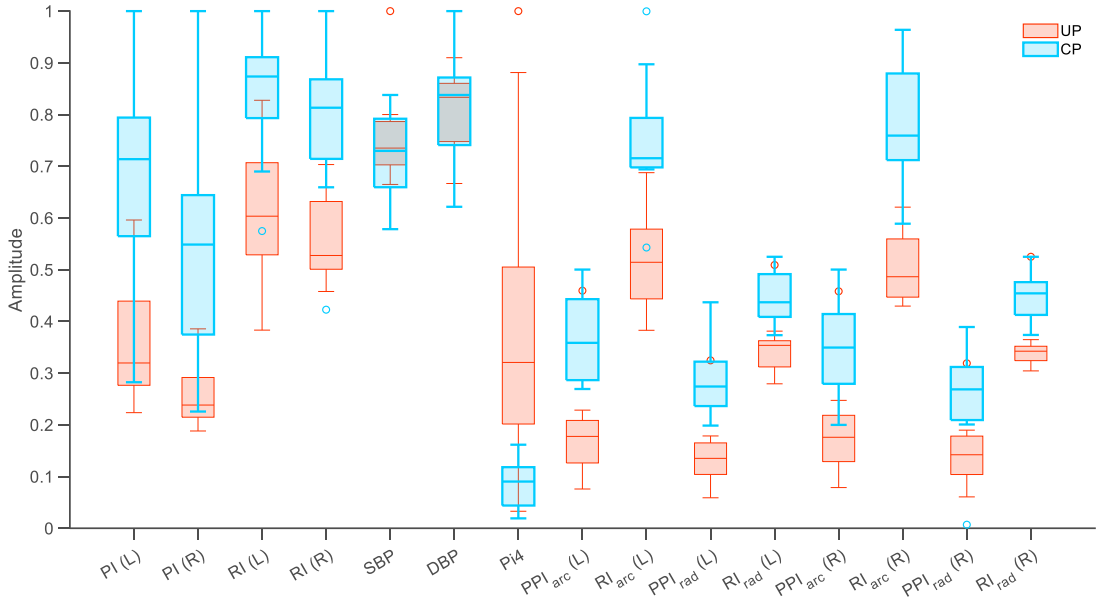

***Figure 20**. Best classifiers comparison to standard clinical biomarkers such as PI, RI, and DBP/SBP.*

3-dimensional power Doppler (3DPD) is a different method used in [121] which calculates new indices called vascularisation index, flow index and vascularisation flow index. Hafner et al. [122] found a good detection sensitivity of pre-eclampsia using this method, however, it is questionable when it comes to validity and reproducibility [121].

As such, using the computational model to generate the flow and pressure in the spiral/radial arteries is a more advantageous method. The use of 1D modelling integrated with the Wave Intensity analysis (WIA) to capture the wave propagation is an important factor related to pre-eclampsia and the physiological changes that it generates.

In Figure 19, the normalised values of *SBP* for the two groups can be seen. *SBP* is the most reliable biomarker that is used in the diagnosis of pre-eclampsia by clinicians. However, in cases where the pregnant women develop hypertension, it becomes harder to differentiate between pregnancy induced hypertension and pre-eclampsia. This problem can be seen in Figure 20, as the uncomplicated group contains hypertensive women that did not develop pre-eclampsia while the complicated group developed pre-eclampsia. For *SBP*, the two groups' ranges overlap, making a diagnosis based simply on the pressure measurement difficult. When comparing *SBP*'s boxplots to those of the other classifiers, it is clear that *PI* and *RI* can distinguish between the two groups better than *SBP* (the values in Figure 19 for *PI* and *RI* are normalised; the figure showing the boxplots using the original values can be seen in Appendix).

This study comprised pregnancies that had already developed or were developing pre-eclampsia at the time of the CP assessments. The *SBP* of the two groups overlaps significantly, making pre-eclampsia diagnosis more difficult. Nonetheless, the proposed classifiers yielded encouraging results, and in the event of uncomplicated pregnancies in healthy normotensive women, it will yield much better outcomes. However, the capacity to predict which pregnancies may develop pre-eclampsia in the future is unknown and will need to be examined more in future research.

Lastly, it should be discussed the issue of finding positive markers by chance when calculating this range of biomarkers (*PPI* and RI_{arc}/RI_{rad} terms) in the context of the given dataset. After analysing the results it was found that PPI_{arc} (L) and RI_{arc} (R) had the highest accuracy when classifying the 2 groups. These findings only apply for the current dataset and should not be considered as general biomarkers that will classify pre-eclamptic women best. The method of calculating these biomarkers should be used the calculate both the radial and arcuate *PPI* and *RI* and then assess the results together with other parameters such as blood pressure, proteinuria, possible notching etc. However, this will raise the following question: how are the new biomarkers better than the clinical *PI* and *RI* when a range of new biomarkers needs to be calculated and they still need to be used together with the standard predictors such as blood pressure and proteinuria? One option to solving the problem is to prove that among the range of new biomarkers (*PPI* and RI_{arc}/RI_{rad} terms) there is always one that always performs better than all others, however, this cannot be investigated in this work as it requires an extended dataset to validate it. By doing this, the issue of finding random positive markers will also disappear and a better confidence and understanding of the new biomarkers will be given.

In summary, the conclusion of this work can be that a new set of biomarkers was found, and it was proven they can perform better than the current biomarkers. Also, the method of using computational modelling is a reliable approach in understanding the cardiovascular changes in the smaller arteries of the uterine system which is currently not easily accessible through clinical means.

5. Conclusion

The main objective of this work of finding a new biomarker that can classify pre-eclampsia has been fulfilled. As shown in 4. Results and Discussion, PPI_{arc} (L) and RI_{arc} (R) showed better results at classifying complicated pregnancies compared to *PI*, *RI* or *SBP*. This suggests that the use of computational modelling of the cardiovascular system can provide additional information that is essential in diagnosis of pre-eclampsia. The accuracy of the proposed biomarkers was higher than the PI and RI for the supervised and unsupervised classification. It is also worth mentioning that the uncomplicated pregnancies group had a high mean blood pressure suggesting that some patients were suffering from hypertension at the time of measurements. This points at how the proposed biomarkers can differentiate between hypertension and pre-eclampsia well. When compared to *DBP* and *SBP*, it was shown that it would be considerably harder to provide a diagnosis of pre-eclampsia solely on blood pressure.

The results of the maternal parameters assessed are also worth mentioning as they confirm some of the literature findings. *Area of aorta*, *PWV* and *SV* were found to be important parameters in the classification of the two groups and the difference in values (Figure 17) seen between the two groups is worth mentioning. The group with complicated pregnancies meaning the pre-eclamptic women showed increased values in the area of the aorta, *PWV* and *SV*.

6. Future direction

The next step is to further investigate the effect of the proposed biomarkers on a bigger dataset. To do this, the computational model needs to be adjusted. Currently, the model has disadvantages that would not allow it to be used in a clinical setting such as increased computational time to run a case and high complexity. An option would be to use a neural network which is faster and easier to use. This is currently pursued as part of a PhD project. However, implementation of a model of this complexity into a neural network will come with its difficulties.

Looking at the bigger picture, the model was able to find new biomarkers that would be much more difficult to measure clinically, and it would be a good opportunity to use the model to its full potential. This could mean proposing more biomarkers and analysing the simulations of the pregnant women in more depth. This will provide a better understanding of the cardiovascular changes and the effects of the pregnancy on the maternal parameter. One good example would be how Area of aorta, PWV and SV showed to be important parameters in classification of the two groups (Figure 15), however, the proposed biomarkers that included these parameters did not show good results during the classification analysis. As such, more work related to the maternal parameters would be a good direction as promising results were shown here but also in literature (discussed in 2. Literature review).

7. Case Study: Effect of maternal positioning on maternal and foetal state

7.1. Introduction

During pregnancy, it is often recommended for conditions such as oedema that the pregnant women should rest in bed [123]. In the case of bed rest or even sleep, the position of the pregnant woman can affect the maternal physiological state. It was reported by Heazell et al. [124] that supine going-to-sleep position is associated with late stillbirth. Regarding the maternal haemodynamic state, it was seen that in the supine position, the blood pressure was not significantly different for different time periods while in the lateral position, the blood pressure decreased even by 15 mmHg [125, 126]. Regarding the cardiac output, it was noticed that it decreased up to 17% in the tilted position of 12.5 degrees on right lateral and 13% in the supine position [127]. Heart rate increased around 10 bpm and Bamber et al. [127] found that SBP increased by 2 mmHg in supine position.

The decrease in cardiac output is caused by compression of inferior vena cava (IVC) which impedes venous return, causing a decrease in cardiac output [128]. This compression is part of aortocaval compression (ACC) that is caused by the uterus and it also compresses the abdominal aorta [128]. ACC is usually asymptomatic as the arterial pressure remains fairly the same due to the increased in systemic vascular resistance (SVR) which is caused by a sympathetic response. Because of this, it is important to investigate the effect of the compression of the IVC in relation to the utero-placental flow. This will provide us with a better understanding of the effects of maternal positioning on the foetus. One study reported no changes in PI and RI for lateral and supine positions [126].

7.2. Methods

The effect of reducing the area of the veins that could be affected by the compression caused by the pillow when the women are positioned in prone position. The case study focuses on the maternal positioning and in this case, on the prone positioning of the women and usage of a pillow. It was seen in N. Introduction that the positioning of the women will cause vessel constriction for the venous system and also the arterial system (i.e. vena cava and abdominal aorta). Figure 21 shows the main veins found in the area of the uterus and belly.

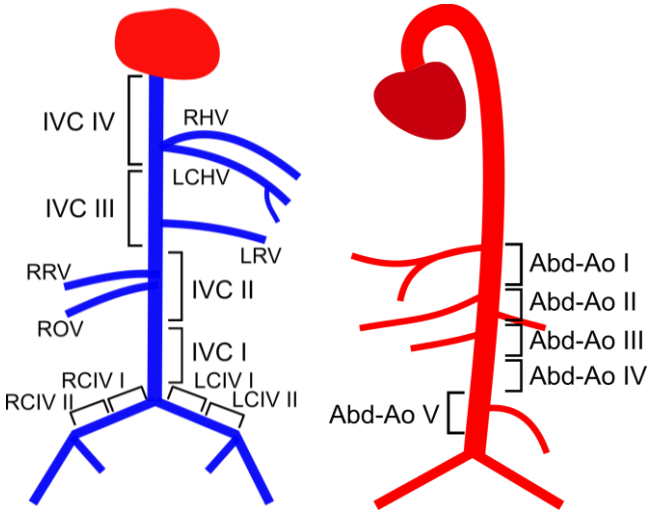

Figure 21. *Venous circulation in the abdominal region (Left) and arterial circulation in the abdominal region (Right); IVC – inferior vena cava, RHV – right hepatic vein, LCHV – left common hepatic vein, LRV – left renal vein, RRV – right renal vein, ROV – right ovarian vein, RCIV – right, LCIV – left common iliac vein, Abd-Ao – abdominal aorta common iliac vein*

The vessels that will be compressed are: IVC I, IVC II, IVC III, RCIV I, RCIV II, LCIV I, LCIV II, and Abdominal aorta. The vessels will be compressed individually and in groups. When a vessel is compressed, the area of the vessel reduces. Thus, to perform the simulations, the area will be reduced by 70, 80 and 90% to model the compression of the vessel.

The model will contain the closed loop circulation (heart model, venous system and arterial system). The model will not contain any optimisation, but the initial conditions will be based on patient's measurements and solutions from the personalised model (the open loop that converges to Doppler velocities). These initial conditions contain initial areas of arteries based on the area solution from the patient's personalised model, initial resistance and compliance from the personalised model results, initial flow based on flow solution from personalised model, patient's heart rate measurement, and patient's SBP and DBP used for initial pressure.

The simulations of reducing the area will be performed for all 21 patients. The analysis will compare the simulated results to clinical measurements of positioning a group of pregnant women on prone and lateral positions for 20 – 30 minutes. The flow and pressure in the uterine artery will be investigated to determine if compressing the veins and abdominal aorta will affect the blood flow going to the placenta. Lastly, the comparison between uncomplicated and complicated pregnancies will be investigated in the context of compressing the veins.

7.3. Results

Reduction of the Vena Cava and Iliac Veins

The main changes have been observed when reducing the area of the *IVC III* by 90% (Figure 22). The clinical data used to compare the simulated results has been provided by St. Mary's Hospital, Manchester, UK.

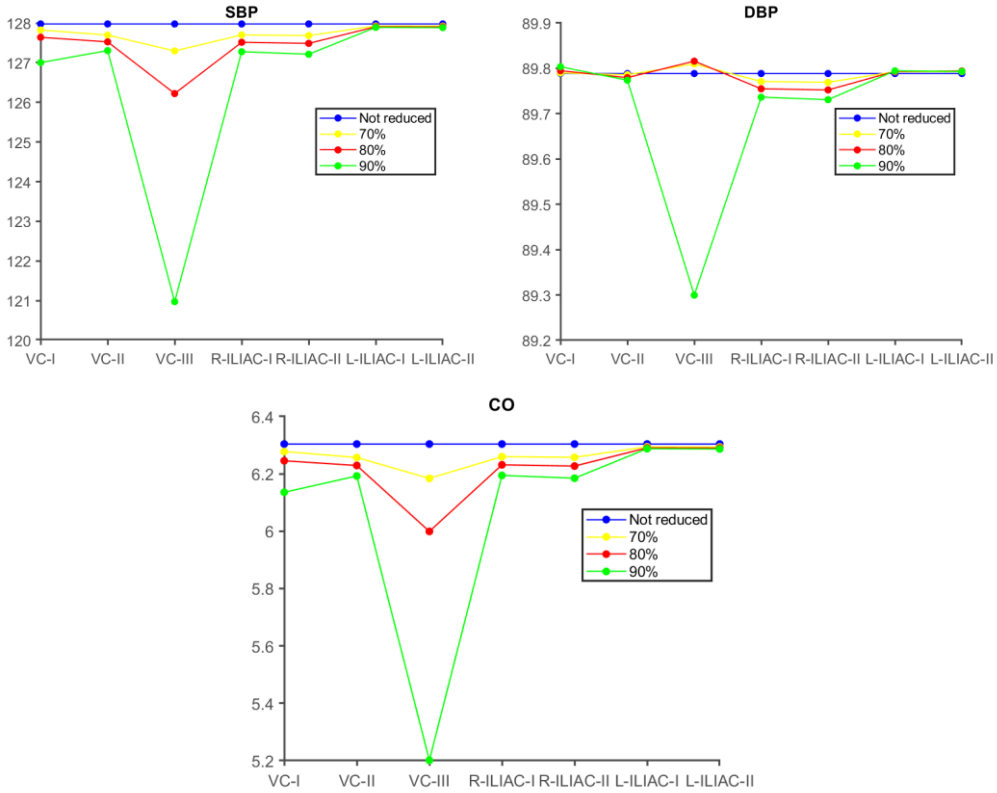

Figure 22. *Reduction of different vessel areas and their effect on different parameters; x-axis shows which vein was reduced, the title indicates which parameter is assessed; on y-axis is plotted SBP (mmHg), DBP (mmHg), and CO (L/min) respectively. VC-I – Vena cava I, VC-II – Vena Cava II, VC-III – Vena Cava III, R-ILIAC-I – Right Common Iliac I, R-ILIAC-II – Right Common Iliac II, L-ILIAC-I – Left Common Iliac I, L-ILIAC-II – Left Common Iliac II*

The changes in the cardiovascular system caused by the compression of the Vena Cava can be high, e.g. from 6.3 to 5.2 for *CO* when reducing *IVC III* by 90%. The *SBP* doesn't change by more than 10 mmHg and *DBP* changes by less than 1 mmHg. *PWV* is similar to *DBP* as it doesn't change greatly, it stays it the range of 7 m/s, and for the uterine artery, the flow doesn't decrease by more than 4 $\frac{cm^3}{s}$ for the worst case (*IVC III* reduced by 90%) and 5 mmHg drop in pressure. The total resistance also increased the most for the case of *IVC III* reduced by 90%.

Based on this, it was shown that the *IVC III* section affects the output of flow and pressure the most and the reduction of area by 90% is the most significant (Figure 22). One reason why *IVC-III* affects the pressure and flow output more than the other veins or segments of the vena cava is that the incoming flow going in the *IVC-III* is higher than the one in *IVC-II* and *IVC-I (IVC-IV* is not included as compression this segment results in the model not being able to deal with big area reductions). Flow in vena cava segments when there is no compression: flow in *IVC-I* is 6.6 $\frac{cm^3}{s}$, in *IVC-II* is 9.1 $\frac{cm^3}{s}$, in *IVC-III* is 16.6 $\frac{cm^3}{s}$ and lastly, in *IVC- IV* is 21.9 $\frac{cm^3}{s}$.

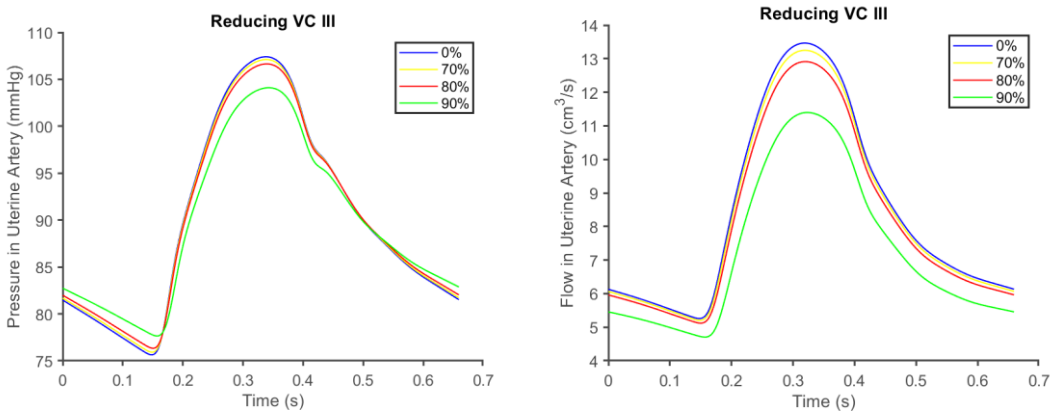

***Figure 23**. Pressure and Flow changes in uterine artery when IVC-III is reduced for patient 1*

The flow and pressure waveforms in the uterine artery are shown in Figure 23. When the *IVC III* is reduced by 90%, the flow in the uterine artery reduced by 2.5 $\frac{cm^3}{s}$ meaning that less blood gets to the fetus when the mother lies in a position that compresses the vena cava.

***Table 13.** Comparing the not reduced case to 90% area reduction of IVC III to clinical results.*

	Not reduced Mean ± Std	***90% area reduction Mean ± Std***	***Difference (90% area reduction – not reduced)***	***Clinical difference***
SBP (mmHg)	126.73 ± 6.55	119.92 ± 6.79	-6.81	6
DBP (mmHg)	89.34 ± 8.52	88.98 ± 8.48	~ 0	7
PWV (m/s)	7.69 ± 0.1	7.64 ± 0.12	~ 0	-
CO (L/min)	6.44 ± 0.42	5.30 ± 0.30	-1.14	-1.5
SVR ($dyne{\cdot}s/cm^5$)	1398.9 ± 157.5	1634.7 ± 178.4	235.8	243
Peak uterine artery Pressure (mmHg)	104.18 ± 6.04	100.53 ± 6.27	-3.65	-
Peak uterine artery Flow (cm^3/s)	14.01 ± 0.47	11.77 ± 0.33	-2.24	-

Table 13 shows how the blood pressure increases clinically while in the simulations, *SBP* decreases while *DBP* stays the same. The difference in *CO* is similar between clinical and simulations together with *SVR.* This suggests that in the prone position, the abdominal aorta could get compressed together with the vena cava. Another possibility related to the increase of the blood pressure could be that the resistance in the vascular beds increases to account for the compression as a physiological response.

Healthy vs. Pre-eclamptic comparison

In the results presented above, the dataset included both groups. Here, the two groups will be compared to see if there are any differences.

***Table 14.** Healthy (n = 12 patients) vs. pre-eclamptic (n = 9 patients). The area of the IVC III has been reduced.*

	Hypertensive		***Pre-eclamptic***	
	Not reduced Mean ± Std	***90% area reduction Mean ± Std***	***Not reduced Mean ± Std***	***90% area reduction Mean ± Std***
SBP (mmHg)	126.73 ± 6.55	119.92 ± 6.79	129.63 ± 10.79	122.38 ± 10.94
DBP (mmHg)	89.34 ± 8.52	88.98 ± 8.48	90.39 ± 12.95	89.73 ± 12.74

PWV (m/s)	7.69 ± 0.1	7.64 ± 0.12	7.66 ± 0.07	7.62 ± 0.08
CO (L/min)	6.44 ± 0.42	5.30 ± 0.30	6.12 ± 0.47	5.07 ± 0.33
Peak uterine artery Pressure (mmHg)	104.18 ± 6.04	100.53 ± 6.27	107.15 ± 10.36	102.94 ± 10.5
Peak uterine artery Flow (cm^3/s)	14.01 ± 0.47	11.77 ± 0.33	14.13 ± 0.97	11.85 ± 0.69

The results are similar between the two groups. The pre-eclamptic groups has slightly increased pressure values (*SBP* and *Peak uterine Pressure)* compared to the healthy group.

This analysis does not consider the duration of compression (e.g. 5 minutes in prone position) meaning that it does not account for physiological responses caused by the compression of the vein.

Reduction of the Vena Cava and Abdominal Aorta

Checking how reducing the area of one section of the abdominal aorta together with *IVC III* by 90% compares to only reducing the *IVC III* by 90% and the case when no vessel was reduced. The summary can be seen in Table 15. Abdominal aorta I (vessel number 40) was also reduced but did not show an increase in BP as great as reducing Abdominal aorta II (vessel number 46).

Table 15. *0% – shows the results where no vessel is reduced; Only IVC III reduced 90% - shows the results when only IVC III was reduced. Abd-Ao II 90% - shows the results when abdominal aorta II and IVC III were reduced by 90%*

	0%	***Only IVC III reduced (90%)***	***Abd-Ao II-90%***	***Difference (Abd-Ao 90% - 0%)***	***Clinical difference***
Parameters	***Mean ± Std***	***Mean ± Std***	***Mean ± Std***		
SBP (mmHg)	128.0 ± 8.5	121.0 ± 8.6	134.0 ± 8.6	6	6
DBP (mmHg)	89.8 ± 10.3	89.3 ± 10.2	89.8 ± 10.2	0	7
PWV (m/s)	7.7 ± 0.1	7.6 ± 0.1	6.1 ± 0.1	-1.6	-
CO (L/min)	6.3 ± 0.5	5.2 ± 0.3	5.5 ± 0.3	-0.8	-1.5
*SVR (dynes*s/cm^5)*	1398.9 ± 157.5	1634.7 ± 178.4	1626.4 ± 178.8	228	243
P ut (mmHg)	105.5 ± 8.1	101.6 ± 8.2	62.5 ± 8.1	-43	-
Q ut (cm^3/s)	14.1 ± 0.7	11.8 ± 0.5	5.8 ± 0.5	-8.3	-

It can be seen that the *SBP* increased and had a similar difference to the clinical results. However, the cardiac output increased compared to the case when only the *IVC III* was reduced and made the difference between the 0% and Abd-Ao II reduction to be only 0.8 L/min which is considerably lower than the clinical one.

Table 16 looks at reducing all segments of the abdominal aorta by 70, 80, and 90% together with the reduction of 90 % of *Left and Right iliacs, IVC I and IVC II.* Here the cardiac output barely decreased suggesting that the cause in the decrease of the cardiac output is *IVC III* segment.

Table 16*. Abdominal aorta I,II,III,IV,V together with 90% reduction of Left and Right Iliacs, VC-I and II*

Parameters	0%	70%	80%	90%	Difference (90%-0%)	Clinical difference
	Mean ± Std	Mean ± Std	Mean ± Std	Mean ± Std		
SBP (mmHg)	128.0 ± 8.5	131.9 ± 8.4	133.7 ± 8.3	135.6 ± 8.3	7.6	6
DBP (mmHg)	89.8 ± 10.3	89.8 ± 10.3	89.8 ± 10.3	89.9 ± 10.3	~0	7
PWV (m/s)	7.7 ± 0.1	7.4 ± 0.1	6.9 ± 0.1	5.7 ± 0.1	-2	-
CO (L/min)	6.3 ± 0.5	6.1 ± 0.4	6.1 ± 0.4	6.2 ± 0.5	-0.1	-1.5

SVR *(dynes*s/cm^5)*	1398.9 ± 157.5	1460.0 ± 161.7	1471.3 ± 162.4	1476.4 ± 161.5	78	243
P ut (mmHg)	105.5 ± 8.1	93.0 ± 7.8	79.6 ± 7.3	50.6 ± 5.7	-49	-
Q ut *(cm^3/s)*	14.1 ± 0.7	10.9 ± 0.6	8.4 ± 0.5	4.1 ± 0.3	-10	-

It is worth mentioning that the flow in the uterine artery decreases considerably and the pressure in the uterine artery is close to half of what it is in the not reduced case (0%). This confirms that the flow going to the placenta will decrease when the abdominal aorta and inferior vena cava are compressed.

Table 17*. The results of normal cardiac cycles where no vessel has been compressed (Not reduced); the results of compressing IVC I, II, III and the abdominal aorta II, III, IV and V by 90% (Area reduction of 90%) together with the resistance in vascular beds increased by 4 times the initial one and compliance in uteroplacental beds increased by 1.0005 times the initial one (Reduced). The number of patients is 10*

Parameters	***Not reduced***	***Reduced***	***Difference (Reduced – Not reduced)***	***Clinical difference***
	Mean ± Std	***Mean ± Std***		
SBP (mmHg)	127.7 ± 6.5	136.0 ± 11.9	8.3	6
DBP (mmHg)	90.3 ± 8.5	94.6 ± 13.9	4.3	7
PWV (m/s)	7.7 ± 0.1	5.1 ± 4.1	-2.6	-
CO (L/min)	6.4 ± 0.4	5.5 ± 0.4	-0.9	-1.5
SVR ($dyne{\cdot}s/cm^5$)	1380.5 ± 6.0	1698.2 ± 15.5	318	243
P ut (mmHg)	105.2 ± 9.0	66.4 ± 11.3	-38.8	-
Q ut (cm^3/s)	14.0 ± 0	3.5 ± 0.1	-10.5	-

In Table 17, the results of compressing *IVC I, II,* and *III* and *abdominal aorta II, III, IV* and *V* by 90% together with an increase in resistance in vascular beds of 4 times the original one and compliance in the utero-placental beds by 1.0005 times the original one. This showed the most similar results to the clinical ones. It can be seen that the additional changes of increasing the resistance and compliance resulted in an increase in *SBP* and *DBP* and decrease in *CO*. The change in *SVR* is also similar to the clinical one (318 $dyne{\cdot}s/cm^5$ vs. 243 $dyne{\cdot}s/cm^5$). This suggests that the positioning of the pregnant woman in prone position would result in a significant compression of the inferior vena cava and abdominal aorta which causes a major drop in stroke volume and because of this, the sympathetic nervous system kicks in and increases the peripheral resistance which causes an increase in blood pressure. However, this explanation is based on a small dataset and rough changes to resistance and reduction in area of the veins/arteries in the abdominal region. It was seen in other work that the changes in pressure, cardiac output and resistance can differ depending on the duration of sitting in given position, the type of position inspected, the number of participants and so on [125–127].

7.4. Conclusion

In summary, it was possible to reproduce similar results of the effect of prone position on pregnant women to the clinically observed ones. This could mean that the sympathetic system plays a role. Another useful observation is that the obstruction of the vena cava and abdominal aorta needs to be significant to observe any major changes. Similarly, it was observed that for such major obstruction, the blood flow in the uterine system significantly decreased. Lastly, the difference between hypertensive and pre-eclamptic women when obstructing the venous and arterial vessels was insignificant.

The investigation presented in this work was only at the start and it is not finished. As such, future work is needed to understand the overall changes that cause an increase in the pressure and a decrease in cardiac output (as seen in the clinical tests performed on pregnant women by positioning

them in a prone position on a pillow). As mentioned before, the resistance will play an important role in these simulations and because of that, a further investigation on the effect of changing the resistance together with the area reduction would be useful.

8. Data cleaning

8.1. Introduction

This chapter focuses on one of the steps that need to be taken to implement a possible neural network as mentioned in the *Future Direction* section. That step is data cleaning. As it is well known, a model, be a mathematical model or a neural network, needs to be validated. Especially for a neural network, data plays a main role in its optimisation as it is used to train the algorithm and validate it. There are different options to train neural networks. One would be to use synthetic data rather than actual data from patients (which is often used as it is easier to acquire). However, actual data still needs to be used at some point (only using synthetic data could cause issues such as training the network to output solutions that are not physiologically possible). This chapter serves as an introduction to how to clean large datasets.

In clinical settings, the platform used for recording data is not always standardised (there could be devices that have a standard format and are the same across multiple facilities. However, this is rarely the case). This is mentioned because not having a standard platform can cause variability. This means that even small differences in data inputs can result in data that would be hard to use for computational applications. Currently, the majority of data is manually inputted in the system. Again, this is mentioned because it plays a big role in data cleaning. The majority of errors are made during the manual recording of the data (e.g. writing the clinical measurements in an excel sheet and making mistakes such as writing word wrong, using capital letters for some word but not for others, putting a '.' In the wrong place and so on).

Data cleaning is a process that removes duplicated data, incorrectly formatted data, corrupted or incorrect data and can also fill incomplete data. Different methods used in data cleaning will be presented here and used to clean a large clinical dataset.

8.2. Foetal measurements

Besides the ultrasound scan performed for the assessment of the uterine artery velocity waveform, an ultrasound scan is also performed for the assessment of the foetus, and it is called sonography.

Foetal measurements are taken by clinicians in second and third trimester to assess the development of the foetus, foetal weight and gestational age. Generally, gestational age (dating) is calculated from the first day of the last menstrual period (LMP), but this method can be unreliable as this information is not always known [129]. An alternative method to calculate gestational age is to measure crown-rump length (CRL) and head circumference (HC). For assessing foetal size, foetal size charts are used where the calculated foetal size is compared to reference data in charts [130]. Finally, foetal weight estimation (or estimated foetal weight, EFW) is generally calculated using Shepard and Hadlock formulas [131].

The main measurements taken are head circumference (HC), biparietal diameter (BPD), abdominal circumference (AC), and Femur length (FL). There are multiple clinical practices for taking the measurements of the head such as measuring BPD using outer to outer (BPDoo) or outer to inner (BPDoi) calliper placement and HC using the ellipse facility on the ultrasound machine or calculating it using the occipitofrontal diameter (OFD) [132]. AC is measured using the transverse section of the

ultrasound image; FL is measured by locating the femur and needs to be close to the horizontal plane [133].

Table 18. *Assessment of typical ranges for BPD, AC, HC, and FL* [134, 135]

	Gestational age range (weeks)	Measurements range
BPD (cm)	13 – 42	2.5 – 10
HC (cm)	13 – 42	8 – 36
AC (cm)	13 – 41	10 – 37
FL (cm)	13 – 41	1 – 8
EFW (g)	20 – 36	343 - 2624

Shepard and Hadlock formulas typically used for calculating EFW are shown below [136]:

$$Shepard: Lg(weight) = -1.7492 + 0.166 * \boldsymbol{BPD} + 0.046 * \boldsymbol{AC} - \frac{2.6460(\boldsymbol{AC} * \boldsymbol{BPD})}{1000} \quad (27)$$

$$Hadlock\ 1: Lg(weight) = 1.304 + 0.05281 * \boldsymbol{AC} + 0.1938 * \boldsymbol{FL} - 0.004 * \boldsymbol{AC} * \boldsymbol{FL} \quad (28)$$

$$Hadlock\ 2: Lg(weight) = 1.335 + 0.0034 * \boldsymbol{AC} * \boldsymbol{FL} + 0.0316 * \boldsymbol{BPD} + 0.0457 * \boldsymbol{AC} + 0.1623 * \boldsymbol{FL} \quad (29)$$

$$Hadlock\ 3: Lg(weight) = 1.326 - 0.00326 * \boldsymbol{AC} * \boldsymbol{FL} + 0.0107 * \boldsymbol{HC} + 0.0438 * \boldsymbol{AC} + 0.158 * \boldsymbol{FL} \quad (30)$$

$$Hadlock\ 4: Lg(weight) = 1.3596 - 0.00386 * \boldsymbol{AC} * \boldsymbol{FL} + 0.0064 * \boldsymbol{HC} + 0.00061 * \boldsymbol{BPD} * \boldsymbol{AC} + 0.0424 * \boldsymbol{AC} + 0.174 * \boldsymbol{FL} \quad (31)$$

Obstetricians need to assess the foetal size in relation to gestational age to determine whether the foetus is small for gestational age (SGA), large for gestational age (LGA) or appropriate for gestational age (AGA)[137]. SGA foetuses have EFW and AC below 10th percentile while LGA foetuses have EFW and AC above 90th percentile.

Similar to SGA, foetal growth restriction (FGR) foetuses have EFW below the 10th percentile, however, not all FGR foetuses are SGA foetuses. A FGR foetus can be defined as a foetus that did not achieve its potential growth and it can result in adverse perinatal outcome such as pre-term birth or even stillbirth [137, 138]. When paired with pre-eclampsia, this could result in a baby at risk of developing cardiovascular diseases and neurodevelopmental conditions [138]. Thus, it is important to keep track of fetal size throughout the pregnancy and to screen for possible FGR.

8.3. Methods

Compared to before, this section focuses on large datasets as data cleaning is useful for datasets that are difficult to manually clean. The dataset used in this section is acquired from St. Mary's Hospital, Manchester, UK with the approval of NHS Research Ethics Committees (RECs) as the previous one. The dataset on which data cleaning was performed includes 9711 rows (rows signify the visits) and 30 columns (meaning 30 parameters that were recorded). The main columns contains clinical measurements such as HC, AC, BPD, FL, EFW, Umbilical PI, Umbilical RI, Umbilical EDF, Uterine artery PI, RI, and Notch, Impression (assessment of any diseases present during consultation, history etc.), Outcome (developed pre-eclampsia, other diseases or healthy), Department and Examination date. Compared to the previous dataset which only contained 21 patients, this dataset has thousands of patients. Also, this dataset focuses on foetal measurements rather than maternal cardiovascular measurements.

The cleaning was performed using Python on the JupyterLab platform (JupyterLab was chosen as it is an accessible platform that can be used without extensive knowledge). The main libraries used are SciPy, NumPy, matplotlib, pandas, and sklearn (Table 19).

Table 19*. Python libraries that are often used in data cleaning*

Library	**Details**

SciPy	Contains complex algorithms (ODE, Fourier solvers) and can be used in statistics, optimisation, integration and others [139]
NumPy	Main module for scientific computing and can be used for sorting, indexing, linear algebra and others [140]
Matplotlib	Fundamental package for creating figures in Python
Pandas	Main package used for data analysis and data cleaning as it can easily manipulated data (delete/insert columns, group data, handles missing data well etc.) [141]
Sklearn	Package that focuses on machine learning algorithms to use in Python

The main steps taken for cleaning the data are:

- Removing unwanted columns (or columns that are not needed such as Exam Date or Department)
- Removing duplicated rows (all values in each column same as another row's values)
- Generating a Profile report of the dataset and check any abnormal values
- Replacing abnormal values to values that are physiological correct e.g. replacing PI value of 70 to 0.7. This step refers back to the Introduction (Section Data Cleaning – R. Introduction) as one of the functions of data cleaning is to spot inconsistent data. This should not be confused with outliers. Outliers can still be physiological correct (for example: having a blood pressure of 160 mmHg while the mean of the dataset is 120 mmHg means 160 mmHg is an outlier. If the value would be 1600 mmHg then this is considered an inconsistency as it is not physiological possible)
- Filling missing values in the "string" columns (e.g. in the notch column, fill missing values with "missing notch")
- Changing strings values to integers: identify typos such as "preeclampsia", "pre-eclampsia" ,"Pre-eclampsia with diabetes" and replace it with "Pre-eclampsia" which will then be changed to an integer. This step was performed by first identifying all string that contain a specific word or phrase, and then replacing it with the wanted string/integer
    - For the Outcome column, 5 categories have been selected: Pre-eclampsia (patients that developed pre-eclampsia), Maternal disease (other disease than pre-eclampsia), Normal foetal growth (healthy), Abnormal foetal growth (foetal abnormality), and unknown outcome
- Imputation of missing data: this step will be performed on the columns containing numeric data such as FL, HC, AC, BPD, PI and RI
    - 4 methods have been selected for performing the data imputation: calculating the mean of the category (first method), k-means (second method), kNNI (kNN Imputation) (third method), and XGBoost (fourth method)
    - Separate filling of EFW column using Hadlock and Shepard formulas based on the foetal measurements. To select a formula, the error for each formula (equations 27-31) will be calculated and the formula with the lowest error will be used for imputation.

Calculating error as:

$$error = \frac{actual\ value - calculated\ value}{actual\ value} \times 100 \quad (32)$$

where the actual value is the original data value and calculated value is the value calculated by the formulas.

The first data imputation method, calculating the mean of the category, is one of the most common methods used in data imputation. The categories are the ones mentioned in column labelled *Outcome* (as the name suggests, it gives information about the outcome of the pregnancy). The mean will be calculated using the data that is linked to the specific category.

The second data imputation method is k-means. The first step is to normalise the data. This can be performed using the MinMaxScaler function in Python (it scales from 0 for minimum to 1 for

maximum). Next, the ideal number of clusters needs to be identified. To do this, the elbow method is used (the elbow method is used in k-means clustering to find the optimal number of clusters; it plots the average data dispersion on the y axis and k or the number of clusters on the x axis. The plotted line will look like an elbow, hence the name. The optimal number of clusters is where the elbow is). The imputation uses the clusters' centroids values for filling the missing values. Lastly, reverse scaling is performed to revert from the normalised values.

The third data imputation method is kNNI. Similar to k-means, the data is normalised. The imputation uses the k nearest neighbour algorithm which involves selecting a distance measure (e.g. Euclidean) and the number of neighbours, k. Here, the missing values will be replaced by the mean value of 5 nearest neighbours measured by Euclidean distance (it can be said the neighbours form a cluster, however in this method, the number of neighbours can be changed based on the dataset compared to k-means which looks at the entire dataset and the clusters formed inside it while kNNI can chose to ignore data points if the number of neighbours chosen is smaller than the actual number of datapoints in that cluster). Then, the data is scaled back.

The fourth and final data imputation method used is XGBoost. This method is designed for large datasets due to its high speed. Besides that, it uses predictive mean matching to improve the variance of the imputations. It is using a tree algorithm and it is fairly easy to implement. It was chosen as the algorithm is more complex than the first method and it is also different compared to KNNI and k-means. This methods should cover a range of algorithms and provide a general idea on which type of method would be more suitable for a dataset as the one in this chapter.

8.4. Results

Removal of duplicate rows

Not all columns are required for the next step after data cleaning. So, the columns left are Exam date, Indication, *BPD, HC, AC, Femur, EFW, Umbilical PI, Umbilical RI, Umbilical EDF* (End-diastolic flow), *Uterine PI* (Right and Left), *Uterine RI* (Right and Left), *Uterine Notch* (Right and Left), and *Impression.* To remove duplicate rows, the data in all columns need to be identical to another row's data. One example can be seen in the table below.

***Table 20**. Example of duplicated rows. Note: Not all columns have been displayed*

Exam date	***Indication***	***BPD (mm)***	***HC (mm)***	***AC (mm)***	***Femur (mm)***	***EFW (g)***	***Umbilical PI ()***	***Umbilical RI ()***
26/12/ 2019	Preeclampsia with FGR						1.46	
26/12/ 2019	Preeclampsia with FGR						1.46	
27/12/ 2019	Maternal disease in current pregnancy	85.5	309.6	306.5	65.8	2,419	1.07	0.67
27/12/ 2019	Maternal disease in current pregnancy	85.5	309.6	306.5	65.8	2,419	1.07	0.67

As it can be seen in the table above, first and second rows are identical and third and fourth rows are identical too. After removing the identical rows, the number of total rows reduced from 9711 rows to 2382 rows.

Assessment of typos in the dataset

There are two types of data in this dataset: text and numeric. The text data will include typos, writing with a capital letter, lower case letter, using '-' or others and will be dealt with during the grouping step. The numeric data needs to be in the correct ranges for each parameter, if not, it can be considered a typo. The physiological ranges for the foetal measurements are found in Section

Background – Foetal measurements. For the PI and RI ranges, it is safe to say that values below 0 and over 5 are abnormal. Lastly, it is important to consider that many women assessed in this dataset have maternal diseases and some impressions of these pregnancies are unfavourable (small for gestational age or large for gestational age) which results in abnormal measurements.

As the dataset is large, a report was generated using pandas-profiling v3.2.0. It was found that the maximum of Umbilical RI and Uterine RI was over 60 suggesting that there are typos in these columns. The typical range for RI is [0, 1] but there could be outliers (the definition of RI is maximum velocity minus minimum velocity divided by maximum velocity so based on this, the range should be from 0 to 1. However, minimum velocity could be negative, meaning the flow is going in the opposite direction) [142].

To remove these typos, the values that are over 3 (the value of 3 was chosen to account for any outliers in the range for RI) in these columns have been divided by 100 as it is presumed that the clinician probably wanted to type, for example, 0.6 rather than 60. The summary of the Umbilical RI can be seen in the Figure 24.

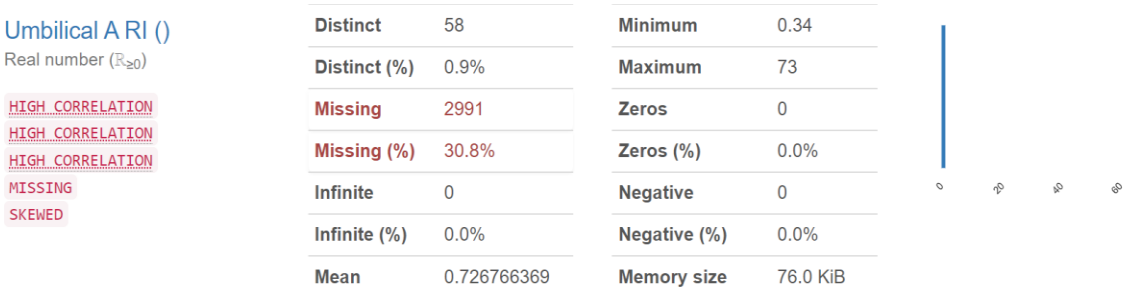

***Figure 24**. Summary of data in the Umbilical A RI () column (Umbilical A RI () = Umbilical RI). This report was done on the original dataset. On the right side, a histogram is displayed.*

It can be seen that the mean of the data in this column is 0.73, so values of 73 are far from the mean. The histogram is not displaying the distribution properly due to the typo.

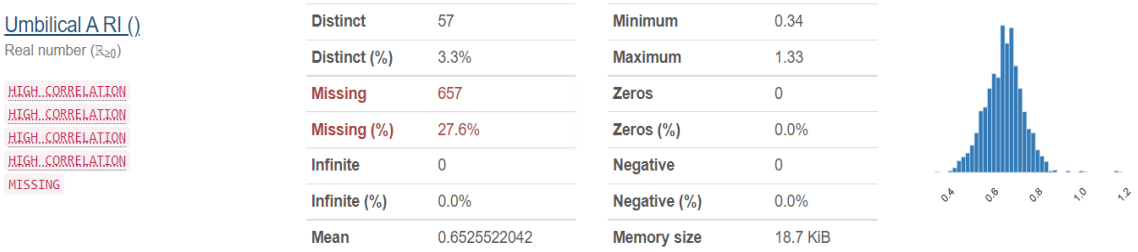

***Figure 25**. Summary of data in the Umbilical A RI () column (Umbilical A RI () = Umbilical RI) after removing the duplicated rows and the typos.*

Figure 25 shows the data distribution after removing the typos. It can be seen in the histogram that the distribution is a normal distribution with a maximum of 1.33 and minimum of 0.34

Grouping of data in different categories

As mentioned above, the categorical data shows many different inputs and variations of them. A summary of the inputs seen in the *Impression* and *Indication* columns can be seen in Figure 26.

Common Values

Value	Count	Frequency (%)
Maternal disease in current pregnancy	6121	63.0%
Previous pregnancy with likely placental dysfuncti…	218	2.2%
Preeclampsia	215	2.2%
Possible FGR	81	0.8%
Maternal disease in current pregnancy. Preeclam…	63	0.6%
SLE Budd chiari	60	0.6%
SLE budd chiari	60	0.6%
Evaluation of fetal well-being	48	0.5%
di/di twins	42	0.4%
Follow-up evaluation for fetal growth	29	0.3%
Other values (219)	1169	12.0%
(Missing)	1605	16.5%

Common Values

Value	Count	Frequency (%)
Normal fetal growth. (Please note this is an estim…	4019	41.4%
Likely FGR: Stable Doppler assessment	483	5.0%
Preeclampsia	244	2.5%
Normal fetal growth. (Please note this is an estim…	232	2.4%
Likely FGR: (See comments)	230	2.4%
Likely SGA	93	1.0%
No obvious fetal abnormality detected	42	0.4%
Normal fetal growth. (Please note this is an estim…	38	0.4%
Hypertension: Chronic	33	0.3%
FM seen. Normal LV. Only very fleeting AEDF. Hig…	30	0.3%
Other values (670)	2607	26.8%
(Missing)	1660	17.1%

Figure 26*. Summary of data in the Impression (Right) and Indication (Left) columns of original dataset.*

In the Figure above (Figure 26 Right), 'Normal fetal growth' can be seen twice. This is caused by an additional phrase added and because of that, it becomes separated from the category with the frequency of 41.4%. At the bottom of the figure, it is shown that there are 670 other values that account for 26.8% of the data inputs. In the Indication column (Left), it can be seen that even a lower case letter separates the same disease into two different categories (e.g. Budd vs. budd). To group the data values in different categories, common words/phrases such as 'Pre-eclampsia', 'maternal disease', 'Normal', 'Abnormal' etc. have been selected and based on this, different categories implemented i.e. if a phrase in the Impression column contained the word 'Normal' or 'normal' then it will change to 'Normal fetal growth'. Following this, the categories that summarise the values in the *Impression* column are Normal fetal growth, Abnormal fetal growth, Maternal disease, Pre-eclampsia and Unknown where Unknown was given to missing values in this column. All other columns that contained categorical data and had missing values had those values filled as 'unknown'.

After grouping the categorical data in different categories, the categories were converted from strings to integers to remove all strings from the dataset.

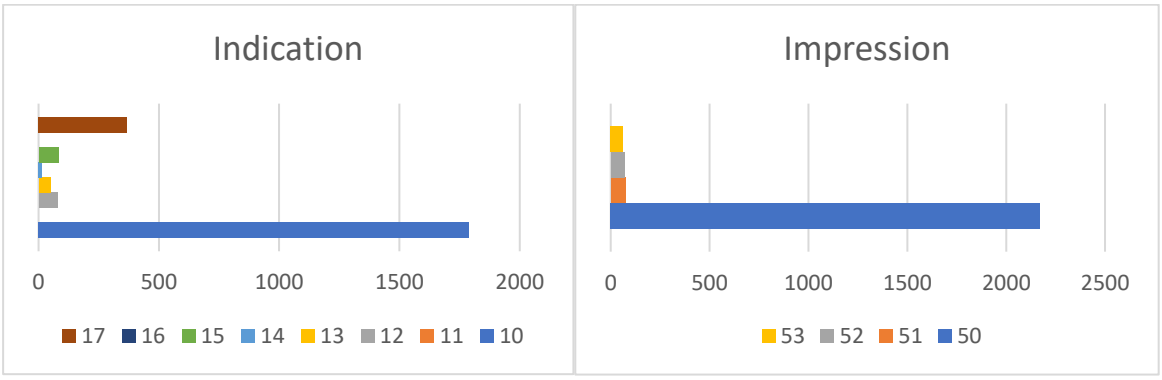

Figure 27*. Summary of data in the Impression and Indication categories; 50 – Normal fetal growth, 51 – Abnormal fetal growth, 52 – Maternal disease other than pre-eclampsia, 53 – Pre-eclampsia, 10 – Maternal disease before pregnancy (e.g. diabetes), 11 – Previous pregnancy with maternal disease, 12 – Fetal abnormality, 13 – Fetal evaluation, 14 – Previous stillbirth or miscarriage, 15 – Pre-eclampsia, 16 – Previous pregnancy with pre-eclampsia, 17 - Unknown*

Based on Figure 27, the category with most values in the *Indication* column is Maternal disease and in the *Impression* column is Normal fetal growth. This suggests that many pregnancies where the mother has a maternal disease can result in normal growth. The *Impression* column also has a Maternal disease category which contains diseases such as SGA, LGA, FGR, hypertension and other diseases except pre-eclampsia.

Other columns that have categorical data are the *Notch* columns and *Umbilical EDF* (end-diastolic flow*)*. Summary of the Right and Left uterine notch can be seen below.

In the Notch column, the most values are found in Category 2 which includes the missing values. The second category with most values is the no notch seen for both left and right uterine arteries and lastly, 1 or notch seen.

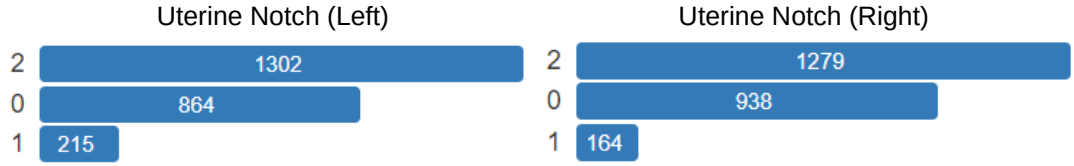

Figure 28*. Summary of Uterine Notch columns (Left and Right), 0 – no notch seen, 1 – notch seen, 2 – unknown*

Imputation of missing data

The most important part of data cleaning is data imputation. Data imputation can be performed using many methods such as using the mean of the column or using more complex methods such as category mean, k-means, KNNI, and XGBoost which have been used here. Table 21 shows that on average, over 30% of data is missing for most columns.

Table 21. *Percentage of data missing for most columns with numerical data (after duplicated rows have been removed)*

Column	Missing (%)
BPD (mm)	39.6
HC (mm)	34.2
AC (mm)	32.3
Femur (mm)	32.0
EFW (g)	33.2
Umbilical PI	26.5
Umbilical RI	27.6
Uterine PI (R)	46.2
Uterine RI (R)	46.2
Uterine PI (L)	47.1
Uterine RI (L)	47.0

The results of the four methods used to impute data for the BDP (bi-parietal diameter) column can be seen in Figure 29.

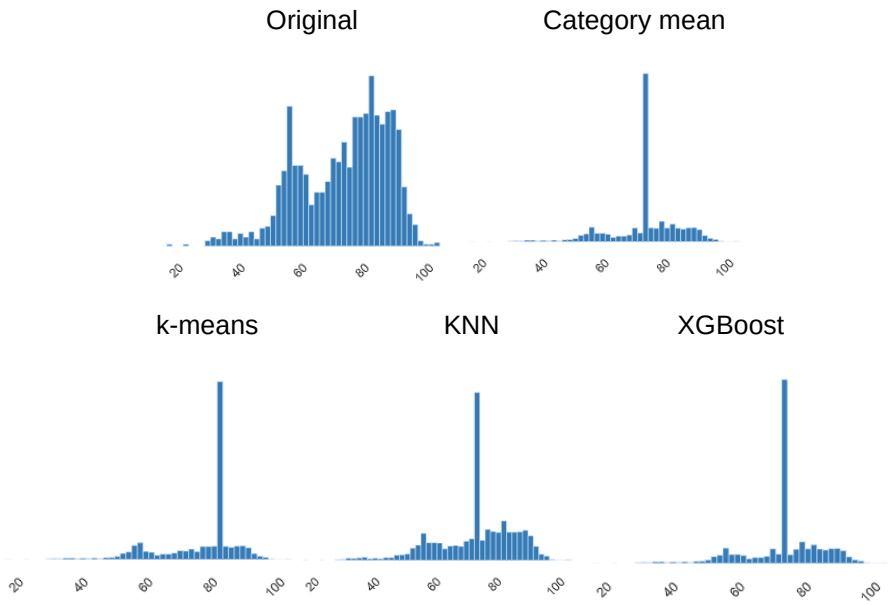

***Figure 29**. Summary of data imputation in column BPD (bi-parietal diameter) where original shows the distribution before data imputation. The y-axis represents the frequency while the x-axis is BPD (mm)*

After data imputation, all methods show similar results as the most common values are found around BPD = 70 mm. This shows that all methods investigated fail at filling the missing values in a distributed way of the original range (it can be seen in the graphs for all methods other than the original that the distribution is not normal anymore due to the high frequency of missing values being imputed at 70 mm). One reason why it fails in filling the missing values with different distinct values is that the main category with most data values is the Normal fetal growth. As such, the category mean method will fill the missing values in specific categories with the mean of that category which resulted in the high frequency of the value 73 in Figure above (for category mean). This type of imputation was seen in the other columns as well. Overall, it can be concluded that these methods show little variation in the data that was imputed making these methods unreliable. One option that could improve the imputation would be to consider adding noise to each value and thus, increase the variance of the population. However, random noise could not be appropriate when dealing with physiological data.

The formulas used for calculating EFW (estimated fetal weight) (formulas can be found in Chapter 8.2) have been compared to assess which one is the best to use for this data. To assess this, the formulas were used to estimate the EFW for patients that already had it calculated by the clinicians and then using eq. 32 in Chapter 8.3 to calculate error (the actual values are the ones already in the data and the estimated values are the ones calculated using the formulas. Then the formulas with the smallest error will be chosen to estimate the missing values of EFW). Table 22 shows the results of the different formulas:

***Table 22**. Number of rows where the error is of above 10% for each method of data imputation*

	Category mean	**k-means**	**KNN**	**XGDBoost**
Shepard	2381	1591	1591	1591
Hadlock 1	827	36	34	38
Hadlock 2	902	40	31	116
Hadlock 3	863	36	32	77
Hadlock 4	865	39	32	80

From Table 22, two conclusions can be drawn. Firstly, Shepard formula generated an error above 10% for the majority of the dataset. Secondly, the Category mean method will have an error above 10% in more than 800 rows which suggest that this method is not suitable for data imputation of EFW. The

other three methods show similar results as Hadlock 1 formula found around 35 values that had an error above 10% which is significantly lower compared to Category mean and can be deemed acceptable due to the large dataset. The results of the data imputation on EFW column can be seen in Figure 30.

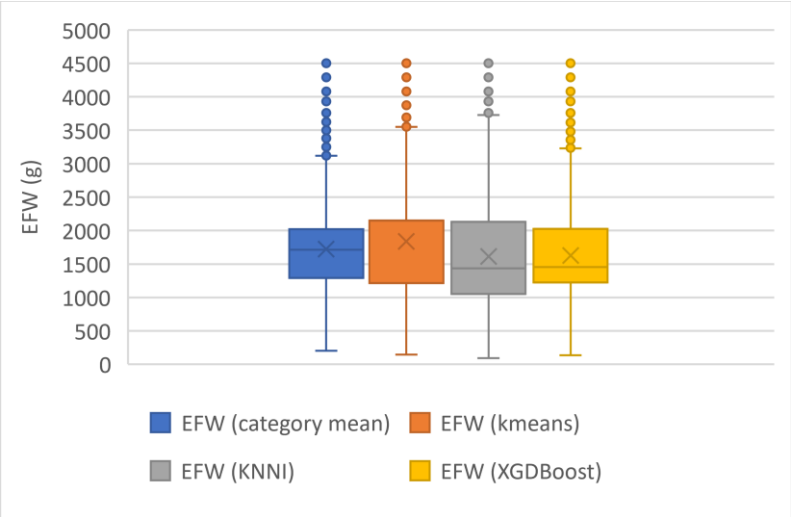

***Figure 30**. EFW spread using category mean, kmeans, KNNI, and XGDBoost methods*

8.5. Conclusion

During this work, it was possible to show how a large dataset can be cleaned and how data imputation can be performed. Although the results of the data imputation are not ideal, the methods used here provide a general idea of the process that can be useful in future work.

This chapter only shows a portion of the results that were deemed as representative of the data cleaning results. The results presented for BPD are similar to the other parameters. Data cleaning is necessary for large datasets as the one presented in this chapter and data imputation is an important process that can fill missing values. However, the results of the methods shown here do not seem to fill the missing values in a nicely distributed manner. One of the reason could be that data imputation was constrained by the category (e.g. Normal fetal growth). So, as a next step, imputing the missing values regardless of the category could be pursued. Also, it is worth mentioning that only using a simple method such as calculating the mean and using only that is not a good choice for a large dataset. This will definitely result in a distribution with a value that has a higher frequency than all other as seen in the results section for this method.

Future work needs to be done to improve data imputation as the results presented here show only the basic steps of data cleaning. More understanding of the actual physiological values and distribution of the parameters is needed.

9. References

[1] National Institute for Health and Care Excellence. Antenatal care: NICE; 2021. Available from: www.nice.org.uk/guidance/ng201.

[2] Vanoppen A, Stigter R, Bruinse H. Cardiac output in normal pregnancy: A critical review. *Obstet Gynecol* 1996; 87: 310–318.

[3] Al-Ghazali W, Chapman MG, Allan LD. Doppler assessment of the cardiac and uteroplacental circulations in normal and complicated pregnancies. Br J Obstet Gynaecol. 1988 Jun;95(6):575-80., doi: 10.1111/j.1471-0528.1988.tb09486.x. PMID: 3291935.

[4] McKelvey A, Pateman K, Balchin I, et al. Total uterine artery blood volume flow rate in nulliparous women is associated with birth weight and gestational age at delivery: Uterine blood flow and birth weight. *Ultrasound Obstet Gynecol* 2017; 49: 54–60.

[5] Sanghavi M, Rutherford JD. Cardiovascular Physiology of Pregnancy. *Circulation* 2014; 130: 1003–1008.
[6] Rigano S, Ferrazzi E, Boito S, et al. Blood flow volume of uterine arteries in human pregnancies determined using 3D and bi-dimensional imaging, angio-Doppler, and fluid-dynamic modeling. *Placenta* 2010; 31: 37–43.
[7] Ghi T, Sotiriadis A, Calda P, et al. ISUOG Practice Guidelines: invasive procedures for prenatal diagnosis: ISUOG Guidelines. *Ultrasound Obstet Gynecol* 2016; 48: 256–268.
[8] Dickey R. Doppler ultrasound investigation of uterine and ovarian blood flow in infertility and early pregnancy. *Hum Reprod Update* 1997; 3: 467–503.
[9] Schwarze A, Nelles I, Krapp M, et al. Doppler ultrasound of the uterine artery in the prediction of severe complications during low-risk pregnancies. *Arch Gynecol Obstet* 2005; 271: 46–52.
[10] Lui EYL, Steinman AH, Cobbold RSC, et al. Human factors as a source of error in peak Doppler velocity measurement. *J Vasc Surg* 2005; 42: 972.e1-972.e10.
[11] Khan KS, Wojdyla D, Say L, et al. WHO analysis of causes of maternal death: a systematic review. *The Lancet* 2006; 367: 1066–1074.
[12] National Institute for Health and Care Excellence .Hypertension in pregnancy: diagnosis and management: NICE;2019. Available from: www.nice.org.uk/guidance/ng133. *Hypertens Pregnancy*; 55.
[13] Magee LA, Pels A, Helewa M, et al. Diagnosis, evaluation, and management of the hypertensive disorders of pregnancy. *Pregnancy Hypertens Int J Womens Cardiovasc Health* 2014; 4: 105–145.
[14] Corrigan L, O'Farrell A, Moran P, et al. Hypertension in pregnancy: Prevalence, risk factors and outcomes for women birthing in Ireland. *Pregnancy Hypertens* 2021; 24: 1–6.
[15] Zhang J, Zeisler J, Hatch MC, et al. Epidemiology of Pregnancy-induced Hypertension. *Epidemiol Rev* 1997; 19: 218–232.
[16] Granger JP, Alexander BT, Llinas MT, et al. Pathophysiology of Hypertension During Preeclampsia Linking Placental Ischemia With Endothelial Dysfunction. 5.
[17] Ayoubi. Pre-eclampsia: pathophysiology, diagnosis, and management. *Vasc Health Risk Manag* 2011; 467.
[18] Mynard JP, Smolich JJ. One-Dimensional Haemodynamic Modeling and Wave Dynamics in the Entire Adult Circulation. *Ann Biomed Eng* 2015; 43: 1443–1460.
[19] Carson JM. *Development of a cardiovascular and lymphatic network model during human pregnancy*. PhD, Swansea University. Epub ahead of print 2019. DOI: 10.23889/Suthesis.50058.
[20] Carson J, Lewis M, Rassi D, et al. A data-driven model to study utero-ovarian blood flow physiology during pregnancy. *Biomech Model Mechanobiol* 2019; 18: 1155–1176.
[21] Carson J, Warrander L, Johnstone E, et al. Personalising cardiovascular network models in pregnancy: A two-tiered parameter estimation approach. *Int J Numer Methods Biomed Eng*. Epub ahead of print 13 January 2020. DOI: 10.1002/cnm.3267.
[22] Huxley R. Nausea and vomiting in early pregnancy: its role in placental development. *Obstet Gynecol* 2000; 95: 779–782.
[23] Bower, S., Vyas, S., Campbell, S. and Nicolaides, K.H. (1992), Color Doppler imaging of the uterine artery in pregnancy: normal ranges of impedance to blood flow, mean velocity and volume of flow. Ultrasound Obstet Gynecol, 2: 261-265. https://doi.org/10.1046/j.1469-0705.1992.02040261.x
[24] Mockridge A, Maclennan K. Physiology of pregnancy. *Anaesth Intensive Care Med* 2019; 20: 397–401.
[25] Hunter S, Robson SC. Adaptation of the maternal heart in pregnancy. *Heart* 1992; 68: 540–543.
[26] Gaillard R, Bakker R, Willemsen SP, et al. Blood pressure tracking during pregnancy and the risk of gestational hypertensive disorders: The Generation R Study. *Eur Heart J* 2011; 32: 3088–3097.
[27] Wiles K, Smith P. Renal disease in pregnancy. *Medicine (Baltimore)* 2019; 47: 684–690.
[28] Torgersen CKL, Curran CA. A Systematic Approach to the Physiologic Adaptations of Pregnancy: *Crit Care Nurs Q* 2006; 29: 2–19.
[29] Prowse, C. M., & Gaensler, E. A. (1965). Respiratory and acid-base changes during pregnancy. Anesthesiology, 26, 381–392. https://doi.org/10.1097/00000542-196507000-00003
[30] Chen M, Zeng J, Liu X, et al. Changes in physiology and immune system during pregnancy and coronavirus infection: A review. *Eur J Obstet Gynecol Reprod Biol* 2020; 255: 124–128.
[31] Annamraju H, Mackillop L. Respiratory disease in pregnancy. *Obstet Gynaecol Reprod Med* 2017; 27: 105–111.
[32] Mehta N, Chen K, Hardy E, et al. Respiratory disease in pregnancy. *Best Pract Res Clin Obstet Gynaecol* 2015; 29: 598–611.
[33] Van Heerden, P., Cluver, C. A., Bergman, K., & Bergman, L. (2021). Blood pressure as a risk factor for eclampsia and pulmonary oedema in pre-eclampsia. Pregnancy hypertension, 26, 2–7. https://doi.org/10.1016/j.preghy.2021.07.241
[34] Ma GJ, Yadav S, Kaplan PW, et al. New-onset epilepsy in women with first time seizures during pregnancy. *Seizure* 2020; 80: 42–45.
[35] Hart LA, Sibai BM. Seizures in pregnancy: Epilepsy, eclampsia, and stroke. *Semin Perinatol* 2013; 37: 207–224.
[36] Aminoff MJ, Josephson SA. *Aminoff's neurology and general medicine*, https://www.sciencedirect.com/science/book/9780128193068 (2021, accessed 18 November 2021).
[37] Duley L. The Global Impact of Pre-eclampsia and Eclampsia. *Semin Perinatol* 2009; 33: 130–137.
[38] Hutcheon JA, Lisonkova S, Joseph KS. Epidemiology of pre-eclampsia and the other hypertensive disorders of pregnancy. *Best Pract Res Clin Obstet Gynaecol* 2011; 25: 391–403.
[39] Brown MA, Magee LA, Kenny LC, et al. Hypertensive Disorders of Pregnancy. 20.
[40] Rolnik DL, Wright D, Poon LC, et al. Aspirin versus Placebo in Pregnancies at High Risk for Preterm Preeclampsia. *N Engl J Med* 2017; 377: 613–622.
[41] Wagenseil JE, Mecham RP. Elastin in Large Artery Stiffness and Hypertension. *J Cardiovasc Transl Res* 2012; 5: 264–273.

[42] Lakatta EG, Levy D. Arterial and Cardiac Aging: Major Shareholders in Cardiovascular Disease Enterprises: Part I: Aging Arteries: A “Set Up” for Vascular Disease. *Circulation* 2003; 107: 139–146.
[43] Groenink M. The influence of aging and aortic stiffness on permanent dilation and breaking stress of the thoracic descending aorta. *Cardiovasc Res* 1999; 43: 471–480.
[44] Laurent S, Boutouyrie P, Asmar R, et al. Aortic Stiffness Is an Independent Predictor of All-Cause and Cardiovascular Mortality in Hypertensive Patients. *Cardiovasc Risk Factors*; 6.
[45] Guthold M, Liu W, Sparks EA, et al. A Comparison of the Mechanical and Structural Properties of Fibrin Fibers with Other Protein Fibers. *Cell Biochem Biophys* 2007; 49: 165–181.
[46] Wolinsky H, Glagov S. Structural Basis for the Static Mechanical Properties of the Aortic Media. *Circ Res* 1964; 14: 400–413.
[47] Yu S, McEniery CM. Central Versus Peripheral Artery Stiffening and Cardiovascular Risk. *Arterioscler Thromb Vasc Biol* 2020; 40: 1028–1033.
[48] Anthoulakis C, Mamopoulos A. Augmentation index and pulse wave velocity in normotensive versus preeclamptic pregnancies: a prospective case–control study using a new oscillometric method. *Ann Med* 2022; 54: 1–10.
[49] Shirwany NA. Arterial stiffness: a brief review. *Acta Pharmacol Sin*; 10.
[50] Tihtonen KMH, Kööbi T, Uotila JT. Arterial stiffness in preeclamptic and chronic hypertensive pregnancies. *Eur J Obstet Gynecol Reprod Biol* 2006; 128: 180–186.
[51] Shykoff BE, Hawari FI, Izzo JL. Diameter, pressure and compliance relationships in dorsal hand veins. *Vasc Med*; 6.
[52] Cohn JN, Finkelstein S, McVeigh G, Morgan D, LeMay L, Robinson J, Mock J: Noninvasive pulse wave analysis for the early detection of vascular disease. Hypertension 1995;26:503–508.
[53] Pannier BM, Avolio AP, Hoeks A, et al. Methods and devices for measuring arterial compliance in humans. *Am J Hypertens* 2002; 15: 743–753.
[54] Franz MB, Burgmann M, Neubauer A, et al. Augmentation index and pulse wave velocity in normotensive and pre-eclamptic pregnancies. *Acta Obstet Gynecol Scand* 2013; 7.
[55] Kaihura C, Savvidou MD, Anderson JM, et al. Maternal arterial stiffness in pregnancies affected by preeclampsia. *Am J Physiol-Heart Circ Physiol* 2009; 297: H759–H764.
[56] Katsipi I, Stylianou K, Petrakis I, et al. The use of pulse wave velocity in predicting pre-eclampsia in high-risk women. *Hypertens Res* 2014; 37: 733–740.
[57] Phan K, Schiller I, Dendukuri N, et al. A longitudinal analysis of arterial stiffness and wave reflection in preeclampsia: Identification of changepoints. *Metabolism* 2021; 120: 154794.
[58] Turi V, Iurciuc S, Crețu OM, et al. Arterial function in hypertensive pregnant women. Is arterial stiffness a marker for the outcomes in pregnancy? *Life Sci* 2021; 264: 118723.
[59] Myers JE, Ormesher L, Shawkat E, et al. 296: Arterial stiffness and placental growth factor are independent predictors of adverse pregnancy outcome in women with chronic hypertension. *Am J Obstet Gynecol* 2018; 218: S188.
[60] Orabona R, Sciatti E, Vizzardi E, et al. Elastic properties of ascending aorta in women with previous pregnancy complicated by early- or late-onset pre-eclampsia: Elastic properties of ascending aorta in early- or late-onset PE. *Ultrasound Obstet Gynecol* 2016; 47: 316–323.
[61] Melchiorre K, Sutherland GR, Liberati M, et al. Preeclampsia Is Associated With Persistent Postpartum Cardiovascular Impairment. *Hypertension* 2011; 58: 709–715.
[62] Borzychowski AM, Sargent IL, Redman CW. Inflammation and pre-eclampsia. Semin Fetal Neonatal Med 2006; 11: 309–316.
[63] Castleman JS, Shantsila A, Brown RA, et al. Altered cardiac and vascular stiffness in pregnancy after a hypertensive pregnancy. *J Hum Hypertens*. Epub ahead of print 25 February 2022. DOI: 10.1038/s41371-022-00662-4.
[64] Kalapotharakos G, Salehi D, Steding-Ehrenborg K, et al. Cardiovascular effects of severe late-onset preeclampsia are reversed within six months postpartum. *Pregnancy Hypertens* 2020; 19: 18–24.
[65] Goodman HM. *Basic medical endocrinology*. 4th ed. Amsterdam ; Boston: Elsevier/Academic Press, 2009.
[66] Zia S. Placental location and pregnancy outcome. *J Turk Ger Gynecol Assoc* 2013; 14: 190–193.
[67] Warland, J., McCutcheon, H., & Baghurst, P. (2009). Placental position and late stillbirth: a case-control study. Journal of clinical nursing, 18(11), 1602–1606. https://doi.org/10.1111/j.1365-2702.2008.02779.x
[68] Ito, Y., Shono, H., Shono, M., Muro, M., Uchiyama, A., & Sugimori, H. (1998). Resistance index of uterine artery and placental location in intrauterine growth retardation. Acta obstetricia et gynecologica Scandinavica, 77(4), 385–390.
[69] Granfors M, Stephansson O, Endler M, et al. Placental location and pregnancy outcomes in nulliparous women: A population-based cohort study. *Acta Obstet Gynecol Scand* 2019; 98: 988–996.
[70] King LJ, Dhanya Mackeen A, Nordberg C, et al. Maternal risk factors associated with persistent placenta previa. *Placenta* 2020; 99: 189–192.
[71] Cresswell JA, Ronsmans C, Calvert C, et al. Prevalence of placenta praevia by world region: a systematic review and meta-analysis. *Trop Med Int Health* 2013; 18: 712–724.
[72] Crane, J. M., van den Hof, M. C., Dodds, L., Armson, B. A., & Liston, R. (1999). Neonatal outcomes with placenta previa. Obstetrics and gynecology, 93(4), 541–544. https://doi.org/10.1016/s0029-7844(98)00480-3.
[73] Bahar A, Abusham A, Eskandar M, et al. Risk Factors and Pregnancy Outcome in Different Types of Placenta Previa. *J Obstet Gynaecol Can* 2009; 31: 126–131.
[74] Gargari SS, Seify Z, Haghighi L, et al. Risk Factors and Consequent Outcomes of Placenta Previa: Report From a Referral Center. 5.
[75] Chelmow D, Elleneandrew D, Baker E. Maternal cigarette smoking and placenta previa. *Obstet Gynecol* 1996; 87: 703–706.
[76] Gilliam M, Rosenberg D, Davis F. The Likelihood of Placenta Previa With Greater Number of Cesarean Deliveries and Higher Parity. 2002; 99: 5.

[77] Roberts JM, Escudero C. The placenta in preeclampsia. *Pregnancy Hypertens Int J Womens Cardiovasc Health* 2012; 2: 72–83.
[78] Sun C, Groom KM, Oyston C, et al. The placenta in fetal growth restriction: What is going wrong? *Placenta* 2020; 96: 10–18.
[79] Hypertension in Pregnancy: Executive Summary. Obstetrics & Gynecology: November 2013 - Volume 122 - Issue 5 - p 1122-1131 doi: 10.1097/01.AOG.0000437382.03963.88
[80] Fishel Bartal M, Lindheimer MD, Sibai BM. Proteinuria during pregnancy: definition, pathophysiology, methodology, and clinical significance. *Am J Obstet Gynecol* 2022; 226: S819–S834.
[81] MacDonald TM, Walker SP, Hannan NJ, et al. Clinical tools and biomarkers to predict preeclampsia. *eBioMedicine* 2022; 75: 103780.
[82] Cohen-Overbeek, T., Pearce, J. M., & Campbell, S. (1985). The antenatal assessment of utero-placental and feto-placental blood flow using Doppler ultrasound. Ultrasound in medicine & biology, 11(2), 329–339. https://doi.org/10.1016/0301-5629(85)90132-2.
[83] Clark AR, James JL, Stevenson GN, et al. Understanding abnormal uterine artery Doppler waveforms: A novel computational model to explore potential causes within the utero-placental vasculature. *Placenta* 2018; 66: 74–81.
[84] Hernandez-Andrade, E., Brodszki, J., Lingman, G., Gudmundsson, S., Molin, J., & Marsál, K. (2002). Uterine artery score and perinatal outcome. Ultrasound in obstetrics & gynecology : the official journal of the International Society of Ultrasound in Obstetrics and Gynecology, 19(5), 438–442. https://doi.org/10.1046/j.1469-0705.2002.00665.x
[85] *Marsál K, Olofsson P-A, Lindström K. Doppler uttrasonography:physics and techniques. In Kurjak A, ed. Textbook of PerinatalMedicine, Vol 1. London: The Parthenon Publishing Group, 1998:409–421.*
[86] Papageorghiou AT, Yu CKH, Erasmus IE, et al. Assessment of risk for the development of pre-eclampsia by maternal characteristics and uterine artery Doppler. *BJOG Int J Obstet Gynaecol* 2005; 112: 703–709.
[87] El-Hamedji H, Shillito S, Simpson NA, Walker JJ. Prospective analysis of the role of uterine artery Doppler waveform notching in the assessment of at risk pregnancies. Hypertens Pregnancy 2005;24:137e45.
[88] Axt-Fliedner R, Schwarze A, Nelles I, et al. The value of uterine artery Doppler ultrasound in the prediction of severe complications in a risk population. *Arch Gynecol Obstet* 2005; 271: 53–58.
[89] Espinoza J, Romero R, Nien JK, et al. Identification of Patients at Risk for Early Onset and/or Severe Preeclampsia With the Use of Uterine Artery Doppler Velocimetry and Placental Growth Factor. 2008; 27.
[90] Asnafi N, Hajian K. Mid-trimester uterine artery Doppler ultrasound as a predictor of adverse obstetric outcome in high-risk pregnancy. *Taiwan J Obstet Gynecol* 2011; 50: 29–32.
[91] Zimmermann P, Eirio V, Koskinen J, Kujansun E, Ranta T. Doppler assessment of the uterine and utero placental circulation in the second trimester in pregnancies at high risk for pre-eclampsia and or intrauterine growth retardation: comparison and correlation between different Doppler parameters. Ultrasound Obstet Gynecol 1997;9:330e8.
[92] Schiffer V, Evers L, de Haas S, et al. Spiral artery blood flow during pregnancy: a systematic review and meta-analysis. *BMC Pregnancy Childbirth* 2020; 20: 680.
[93] Clark AR, Lee TC, James JL. Computational modeling of the interactions between the maternal and fetal circulations in human pregnancy. *WIREs Mech Dis*; 13. Epub ahead of print January 2021. DOI: 10.1002/wsbm.1502.
[94] Gleason RL, Sedaghati F. A mathematical model of maternal vascular growth and remodeling and changes in maternal hemodynamics in uncomplicated pregnancy. *Biomech Model Mechanobiol*. Epub ahead of print 2 February 2022. DOI: 10.1007/s10237-021-01555-0.
[95] Iacobelli S, Bonsante F, Robillard P-Y. Comparison of risk factors and perinatal outcomes in early onset and late onset preeclampsia: A cohort based study in Reunion Island. *J Reprod Immunol* 2017; 123: 12–16.
[96] Lisonkova, S., & Joseph, K. S. (2013). Incidence of preeclampsia: risk factors and outcomes associated with early- versus late-onset disease. American journal of obstetrics and gynecology, 209(6), 544.e1–544.e12. https://doi.org/10.1016/j.ajog.2013.08.019.
[97] M. W. Ramsey and M. Sugawara. \Arterial wave intensity and ventriculoarterial interaction." In: Heart and vessels Suppl 12 (1997), pp. 128{134. issn: 0910-8327.
[98] Jonathan P. Mynard and Joseph J. Smolich. \One-Dimensional Haemodynamic Modeling and Wave Dynamics in the Entire Adult Circulation". In: Annals of Biomedical Engineering 43.6 (Apr. 2015), pp. 1443{1460. issn: 1573-9686. doi: 10.1007/s10439-015-1313-8. url: http://dx.doi.org/ 10.1007/s10439-015-1313-8.
[99] Sobol′ IM. Global sensitivity indices for nonlinear mathematical models and their Monte Carlo estimates. *Math Comput Simul* 2001; 55: 271–280.
[100] Xu C, Gertner G. Understanding and comparisons of different sampling approaches for the Fourier Amplitudes Sensitivity Test (FAST). *Comput Stat Data Anal* 2011; 55: 184–198.
[101] Zhang K, Lu Z, Cheng L, et al. A new framework of variance based global sensitivity analysis for models with correlated inputs. *Struct Saf* 2015; 55: 1–9.
[102] Hart J, Gremaud P. An approximation theoretic perspective of the Sobol' indices with dependent variables. *ArXiv180101359 Phys*, http://arxiv.org/abs/1801.01359 (2018, accessed 7 April 2022).
[103] Savine A. Modern Computational Finance. 334.
[104] Helton JC, Johnson JD, Sallaberry CJ, et al. Survey of sampling-based methods for uncertainty and sensitivity analysis. *Reliab Eng Syst Saf* 2006; 91: 1175–1209.
[105] Cannavó F. Sensitivity analysis for volcanic source modeling quality assessment and model selection. *Comput Geosci* 2012; 44: 52–59.
[106] Adamson SL. Arterial pressure, vascular input impedance, and resistance as determinants of pulsatile blood flow in the umbilical artery. *Eur J Obstet Gynecol Reprod Biol* 1999; 84: 119–125.
[107] Lim HS, Gustafsson F. Pulmonary artery pulsatility index: physiological basis and clinical application. *Eur J Heart Fail* 2020; 22: 32–38.

[108] Zhan C, Song X, Xia J, et al. An efficient integrated approach for global sensitivity analysis of hydrological model parameters. *Environ Model Softw* 2013; 41: 39–52.
[109] University Institute of Radiological Sciences and Medical Imaging Technologies (UIRSMIT), Faculty of Allied Health Sciences (FAHS), University of Lahore, Lahaur, Pakistan, Madina SR, Bacha R, et al. Comparison of the resistive indices obtained in the uterine artery and the ophthalmic artery in preeclamptic and normotensive patients in Doppler US. *J Ultrason* 2020; 20: e95–e99.
[110] Wu J-N, Li M-Q, Xie F, et al. Gestational week-specific of uterine artery Doppler indices in predicting preeclampsia: a hospital-based retrospective cohort study. *BMC Pregnancy Childbirth* 2021; 21: 843.
[111] Melchiorre K, Wormald B, Leslie K, Bhide A, Thilaganathan B. First trimester uterine artery Doppler indices in term and preterm pre-eclampsia. Ultrasound Obstet Gynecol. (2008) 32:133–7. doi: 10.1002/uog.540.
[112] Spaanderman MEA, Willekes C, Hoeks APG, et al. The effect of pregnancy on the compliance of large arteries and veins in healthy parous control subjects and women with a history of preeclampsia. *Am J Obstet Gynecol* 2000; 183: 1278–1286.
[113] Ratiu D, Hide-Moser K, Morgenstern B, et al. Doppler Indices and Notching Assessment of Uterine Artery Between the 19th and 22nd Week of Pregnancy in the Prediction of Pregnancy Outcome. *In Vivo* 2019; 33: 2199–2204.
[114] Harrington K, Fayyad A, Thakur V, et al. The value of uterine artery Doppler in the prediction of uteroplacental complications in multiparous women: Uterine artery Doppler in multiparous women. *Ultrasound Obstet Gynecol* 2004; 23: 50–55.
[115] Gomez Y, Hudda Z, Mahdi N, et al. Pulse Pressure Amplification and Arterial Stiffness in Low-Risk, Uncomplicated Pregnancies. *Angiology* 2016; 67: 375–383.
[116] Cnossen JS, Morris RK, ter Riet G, et al. Use of uterine artery Doppler ultrasonography to predict pre-eclampsia and intrauterine growth restriction: a systematic review and bivariable meta-analysis. *Can Med Assoc J* 2008; 178: 701–711.
[117] Nagar T, Sharma D, Choudhary M, et al. The Role of Uterine and Umbilical Arterial Doppler in High-risk Pregnancy: A Prospective Observational Study from India. *Clin Med Insights Reprod Health* 2015; 9: CMRH.S24048.
[118] Makikallio K. First trimester uterine, placental and yolk sac haemodynamics in pre-eclampsia and preterm labour. *Hum Reprod* 2004; 19: 729–733.
[119] Hung, J. H., Ng, H. T., Pan, Y. P., Yang, M. J., & Shu, L. P. (1997). Color Doppler ultrasound, pregnancy-induced hypertension and small-for-gestational-age fetuses. International journal of gynaecology and obstetrics: the official organ of the International Federation of Gynaecology and Obstetrics, 56(1), 3–11. https://doi.org/10.1016/s0020-7292(96)02779-8.
[120] Deurloo KL, Spreeuwenberg MD, Bolte AC, et al. Color Doppler ultrasound of spiral artery blood flow for prediction of hypertensive disorders and intra uterine growth restriction: a longitudinal study: LONGITUDINAL DOPPLER MEASUREMENTS OF SPIRAL ARTERIES. *Prenat Diagn* 2007; 27: 1011–1016.
[121] Gebb J, Dar P. Colour Doppler ultrasound of spiral artery blood flow in the prediction of pre-eclampsia and intrauterine growth restriction. *Best Pract Res Clin Obstet Gynaecol* 2011; 25: 355–366.
[122] Hafner E, Metzenbauer M, Stümpflen I, et al. First trimester placental and myometrial blood perfusion measured by 3D power Doppler in normal and unfavourable outcome pregnancies. *Placenta* 2010; 31: 756–763.
[123] Goldenberg RL, Cliver SP, Bronstein J, Cutter GR, Andrews WW, Mennemeyer ST. Bed rest in pregnancy. Obstet Gynecol 1994;84: 131–6.
[124] Heazell A, Li M, Budd J, et al. Association between maternal sleep practices and late stillbirth - findings from a stillbirth case-control study. *BJOG Int J Obstet Gynaecol* 2018; 125: 254–262.
[125] Myers MC, Brandt DS, Prunty A, et al. Effect of positioning on blood pressure measurement in pregnancy. *Pregnancy Hypertens* 2022; 27: 110–114.
[126] Armstrong S, Fernando R, Columb M, et al. Cardiac Index in Term Pregnant Women in the Sitting, Lateral, and Supine Positions: An Observational, Crossover Study. *Anesth Analg* 2011; 113: 318–322.
[127] Bamber JH, Dresner M. Aortocaval Compression in Pregnancy: The Effect of Changing the Degree and Direction of Lateral Tilt on Maternal Cardiac Output: *Anesth Analg* 2003; 256–258.
[128] Lee SWY, Khaw KS, Ngan Kee WD, et al. Haemodynamic effects from aortocaval compression at different angles of lateral tilt in non-labouring term pregnant women †‡. *Br J Anaesth* 2012; 109: 950–956.
[129] Verburg BO, Steegers EAP, Ridder MD, et al. New charts for ultrasound dating of pregnancy and assessment of fetal growth: longitudinal data from a population-based cohort study. *Ultrasound Obstet Gynecol* 2008; 9.
[130] Loughna P, Chitty L, Evans T, et al. Fetal size and dating: charts recommended for clinical obstetric practice. 2009; 17: 7.
[131] Khadka R. Validation of Hadlock's and Shepard Formulae of Fetal Weight Estimation in Eastern Region of Nepal. *Birat J Health Sci* 2019; 4: 738–743.
[132] Napolitano R, Donadono V, Ohuma EO, et al. Scientific basis for standardization of fetal head measurements by ultrasound: a reproducibility study. *Ultrasound Obstet Gynecol* 2016; 48: 80–85.
[133] Ultrasound Reference Manual for Pregnancy Dating. Developed for the Assessing the Safety of Antimalarials during early Pregnancy (ASAP) Study through support from the Malaria in Pregnancy Consortium (MiPc). 2012.
[134] MacGregor, S, Sabbagha, R, Glob. libr. women's med., (ISSN: 1756-2228) 2008; DOI 10.3843/GLOWM.10206.
[135] Salomon LJ, Bernard JP, Ville Y. Estimation of fetal weight: reference range at 20–36 weeks' gestation and comparison with actual birth-weight reference range. *Ultrasound Obstet Gynecol* 2007; 29: 550–555.
[136] Pinette MG, Pan Y, Pinette SG, et al. Estimation of fetal weight: mean value from multiple formulas. *J Ultrasound Med* 1999; 18: 813–817.
[137] Salomon LJ, Alfirevic Z, Da Silva Costa F, et al. ISUOG Practice Guidelines: ultrasound assessment of fetal biometry and growth. *Ultrasound Obstet Gynecol* 2019; 53: 715–723.

[138] Clark AR, Yoshida K, Oyen ML. Computational modeling in pregnancy biomechanics research. *J Mech Behav Biomed Mater* 2022; 128: 105099.
[139] https://pypi.org/project/scipy/.
[140] https://pypi.org/project/numpy/.
[141] https://pypi.org/project/pandas/.
[142] Geipel A, Hennemann F, Fimmers R, et al. Reference ranges for Doppler assessment of uterine artery resistance and pulsatility indices in dichorionic twin pregnancies. *Ultrasound Obstet Gynecol* 2011; 37: 663–667.
[143] Ding, C., & Peng, H. (2005). Minimum redundancy feature selection from microarray gene expression data. Journal of bioinformatics and computational biology, 3(2), 185–205. https://doi.org/10.1142/s0219720005001004.
[144] Radovic, M., Ghalwash, M., Filipovic, N. et al. Minimum redundancy maximum relevance feature selection approach for temporal gene expression data. BMC Bioinformatics 18, 9 (2017). https://doi.org/10.1186/s12859-016-1423-9.

10. Appendix

The table below shows the full patient data used in section Patient characteristics.

***Table 23**. Patient measurement data. U – uncomplicated, C – complicated*

Patient	Height (cm)	Weight (kg)	GA (Week + days)	SBP (mmHg)	DBP (mmHg)	HR (beat/min)	CO (L/min)	PWV (m/s)	Birth Weight (g)
U1	172	95	24+1	146	96	91	6.6	6.3	2117
U2	155	50	24+2	107	74	94	3.5	5.8	2052
U3	169	114	22+2	145	93	88	4.9	7	3260
U4	166	79	24	122	87	76	5.7	6.7	3370
U5	155	54	22+3	123	79	74	2.5	6	2420
U6	157.5	76	23+6	133	95	96	4.4	7.5	-
U7	166	79	23+1	141	97	83	3.3	8.1	3240
U8	164	44.2	23+4	129	88	84	4.2	7.5	2300
U9	167	123	23+2	146	95	117	5.6	12.3	3800
U10	160	74.1	23+1	155	101	99	3.7	5.9	3369
U11	156	80	22	124	78	89	3.5	7.3	3670
U12	165	80	23+6	136	92	108	7.3	6.6	3694
C13	156	76	28	185	111	81	4.7	12.5	931
C14	172	79	23+4	148	94	69	6.1	8.1	340
C15	153	77	22	127	77	79	7.1	7	350
C16	157	57	28	122	84	79	4.5	7.6	494
C17	165	65	22+5	148	90	81	7.1	9.3	260
C18	166	80	25+4	138	105	99	7.3	9.4	550
C19	176	83	26+4	135	93	71	5.7	7.9	895
C20	164	85	25+1	134	69	74	4.8	9.1	495
C21	166	80.2	25+2	131	93	104	7.3	9.4	550

***Table 24.** Doppler ultrasound scan data. v_{sys} – systolic velocity (cm/s), v_{dia} – diastolic velocity (cm/s), L – left, R – right.*

Patient	v_{sys} (L)	v_{dia} (L)	v_{sys} (R)	v_{dia} (R)	PI (L)	PI (R)	RI (L)	RI (R)	Notch
U1	37.5	15	30	15	1.11	0.6	0.62	0.42	no
U2	80	40	75	40	0.79	0.68	0.52	0.47	no
U3	47	30	70	30	0.62	1.14	0.44	0.64	no
U4	66	30	62	31	0.88	0.72	0.55	0.49	no

U5	110	55	67.5	37.5	0.83	0.86	0.53	0.54	no
U6	60	30	67.5	27.5	0.72	1.23	0.48	0.62	no
U7	40	22.5	50	22.5	0.57	1	0.41	0.61	no
U8	88	30	75	45	1.52	0.69	0.72	0.47	no
U9	45	17.5	32.5	20	1.2	0.63	0.62	0.45	yes, no for R
U10	60	25	37.5	22.5	1.13	0.83	0.61	0.54	no
U11	140	68	130	70	0.8	0.8	0.51	0.46	unsure
U12	58	30	120	70	0.69	0.69	0.48	0.41	no
C13	60	15	50	12.5	2.55	3.19	0.87	0.91	yes
C14	30	10	25	5	1.86	2.49	0.78	0.85	yes for R, unsure for L
C15	80	15	37.5	12.5	2.52	1.91	0.83	0.77	yes
C16	45	15	45	12	1.64	1.75	0.72	0.74	yes
C17	37.5	15	37.5	15	0.85	1.06	0.6	0.6	yes
C18	35	10	35	15	1.82	1.24	0.77	0.69	yes for L, unsure for R
C19	65	15	67.5	15	1.84	1.54	0.76	0.74	yes
C20	60	35	65	40	0.72	0.72	0.41	0.38	no
C21	52	16	30	10	1.77	1.77	0.69	0.66	yes

Table 25. *Normalised values for the 9 variables used in the Buckingham PI analysis. A – area of the aorta, PWV – pulse wave velocity, R_{ut} – resistance in the uterine artery, R_{periph} - peripheral resistance, P_{syst} – systolic blood pressure, ΔP_{pulse} – pulse pressure, Compliance – systemic vascular compliance, CO – cardiac output, SV – stroke volume*

Patient	A	PWV	R_{ut}	R_{periph}	P_{syst}	ΔP_{pulse}	Compliance	CO	SV
U1	0.325	0.509	0.891	0.339	0.784	0.676	0.801	0.904	0.807
U2	0.227	0.459	0.176	0.517	0.576	0.452	1.000	0.479	0.414
U3	0.296	0.565	0.566	0.533	0.781	0.707	0.630	0.671	0.620
U4	0.483	0.532	0.268	0.465	0.659	0.473	0.741	0.781	0.835
U5	0.171	0.487	0.105	1.000	0.667	0.614	0.794	0.342	0.376
U6	0.353	0.606	0.384	0.679	0.723	0.512	0.576	0.603	0.510
U7	0.302	0.655	0.723	0.919	0.764	0.593	0.457	0.452	0.442
U8	0.352	0.601	0.266	0.635	0.694	0.554	0.577	0.575	0.556
U9	0.574	0.918	0.560	0.530	0.788	0.689	0.222	0.767	0.533
U10	0.184	0.492	0.564	0.610	0.851	0.767	0.745	0.507	0.416
U11	0.246	0.585	0.089	0.745	0.663	0.630	0.598	0.479	0.438
U12	0.362	0.540	0.419	0.304	0.741	0.594	0.769	1.000	0.752
C13	0.504	1.000	0.519	0.799	1.000	1.000	0.207	0.644	0.646
C14	0.522	0.645	1.000	0.461	0.807	0.727	0.487	0.836	0.984
C15	0.511	0.574	0.286	0.332	0.693	0.675	0.681	0.973	1.000
C16	0.450	0.619	0.494	0.550	0.657	0.513	0.569	0.616	0.634
C17	0.590	0.705	0.647	0.400	0.791	0.782	0.396	0.973	0.975
C18	1.000	0.751	0.511	0.404	0.754	0.445	0.334	1.000	0.820
C19	0.535	0.615	0.345	0.495	0.720	0.567	0.526	0.781	0.893
C20	0.380	0.721	0.378	0.589	0.713	0.886	0.414	0.658	0.722
C21	0.760	0.709	0.323	0.375	0.705	0.514	0.364	1.000	0.781

Further description of methods used for feature selection:

Minimum Redundancy Maximum Relevance algorithm – the method selects a set of features that are highly uncorrelated to each other but they are highly correlated to the output [143].

Chi-square tests – Uses the null hypothesis to assume there are no differences between classes. Then, for each value, an expected number is found. To find chi-square, the difference between actual and expected values squared divided by expected value is used.

F-test – this method is used when the data has an F-distribution. The f-value is calculated as the division between the larger sample variance and smaller sample variance.

ReliefF algorithm – a common method that is based on the idea that a feature should have similar values for observations of the same class and different values for observations of different classes [144]. To calculate the feature score, it uses the nearest neighbour pair and if the observation value for same class is different, then the score decreases.

Table 26. *Summary of ML methods used for the classification models*

Name	Abbreviation	Description/Settings
Fine Tree	FT	Maximum number of splits: 100 Split criterion: Gini's diversity index Surrogate decision splits: Off
Medium Tree	MT	Maximum number of splits: 20 Split criterion: Gini's diversity index Surrogate decision splits: Off
Coarse Tree	CT	Maximum number of splits: 4 Split criterion: Gini's diversity index Surrogate decision splits: Off
Linear Discriminant	LD	Covariance structure: Full
Quadratic Discriminant	QD	Covariance structure: Full
Logistic Regression	LR	-
Gaussian Naïve Bayes	GNB	Distribution name for numeric predictors: Gaussian Distribution name for categorical predictors: Not Applicable
Kernel Naïve Bayes	KNB	Distribution name for numeric predictors: Kernel Distribution name for categorical predictors: Not Applicable Kernel type: Gaussian Support: Unbounded
Linear SVM	LSVM	Kernel function: Linear Kernel scale: Automatic Box constraint level: 1 Multiclass method: One-vs-One Standardize data: true
Quadratic SVM	QSVM	Kernel function: Quadratic Kernel scale: Automatic Box constraint level: 1 Multiclass method: One-vs-One Standardize data: true
Cubic SVM	CSVM	Kernel function: Cubic Kernel scale: Automatic Box constraint level: 1 Multiclass method: One-vs-One Standardize data: true
Fine Gaussian SVM	FGSVM	Kernel function: Gaussian Kernel scale: 0.25 Box constraint level: 1

		Multiclass method: One-vs-One Standardize data: true
Medium Gaussian SVM	MGSVM	Kernel function: Gaussian Kernel scale: 1 Box constraint level: 1 Multiclass method: One-vs-One Standardize data: true
Coarse Gaussian SVM	CGSVM	Kernel function: Gaussian Kernel scale: 4 Box constraint level: 1 Multiclass method: One-vs-One Standardize data: true
Fine KNN	FKNN	Number of neighbours: 1 Distance metric: Euclidean Distance weight: Equal Standardize data: true
Medium KNN	MKNN	Number of neighbours: 10 Distance metric: Euclidean Distance weight: Equal Standardize data: true
Cosine KNN	CosKNN	Number of neighbours: 100 Distance metric: Euclidean Distance weight: Equal Standardize data: true
Cubic KNN	CubKNN	Number of neighbours: 10 Distance metric: Minkowski (cubic) Distance weight: Equal Standardize data: true
Weighted KNN	WKNN	Number of neighbours: 10 Distance metric: Euclidean Distance weight: Squared inverse Standardize data: true
Bagged Trees	BagT	Ensemble method: Bag Learner type: Decision tree Maximum number of splits: 18 Number of learners: 30
Subspace Discriminant	SubD	Ensemble method: Subspace Learner type: Discriminant Number of learners: 30 Subspace dimension: 1
Subspace KNN	SubKNN	Ensemble method: Subspace Learner type: Nearest neighbours Number of learners: 30 Subspace dimension: 1
RUSBoosted Trees	RUSBT	Ensemble method: RUSBoost Learner type: Decision tree Maximum number of splits: 20 Number of learners: 30 Learning rate: 0.1
Narrow Neural Network	NNN	Number of fully connected layers: 1 First layer size: 10 Activation: ReLU Iteration limit: 1000 Regularization strength (Lambda): 0 Standardize data: Yes

Medium Neural Network	MNN	Number of fully connected layers: 1 First layer size: 25 Activation: ReLU Iteration limit: 1000 Regularization strength (Lambda): 0 Standardize data: Yes
Wide Neural Network	WNN	Number of fully connected layers: 1 First layer size: 100 Activation: ReLU Iteration limit: 1000 Regularization strength (Lambda): 0 Standardize data: Yes
Bilayered Neural Network	BNN	Number of fully connected layers: 2 First layer size: 10 Second layer size: 10 Activation: ReLU Iteration limit: 1000 Regularization strength (Lambda): 0 Standardize data: Yes
Trilayered Neural Network	TNN	Number of fully connected layers: 3 First layer size: 10 Second layer size: 10 Third layer size: 10 Activation: ReLU Iteration limit: 1000 Regularization strength (Lambda): 0 Standardize data: Yes

Monte Carlo simulations additional results:

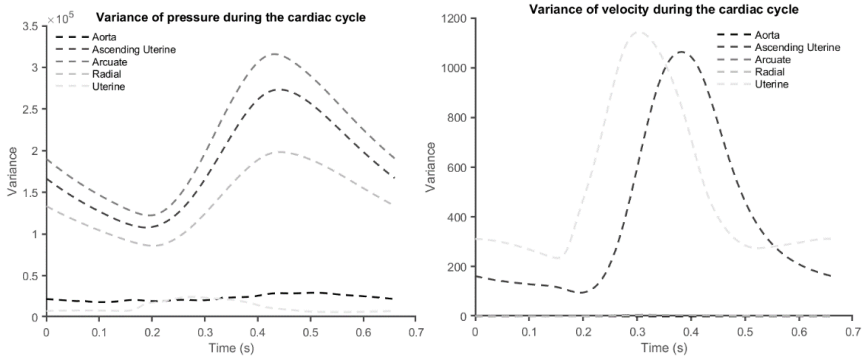

Figure 31. *Variance of Pressure (Left) and Velocity (Right) for different outlet vessels when varying parameter* A_{ut}

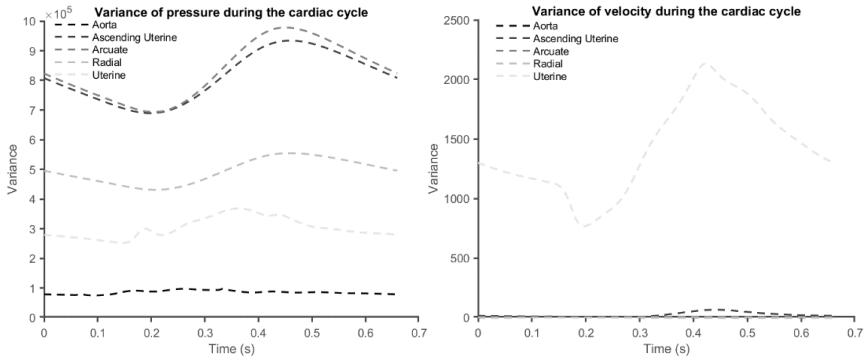

***Figure 32**. Variance of Pressure (Left) and Velocity (Right) for different outlet vessels when varying parameter A_{rad}*

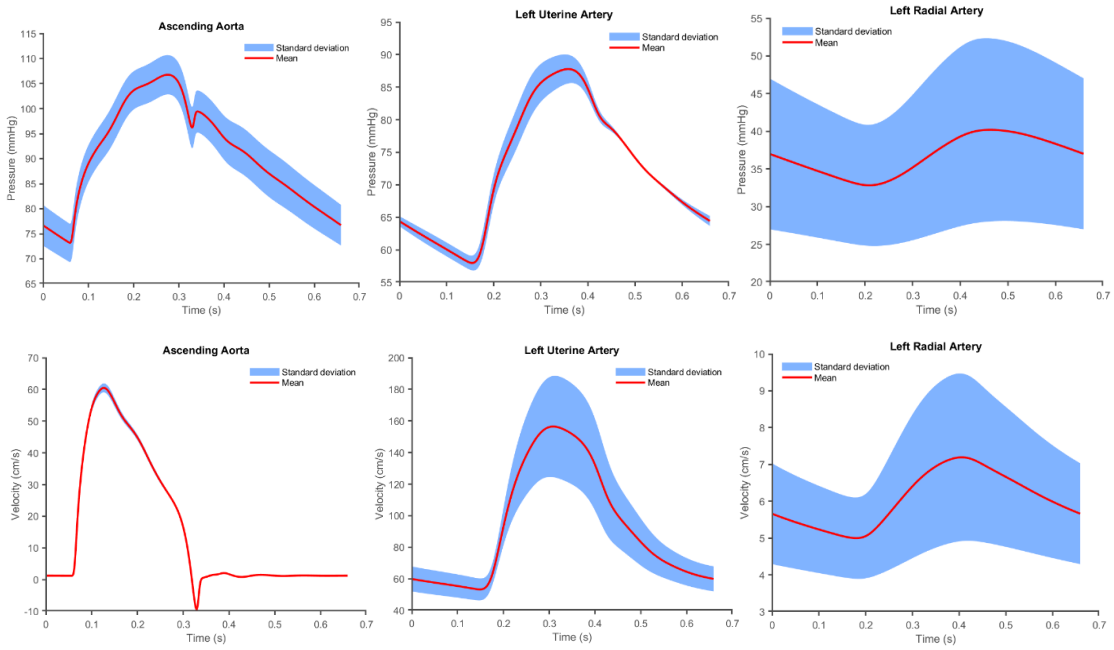

***Figure 33**. Pressure (Top) and Velocity (Bottom) changes of varying A_{ut}*

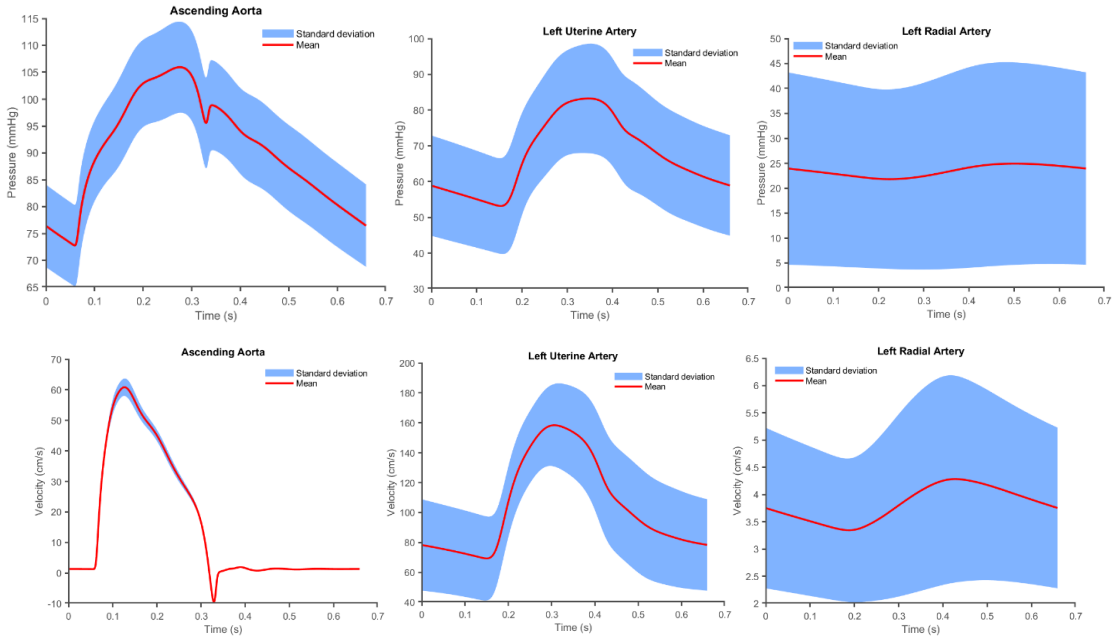

***Figure 34**. Pressure (Top) and Velocity (Bottom) changes of varying A_{rad}*

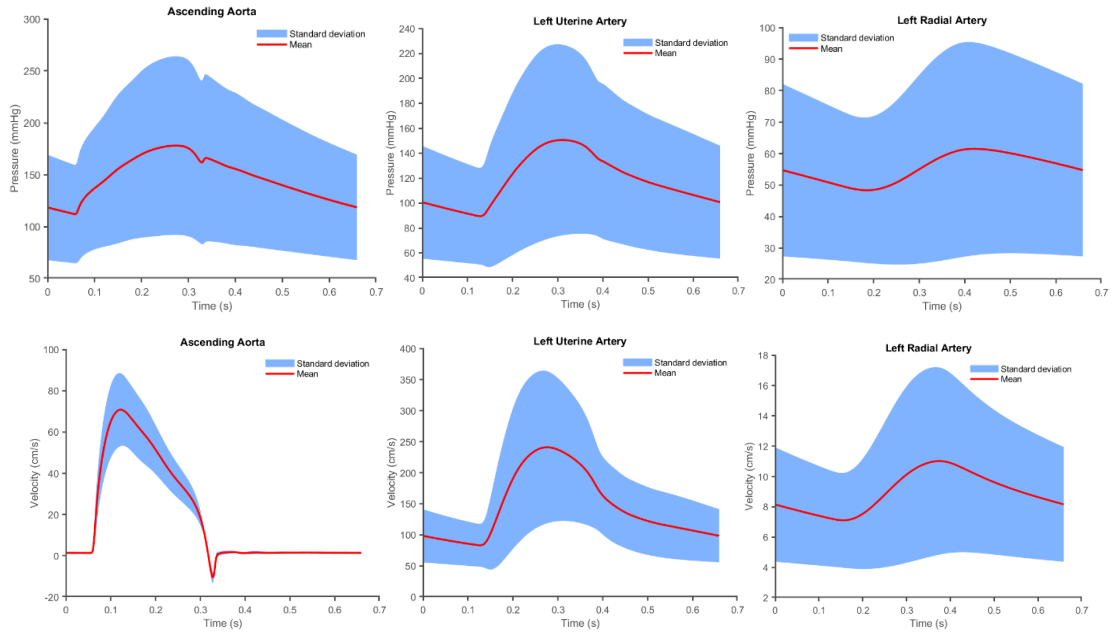

***Figure 35**. Pressure (Top) and Velocity (Bottom) changes of varying $Q_{ao,in}$*

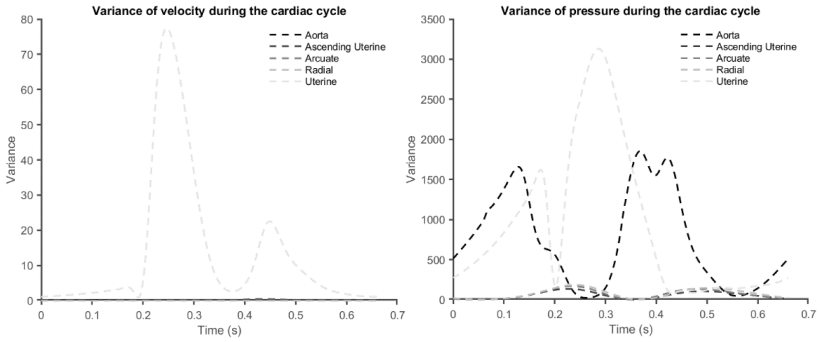

***Figure 36**. Variance of Pressure (Left) and Velocity (Right) for different outlet vessels when varying parameter C*

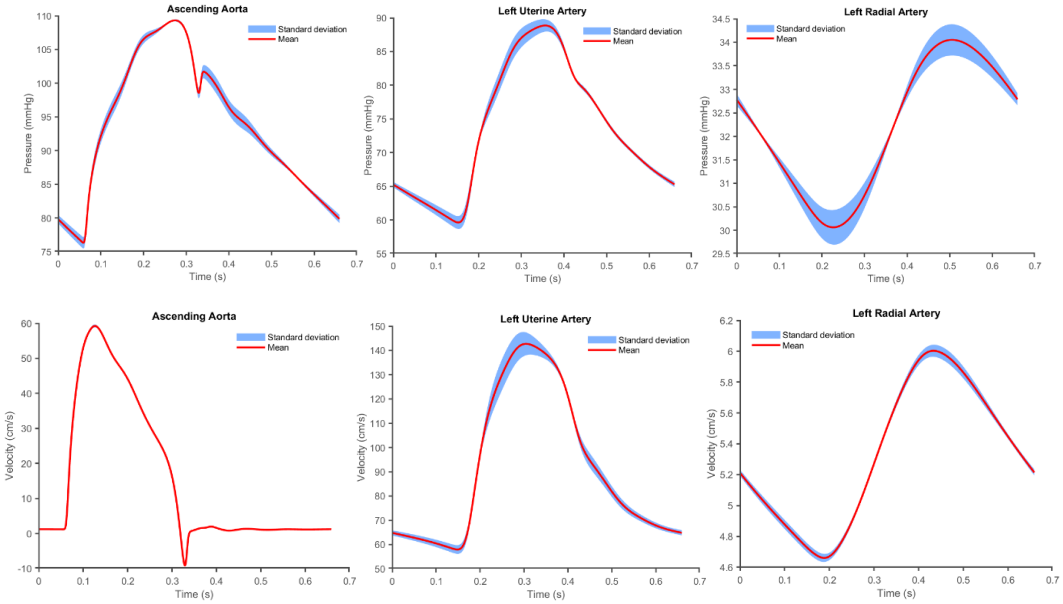

***Figure 37**. Pressure (Top) and Velocity (Bottom) changes of varying $Q_{ao.in}$*

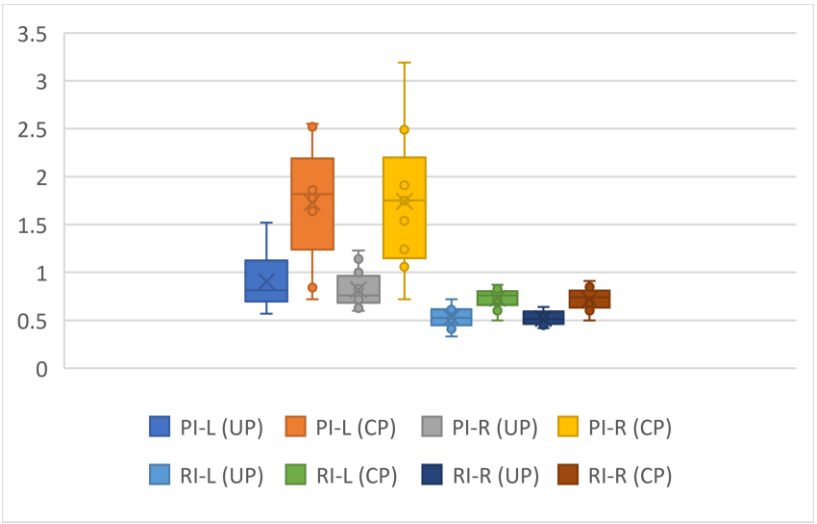

***Figure 38**. Boxplots UP and CP for PI (L/R) and RI (L/R), the values are not normalised*